Lake Champlain Basin Program

TECHNICAL REPORT NO. 100

Evaluating floodplain potential for sediment and phosphorus deposition: Development of a framework to assist in Lake Champlain Basin planning

June 2021

Prepared by:
Rebecca Diehl University of Vermont

For:
The Lake Champlain Basin Program and
New England Interstate Water Pollution Control Commission

This report was funded and prepared under the authority of the Lake Champlain Special Designation Act of 1990, P.L. 101-596 and subsequent reauthorization in 2002 as the Daniel Patrick Moynihan Lake Champlain Basin Program Act, H. R. 1070, through the US EPA. Publication of this report does not signify that the contents necessarily reflect the views of the states of New York and Vermont, the Lake Champlain Basin Program, or the US EPA.

The Lake Champlain Basin Program has funded more than 90 technical reports and research studies since 1991. For complete list of LCBP Reports please visit:
https://www.lcbp.org/news-and-media/publications/technical-reports/

NEIWPCC Job Code: 0100-323-002

Final Report

NEIWPCC Job Code:	0100-323-002
Project Code:	L-2018-017
Prepared by:	Rebecca Diehl University of Vermont
Date Submitted:	January 20, 2021
Date Approved:	June 24, 2021

Evaluating floodplain potential for sediment and phosphorus deposition: Development of a framework to assist in Lake Champlain Basin planning

Contact Information

Rebecca Diehl

University of Vermont, 94 University Place, Burlington, Vermont 05405

Phone: 802-656-2063; Fax: 802-656-3042, Rebecca.Diehl@uvm.edu

This is a Lake Champlain Basin Program funded project
54 West Shore Road
Grand Isle, VT 05482
802.372.3213
www.lcbp.org

This project was selected for funding by the Lake Champlain Basin Program (LCBP) Steering Committee and it has been supported directly by an agreement or sub-award issued by NEIWPCC. NEIWPCC manages LCBP's personnel, contracts, grants, and budget tasks through a partnership with the LCBP Steering Committee.

Although the information in this document may have been funded wholly or in part by the United States Environmental Protection Agency (under agreement CE982720010), the National Park Service, or by the International Great Lakes Fishery Commission, through their respective contracts to NEIWPCC, it has not undergone review by the Agency, Service, or Commission, and no official endorsement of the content of the document should be inferred. The viewpoints expressed here do not necessarily represent those of NEIWPCC, the LCBP, the USEPA, the NPS, or the GLFC, nor does mention of trade names, commercial products, or causes constitute endorsement or recommendation for use.

Suggested Citation:
Diehl, R.M., B.C. Wemple, K.L. Underwood, D. Ross,. 2021. "Evaluating floodplain potential for sediment and phosphorus deposition: Development of a framework to assist in Lake Champlain Basin planning" Report to the Lake Champlain Basin Program, June 2021

Executive Summary

The study described in this report was motivated by a need to provide a baseline understanding of the functioning of floodplains in the Lake Champlain Basin. Because floodplains can store and transform sediment and nutrients derived from the upstream watershed, many stakeholders in the Lake Champlain Basin are interested in restoring, protecting, or enhancing these natural features to optimize their role in water quality improvements. There is a lack of data, however, on the distribution of floodplains and the rate at which river-derived sediment and associated nutrients are deposited.

In this project, we collected and analyzed data that describe the status and function of floodplains along Lake Champlain Basin rivers to assist in watershed planning for improved water quality. First, we created an inventory of floodplains and identified their degree of hydrologic connectivity, through the development of a low-complexity floodplain mapping model. Flood-derived sediment and phosphorus deposition rates collected from a floodplain monitoring network provided a measure of the capacity of floodplains to capture sediment and phosphorus. Statistical models were developed to describe the functional relationship between deposition rates and the physical attributes of the upstream watershed, and more locally along the river channel and floodplain. We then used these statistical models to establish a framework for evaluating where to prioritize floodplain management efforts and the efficacy of such investments in meeting load reduction targets. Our efforts focused on those streams in Vermont whose upstream drainage area was 10 mi^2 or greater, and on a range of watershed settings where it was likely that floodplains can act as sediment sinks. The resulting management framework may be applied throughout the Basin, given the availability of high resolution geo-spatial datasets.

Based on monitoring carried out in 2019 and 2020, we found that floodplains in the Lake Champlain Basin captured between 0.04 and 4.48 kg m^{-2} yr^{-1} of sediment, corresponding to 0.02 to 3.3 g P m^{-2} yr^{-1}, or 0.8 to 164% of annual loads transported. The highest rates of phosphorus deposition were associated with very wide valleys, in watersheds with a relatively higher proportion of impervious surfaces, where channel incision was low, and the floodplain was classified as medium energy (10 < Specific Stream Power < 300 W m^{-2}). Locally, the mass of phosphorus deposition was greatest close to the channel (i.e., within 1 channel width), and where surfaces were regularly inundated. Two types of statistical models developed to predict phosphorus deposition rates through the watershed, and locally across the floodplain, explained 44 to 69% of the measured variability. Application of the floodplain management framework predicted where phosphorus deposition rates were greatest in the Mad River Watershed and the increase in phosphorus deposition with floodplain lowering that resulted in increased hydrologic connectivity.

While the results from this project have made good progress in understanding the controls on spatial variability in deposition rates, numerous limitations exist in the resulting dataset and management framework, which must be understood and acknowledged in its application. Observations are temporally limited (i.e., over one year), masking inter-annual and decadal variability in deposition because of shifts to hydrology, land use, and channel or floodplain morphology. Because of this, predictions from the models have high uncertainties, notably over longer timescales. Additionally, without understanding the full set of processes that determine a floodplain's net sediment and phosphorus budget, we may misjudge the best settings to target. With additional data collection on sediment and phosphorus deposition rates, placed in the context of export and transformations in phosphorus pools, depositional rates such as those presented in this work may then be used to understand the full retentive capacity of floodplains.

Table of Contents

Page

1 Project Introduction

Lake Champlain remains an impaired water body due to excessive phosphorus derived from the surrounding landscape. Water quality improvement plans must focus on both minimizing processes that contribute to watershed export of sediment and nutrients and enhancing features that maximize the retention of those sediments and nutrients (US EPA, 2016). When properly functioning, floodplains can capture, transform, and store sediment and nutrients derived from the upstream watershed (Noe and Hupp, 2009). However, many of the region's rivers have limited floodplain access and often contribute to the export of sediment and phosphorus from excessive bank erosion (Kline and Cahoon, 2010; Langendoen et al., 2012). Investment into restoration, protection, or enhancement projects that improve the hydrologic connection between flood waters and floodplains and reduce flood velocities can reduce fluxes and increase retention of phosphorus-laden sediments. Because of the scope of the problem, it is necessary to thoughtfully target floodplain areas with the greatest potential to store sediment and nutrients for improved water quality (Singh et al., 2019).

From empirical and modelling studies, we have a general understanding of the capacity of floodplains to attenuate the downstream movement of sediment and phosphorus that may point us towards where and how to prioritize floodplain restoration efforts (Lammers and Bledsoe, 2017). Environmental variables, important for determining sediment and phosphorus retention rates, operate at multiple scales. At the watershed-scale, geologic and climatic variability, along with soil and land use/land cover characteristics determine the magnitude of fluxes (i.e., the amount of potential sediment and phosphorus that may be captured by a floodplain; Jones et al., 2001; Ishee et al., 2015; Stryker et al., 2018). Urbanizing watersheds, and those with large swaths of impervious surfaces, for example, often have higher sediment loads and higher total phosphorus (TP) concentrations, resulting in greater deposition, than watersheds dominated by other land use types (Gellis et al., 2008; Pizzuto et al., 2016; McMillan and Noe, 2017). The geologic setting will also influence valley characteristics, important for determining the presence of floodplains and capacity to store sediment over long time periods (Jain et al., 2008). Floodplains located in wide valleys where rivers are sinuous tend to have higher sediment deposition rates (Schenk et al., 2013). Localized variables determine the transport of flood waters from the channel to the floodplain, and the degree to which sediment and sediment-bound phosphorus associated with flood waters are deposited (Pizzuto et al., 2008). While some have found strong relationships between hydroperiod or elevation above the channel and sedimentation (Hupp and Bazemore, 1993; Kleiss, 1996), others attribute depositional patterns on floodplains to the distance from the channel (Asselman and Middelkoop, 1995; Walling et al., 1999), or more localized influences such as floodplain sloughs (Kaase and Kupfer, 2016)..

Our understanding of sediment and phosphorus deposition patterns through a watershed is largely derived, however, from studies conducted outside of the Lake Champlain Basin. Without data specific to the Lake Champlain Basin, we do not know if, and to what degree, these trends apply. Thus, there is a need to build a dataset of the magnitude and variability of sediment and phosphorus deposition on floodplains in the Basin. Development of mechanistic relationships between deposition and physical, hydrologic, or other ecosystem attributes can inform evidence-based prioritization of floodplain projects to improve water quality.

To bridge this critical gap in regional data and build our understanding of floodplain deposition functions, our work was framed around three key objectives:

> **Objective 1. Create an inventory of floodplains.** Map the distribution of floodplain surfaces, and the degree to which they are hydrologically connected to the river channel.
> **Objective 2. Document floodplain deposition.** Build an empirical dataset of sediment and sediment-bound phosphorus deposition rates for floodplains which are representative of the range of settings where long-term storage is likely to occur.

Objective 3. Develop a framework for predicting P deposition on floodplains. Identify statistical models that relate physical attributes at multiple scales to phosphorus deposition rates to provide a framework for basin planning.

For this project, we focused on higher-order, unconfined, lower-gradient river settings that are likely to be associated with floodplain sites of long-term sediment and phosphorus storage. Although deposition can occur in pockets along small streams and those that have steep slopes and are confined within their valley, their role in overall net sediment and nutrient deposition may be small (Swinnen et al., 2020). Thus, we limited the extent of our mapping, monitoring, and modelling to streams with a drainage area greater than 10 mi^2, and whose slope-to-drainage area relationship indicated the likely presence of a floodplain (Jain et al., 2008).

We focused our efforts on floodplain deposition of sediment and sediment-bound phosphorus (i.e., total phosphorus), since in many settings the majority of phosphorus is transported in particulate form (Records et al., 2016; Vidon et al., 2018). A separate LCBP study (Roy 2019) is investigating the complex dynamics of phosphorus transformation in riparian wetland settings, and the degree to which phosphorus in these settings may be converted to more labile forms.

To build a framework to support decision-making around prioritization of floodplain deposition sites, we used statistics to link sediment and phosphorus deposition rates to those physical attributes of the landscape including the river network that are important for determining the production, delivery, and deposition of fine sediment and sediment-bound phosphorus. Because these driving factors occur over multiple spatial scales, from the watershed (10^8 m) to the plot (10^0 m), we designed a study to capture this variability. By creating functional relationships between physical attributes and deposition rates, we built statistical models that are both descriptive of how deposition rates change through the watershed and with shifts to channel and floodplain morphology, and prescriptive of where and how to best improve retention of sediment and phosphorus on floodplains to improve water quality.

Data collection, analyses, and model applications were concentrated in the Vermont portion of the Basin because of the accessibility of high-resolution spatial datasets (geodata.vermont.gov) and convenience of floodplain sites relative to the University of Vermont campus. To achieve our goals of prioritizing over large scales, we developed approaches and built datasets and conceptual frameworks that may be applied to other portions of the basin, notably where high-resolution data exists.

This project benefitted from multiple partnerships. The Vermont Land Trust, USDA Natural Resource Conservation Service Vermont, VT DEC Rivers Program, VT Fish and Wildlife and the Vermont Chapter of The Nature Conservancy (TNC) all assisted in the identification and creation of a floodplain monitoring network, which would not have been possible without the generosity of landowners. Milone and MacBroom, Inc. and Fitzgerald Environmental Associates, LLC provided quality-assured geospatial data sets derived under separate projects. The UVM Gund Institute of Environment provided a platform for the sharing of ideas and financial support to select members of the research team. Students involved in the project were also supported with funding from TNC, VT Department of Transportation, VT EPSCoR, USGS Water Center, UVM College of Arts and Sciences, and the Geography Department.

2 Tasks Completed

We identified six tasks necessary to fulfill the overall goal of improving our understanding of floodplain functions in the Lake Champlain Basin to assist in watershed planning for improving water quality (Table 1). For the first task, we developed a Quality Assurance Project Plan (QAPP), which was approved in February 2019, with amendments to the document in July 2019

and July 2020. The remaining five tasks are associated with the three project objectives as described below.

Table 1. Project Tasks and Deliverables

Project Objective	Task	Task Title	Deliverable or Output	Timeframe of Completion
	1	Develop QAPP	QAPP Approval	Feb 2019; Updated July 2019 and July 2020
Create an inventory of floodplains	2	Develop and execute procedure that identifies floodplains, and their level of hydrologic connectivity	Probabilistic floodplain maps of range of recurrence interval (RI) floods for the Vermont portion of the Lake Champlain Basin	June 2020
Document floodplain deposition	3	Establish floodplain monitoring network	Coordinates and description of floodplain monitoring sites and plots Coordinates and descriptions of floodplain cores	October 2019
	4	Collect and analyze field data	Floodplain deposition dataset from monitoring plots as a result of three flood events Floodplain deposition dataset from cores Comparison metrics between monitoring plot and core deposition Site-averaged floodplain deposition dataset	December 2020
Develop a framework for predicting P deposition on floodplains	5	Identify variables important for total phosphorus (TP) deposition	Physical attributes of floodplain sites and monitoring plots Correlations between physical attributes and metrics describing floodplain deposition	December 2020
	6	Develop models for prioritizing and quantifying impact of restoration	Output from statistical models Description of model use in framework Example applications of framework including prioritization ranking for reaches in a test watershed and change in deposition with restoration on two floodplains	December 2020 January 2021
	7	Write quarterly reports	Approved quarterly reports	April 2019 to December 2020
	8	Write final report	Approved final report and associated deliverables	December 2020 to February 2021

Objective 1. Create an inventory of floodplains.

Task 2. Develop and execute procedure that identifies floodplains, and their level of hydrologic connectivity.

To create an inventory of floodplain maps and identify their level of hydrologic connectivity for rivers draining the Lake Champlain Basin, we developed the probHAND model (Diehl et al., 2020). Unlike traditional floodplain mapping approaches that use data- and resource-intensive hydrodynamic models, the probHAND model is lower in its complexity. Such lower complexity models may be applied over large scales, relatively efficiently. To account for uncertainties that exist in flood inundation mapping, and are exacerbated in low complexity models (Afshari et al.,

2018), we incorporated an uncertainty analysis. Application to the Vermont portion of the Lake Champlain Basin resulted in probabilistic floodplain maps that represent the distribution of floods with recurrence intervals between 2- and 500-years and associated (un)certainty.

Objective 2. Document floodplain deposition

Task 3. Establish floodplain monitoring network.

To measure variability in sediment and TP deposition on floodplains in the Lake Champlain Basin, we established a floodplain monitoring network. This network was designed to capture prominent environmental gradients present in the Lake Champlain Basin, at multiple scales, including those represented at the watershed scale and locally within individual floodplains. We identified 24 floodplain sites and established 170 monitoring plots designed to measure the magnitude and spatial variability of sediment deposition at the temporal resolution of a single flood event.

Task 4. Collect and process field data to develop floodplain deposition dataset.

In an initial reconnaissance of floodplain monitoring sites, we collected core samples following April 2019 snowmelt floods to help guide establishment of plot layout. After the deployment of monitoring plots, field crews collected sediment deposited during three flood events in June, October, and November 2019. All samples were dried, weighed, sieved, and aggregated for plot-scale analyses of TP. Data derived from cores were compared to monitoring plot observations, and observations were converted to sediment and TP deposition rates based on the flood event's recurrence interval and extrapolated to site-scale TP deposition. As a result, we developed a dataset of sediment and phosphorus deposition at 126 plots at 22 different sites (2 sites and 44 plots did not have data).

Objective 3. Develop a framework for floodplain management.

Task 5. Identify variables important for TP deposition

From the peer-reviewed literature, we identified a list of physical attributes of the river channel, floodplain, and watershed likely to describe variability in measured TP deposition. These attributes are indicative of processes important for the generation, transport, and deposition of sediment and phosphorus. Watershed scale characteristics, such as valley setting and upstream soils, are important for determining channel fluxes, while reach-scale and local characteristics, such as channel slope and floodplain width, are important for determining the transport and subsequent deposition of water, sediment, and nutrients onto the floodplain. For each of the floodplain sites, we calculated 11 variables that describe the upstream watershed and reach characteristics. At the 170 monitoring plots, we calculated an additional 6 variables that describe the local physical characteristics. With these 17 variables, we explored significant relationships between environmental controls and the floodplain deposition dataset from Task 4.

Task 6. Identify and apply models to help prioritize and evaluate floodplain restoration

To develop a framework for floodplain management and extrapolate plot- and site-scale observations of TP deposition to the Lake Champlain Basin, we identified statistical models that describe the greatest variability in measured TP deposition rates and have the most empirical support. We prescribed the application of the models to watersheds, and sites of interest to evaluate 1) where in the watershed to prioritize efforts, and 2) how a specific intervention is associated with a change in TP deposition rates. In this report, we provide example applications by 1) creating a map of relative TP deposition rates along the Mad River based on watershed

and reach characteristics and 2) evaluating restoration interventions at two floodplains in the Mad River and Potash Brook Watersheds.

3 Methodology

Task 2. Develop and execute procedure that identifies floodplains, and their level of hydrologic connectivity.

To map floodplains in the Lake Champlain Basin, we formalized and extended the functionality of the low-complexity Height Above Nearest Drainage (HAND) floodplain mapping approach into the probHAND model (Diehl et al., 2020). In the existing approach, HAND maps derived from a digital elevation model (DEM), are used in conjunction with synthetic rating curves, to identify the inundation zone for a specified flood magnitude on a reach-by-reach basis (Zheng et al., 2018). To account for large uncertainties associated with floodplain maps, we incorporated a Monte Carlo simulation to create probabilistic maps. For a description of the probHAND model and its application to the Vermont portion of the Lake Champlain Basin see "Improving flood hazard datasets using a low-complexity, probabilistic floodplain mapping approach", accepted for publication to PLOS ONE on March 4, 2021 (Appendix A).

Task 3. Establish floodplain monitoring network.

We identified 24 floodplain monitoring sites based on the following criteria:

1) *Accessible.* Willing landowners agreed to the placement of monitoring equipment and multiple visits/year from field crews. Sites were also a relatively short walk from a road or trail
2) *Regularly inundated.* Because of the short duration of this project, we focused on sites for which at least a portion of the floodplain is likely to experience floods on an annual basis.
3) *Spatially distributed.* Located within each of the major drainage basins in Vermont and distributed along rivers whose drainage areas span three orders of magnitude (11-2500 km^2), and slopes span four orders of magnitude (0.01 to 0.00001 m/m; Figure 1).
4) *Likely sediment sink.* Based on established relationships between drainage area and slope that define process domains (Jain et al., 2008) along with on-the-ground observations of recent deposition, we focus on sites that are likely to be net depositional over longer time-scales (Figure 2).

In the summer and fall of 2019, we installed 170 monitoring plots at 23 of the 24 sites (Figure 3, Table 2). Depending on the size and topographic and land cover variability of the studied floodplains, we established 3-12 monitoring plots at each site. At most sites, transects perpendicular to the channel best captured gradients in elevation and therefore likely inundation. Each monitoring plot consists of a 6' bamboo pole, surrounded by 4 artificial turf pads (15 cm by 15 cm) orthogonally placed 1-meter from the center pole. A pin flag was placed an additional 0.5 meters from the turf mat. We collected a GPS point initially in ArcGIS's Collector mobile application with an external antenna (horizontal accuracy ~5 meters) to determine the plot's location for analyses and re-location. Field crews returned in 2020 to re-survey plot locations using an RTK-GPS (horizontal accuracy < 1 meter).

At each site, we co-located a stage crest gage with one of the monitoring plots. Each crest gage consists of a 2.22 cm diameter by 6 ft tall acrylic tube and 4 ft long piece of rebar placed in the ground and fastened to each other. The tube has three small holes drilled 10 cm apart starting at the ground surface to allow for water to enter the tube, and one small vent hole close to the top of the tube to allow for air to escape. Ground cork resting at the bottom of the tube floats on top of the rising flood waters, adhering to the side of the acrylic tube, thereby providing an indicator of the maximum flood stage encountered in the time interval since the crest gage was last inspected.

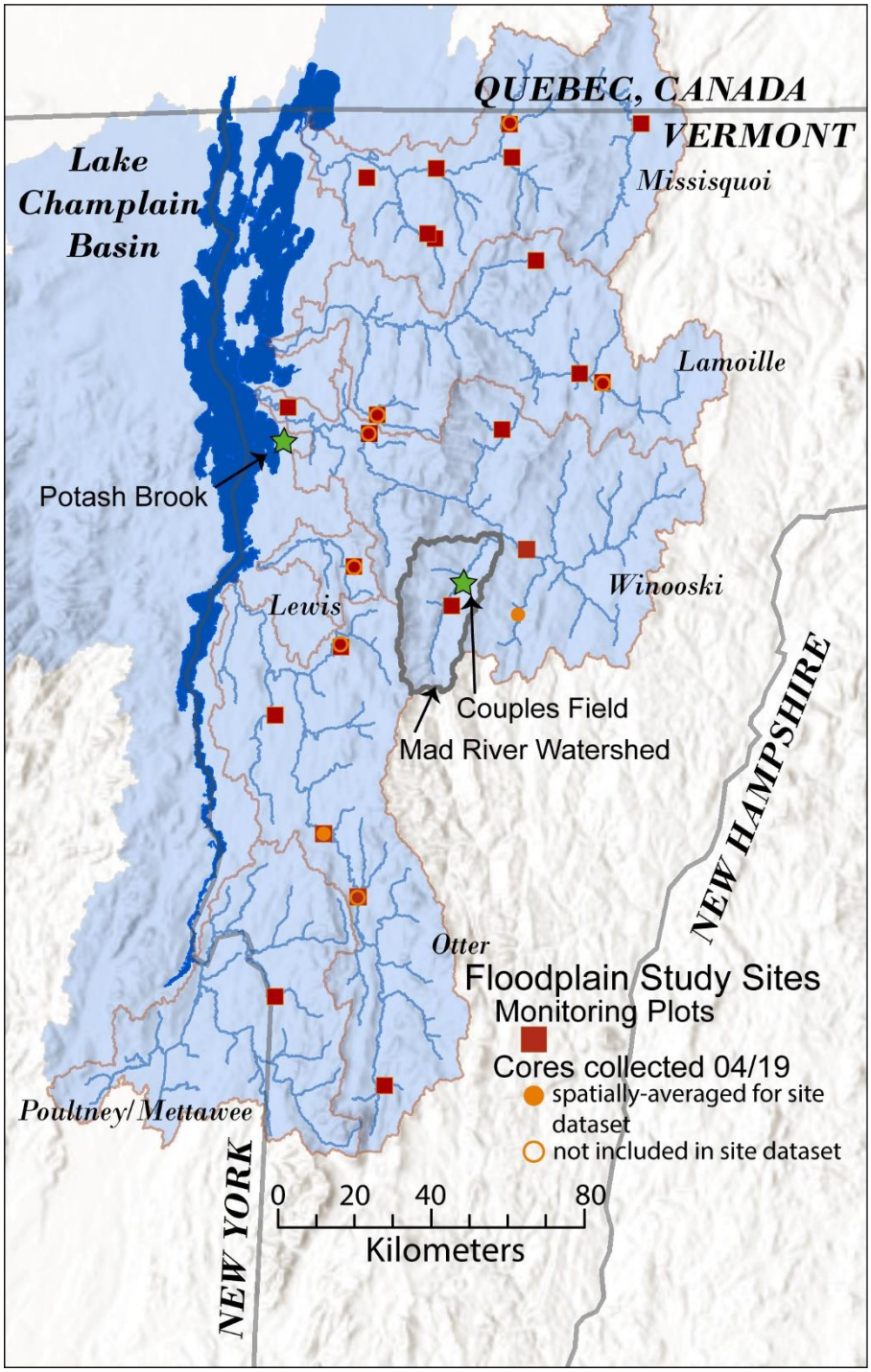

Figure 1. Location of floodplain monitoring sites in the Lake Champlain Basin. We applied the restoration framework to the Mad River Watershed, and two floodplain sites on Potash Brook and at Couples Field.

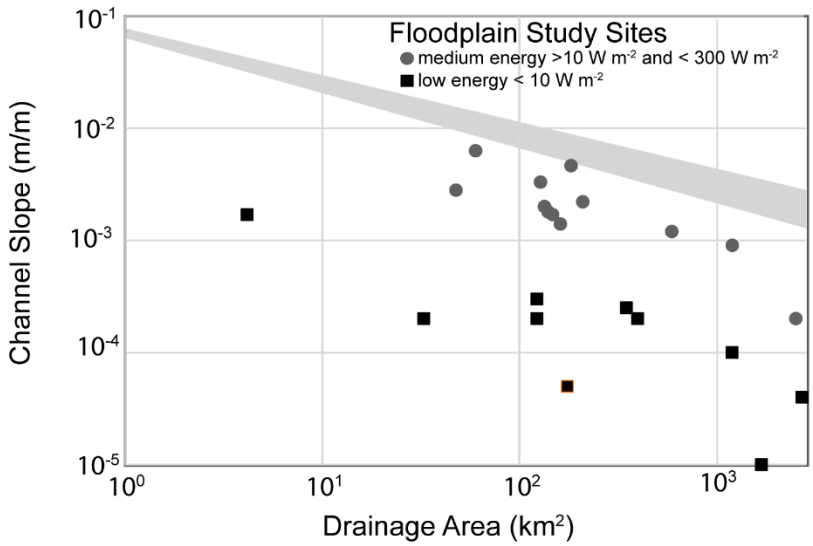

Figure 2. Slope-drainage area relationship for floodplain study sites in the Lake Champlain Basin, Vermont. Gray line is process threshold differentiating areas where floodplains are likely to occur within a watershed, and therefore indicative of settings likely to store sediment over long timescales, as defined in Jain et al 2008. Floodplain sites are also differentiated based on the Nanson and Croke (1992) classification of floodplains by specific stream power, either as low or medium energy floodplains.

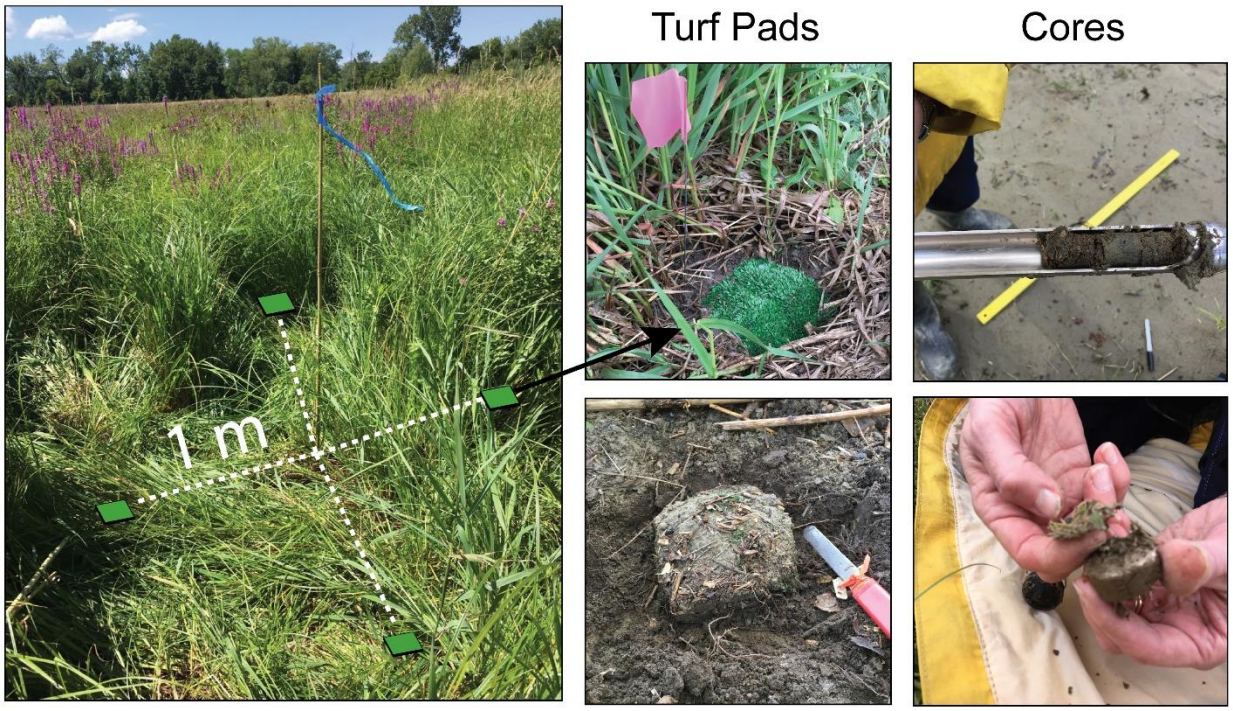

Figure 3. Floodplain monitoring plot design. A 6' bamboo pole at the center of each plot was used to identify the location of four 15 cm by 15 cm square artificial turf pads. Following flood events, we excavated each pad (bottom middle photo) to retrieve flood-deposited sediment and organics. Cores were collected following snowmelt floods in April 2019. We identified contacts between recent deposits and the previous ground surface.

Table 2. Summary of floodplain study sites

ID	Site Name	River	HUC8 Watershed	Drainage Area (km^2)	Channel Slope ($m\ m^{-1}$)	SSP ($W\ m^{-2}$)	# of cores	# of plots	Depths from Cores (m)[a]	Depths from Plots (m)[b]
1	**EPSCoR**	Trib to Hungerford Brook	Missisquoi	11	0.00170	5.0		3		0.3 (0.2-0.4)
2	**Black Creek #1**	Black Creek	Missisquoi	102	0.00020	4.5	1	2	0.7	1.3 (0.1-2.5)
3	**Black creek #2**	Black Creek	Missisquoi	129	0.00030	8.4	2	5	1.2 (0.6-1.7)	2.2 (0.6-7.0)
4	**Trout River**	Trout River	Missisquoi	212	0.00220	67.9		10		4.7 (0.1-10.5)
5	**North Troy**	Missisquoi	Missisquoi	352	0.00030	12.2	1	6	1.6	2.3 (0.2-5.3)
6	**Richford Farm**	Missisquoi	Missisquoi	1215	0.00090	64.6		6	1.4 (0.1-3.3)	3.3 (0.5-5.8)
7	**Enosburg Falls Farm**	Missisquoi	Missisquoi	1707	0.00001	0.8		10		4.3 (0.1-9.7)
8	**Atlas**	N. Branch Lamoille	Lamoille	33	0.00020	1.9		5		0.9 (0.1-2.0)
9	**Browns**	Browns	Lamoille	141	0.00180	43.7	5	9	2.6 (0.7-4.9)	4.9 (0.5-9.4)
10	**Wolcott**	Lamoille	Lamoille	401	0.00020	5.9		6	2.0 (0.2-3.3)	1.5 (0.1-4.9)
11	**Ryder**	Lamoille	Lamoille	601	0.00120	39.8		8		1.1 (0.1-3.5)
12	**Idletyme**	W. Branch Little River	Winooski	60	0.00630	137.0		3		1.3 (0.3-2.3)
13	**Dog River**[c]	Dog River	Winooski	135	0.00200	55.9	9		6.0 (2.8-11.4)	N/A
14	**Lareau**	Mad	Winooski	148	0.00170	37.2		4		2.6 (0.1-5.6)
15	**Dubois**[d]	Winooski	Winooski	1269	0.00020	35.4		10		N/A
16	**Jericho Settlers Farm**	Winooski	Winooski	2554	0.00020	15.9	10	10	2.3 (0.1-4.9)	1.9 (0.2-4.5)
17	**McKenzie Park**	Winooski	Winooski	2745	0.00004	3.4		9		1.8 (0.1-4.5)
18	**Cota**[e]	Lewis Creek	Lewis	48	0.00280	48.6	10	12		2.6 (0.1-5.4)
19	**Otter Creek WMA**	Otter Creek	Otter	162	0.00140	43.8		6		0.4 (0.1-0.7)
20	**Lemon Fair**	Lemon Fair	Otter	177	0.00005	0.8		9		0.6 (0.2-2.3)
21	**Saunders**[e,f]	New Haven	Otter	184	0.00510	83.4		8	1.7 (0.4-4.4)	5.0 (0.1-12.9)
22	**Adams**[g]	Otter Creek	Otter	947	0.00008	9.1	12	8	2.8 (1.3-5.8)	0
23	**Desmarais**[a,g]	Otter Creek	Otter	1209	0.00010	8.6	9	12	2.7 (0.1-5.6)	0
24	**Green Mountain College**	Poultney	Poultney	129	0.00330	62.5		9		0.4 (0.1-1.8)

a. interpreted to represent floods that occurred between Fall 2018 and April 15 2019
b. from monitoring plot data collected after November 1, 2019 flood unless where otherwise noted
c. sediment deposition from cores assuming bulk density of 1.23 g cm^{-2}. TP concentrations also measured from cores
d. site was not inundated during the study period
e. data also collected from monitoring plots following October 17, 2019 flood
f. data was also collected from monitoring plots following June 22, 2019 flood
g. monitoring plots were inundated during the study period but had no sediment

Task 4. Collect and process field data to develop floodplain deposition dataset.

Following floods, we sampled sediment deposited on floodplains and analyzed it for TP to develop a dataset of 1) plot-scale sediment and TP deposition rates (n=126) and 2) site-scale average annual TP deposition and efficiencies (n = 22).

Field data collection

Following flood events, field crews were deployed to those sites with suspected inundation. Once on site, crews re-located monitoring plots and noted evidence of inundation and sediment deposition. If artificial turf pads were buried under sediment, we triangulated their location using the bamboo pole and pin flags. If sediment was deposited on the turf pad, field crews excavated around the mat and noted deposition depths (Figure 3). To continue monitoring, clean turf pads were installed in a similar configuration. Flood-derived sediment and associated organics, along with the turf mat were placed in a labelled bag for transport to the University of Vermont for processing. During site visits, we noted maximum flood depths from the crest gage, measuring the cork strand lines from the ground and the top of the rebar. Crest-gages were then reset by pouring water to clean off the pipe and re-filling with fresh cork.

We also measured floodplain deposition during a limited field campaign carried out prior to the installation of monitoring plots. Following snowmelt floods in April 2019, we visited 9 sites with visible flood deposits, and collected cores along transects from the river using a 2 cm soil corer. At each sampling location, we collected an average of three cores, from which we identified the recent deposit depth using an indicator of the previous ground surface (eg., leaf litter, moss) along with a change in texture (Figure 3). Because interpretation of the core was sometimes difficult (i.e, multiple leaf litter layers), we only report on samples for which we had relatively high confidence in the contact. Once identified, we measured the depth of the recent deposit, separated it from the previous surface, and placed it in a labelled bag. Three cores collected at one sampling location were composited in the same bag. To compare sedimentation measurements from cores to those collected from turf pads, we collected three cores in proximity to seven monitoring plots during pad excavation following summer and fall 2019 floods.

Laboratory Analyses

Floodplain samples were dried in a 70 degree C oven at approximately 12-hour intervals, between which samples that appeared dry were weighed. When sample weights were within 5% of the previous weight, they were removed from the oven. Samples from monitoring plots were weighed with their turf pads. Turf pads were then removed, cleaned by shaking sediment loose, and weighed separately.

We analyzed floodplain deposits for TP concentration (TP_{conc}, mg kg^{1}) in the Agriculture and Environmental Testing Laboratory at the University of Vermont. First, samples from each pad were sieved to remove any gravel (> 2mm) and large sticks or leaves. Subsamples of approximately 7.5 ml (0.5 tablespoon) from two pads at each plot were then composited, ground and passed through a #35 (< 0.5 mm) sieve for TP analysis. Approximately 0.5 g of this composited, < 2 mm fraction was weighed to 0.001 g and digested using either a microwave-assisted (for samples analyzed prior to July 29, 2020) or hotblock-assisted procedure (EPA method 3051 or 3050, respectively). These two procedures are designed to produce the same results. A shift from the microwave-assisted digest (capacity 14 slots per run) to the hotblock-assisted digest (capacity 36 samples per run) was implemented in summer 2020 to allow for a larger capacity of sample processing per digest. Digests were analyzed for TP by ICP-OES (Avio 300, Perkin Elmer Corp., Norwalk, CT, USA).

Small differences in pad weights reflect differences in hand-cut pad size. To account for small differences in pad area, we precisely measured 36 pads (to the nearest mm) and regressed those dimensions with their weight (Appendix B). We applied this regression to the remaining samples to determine the area of the pad to calculate the sediment deposition per area (dep_{sed}, kg m^{-2}). Accounting for the TP_{conc} of the sample, we calculated the phosphorus deposition per area (dep_{TP}, g P m^{-2}).

Deposition Dataset

Flood events that inundated monitoring sites during the project varied considerably in their lateral extents, elevations, durations, and recurrence intervals. Additionally, for a given flood event, sediment deposition varied considerably at a given site, both across plots (e.g., inundating one or more plots at a given site) and within a given plot (e.g., inundating one or more pads comprising a plot). To compare deposition rates between sites and between plots we converted dep_{sed} and dep_{TP} averaged over all turf pads for each plot to annual sediment and phosphorus deposition rates ($dep_{sed,yr}$ in kg m^{-2} yr^{-1} and $dep_{TP,yr}$ in g P m^{-2} yr^{-1}) based on the event's recurrence interval. We identified flood recurrence intervals associated with each flood event using data from nearby stream gages, referenced to regional flood frequency curves (Olson, 2014). For our monitoring sites, and all stream gages within the Lake Champlain Basin in Vermont, we calculated site or gage coordinates, % of watershed water bodies/wetlands, and % of watershed at or above 1200 feet using the USGS StreamStats online application (streamstats.usgs.gov). These variables are important for describing variability in flood frequency in Vermont (Olson, 2014). Additionally, since the storm event that caused the November 1, 2019 flood impacted the full study area, we calculated the storm rainfall total for all sites/gages to use as an additional point of comparison. Daily precipitation totals for October 31 and November 1 were downloaded from the National Weather Service (https://water.weather.gov/precip/). We identified relationships between location, watershed characteristics, or precipitation totals (for the November 1 flood) and the recurrence interval at nearby gages and applied these relationships to predict the recurrence interval associated with each flood that impacted each site during the study period (see Appendix C). Most sites were impacted by only one flood event that resulted in measurable sediment deposition: the November 1, 2019 event. Therefore, for most of the plots, sediment and TP deposition rates were calculated from this one event. Multiple inundating flood events at two sites (Saunders and Cota) resulted in two to three measures of annual deposition rates for thirteen plots. For these plots, we averaged the resulting annual deposition rates derived from each flood event.

To evaluate the feasibility of including deposition rates from cores and turf mat plots in the same dataset, we compared rates for the seven plots which had concurrent measurements using both cores and pads. Depths measured from cores were converted to mass of deposited sediment, by applying a bulk density of 1.23 g cm^{-3}, the average value from pads, measured as average pad depth divided by average dry mass. We did not get reliable measures of bulk density from cores. Cores overestimated $dep_{TP,yr}$ by 12%, on average (-34% to 32%; See Section 4 for more details). Because of differences between the two methods, we did not use rates derived from cores in the detailed plot-scale analyses. However, we identified two opportunities to use $dep_{TP,yr}$ calculated from cores to estimate site-average values, where deposition rates were not available from monitoring plots. The Dog River and Desmarais sites had relatively good spatial coverage and high confidence in identification of the flood surface contact. To account for the average overestimation of $dep_{TP,yr}$ by cores, we decreased rates for the Dog River and Desmarais sites by 12%. For these two sites, we added the recurrence intervals together of all likely inundating floods that occurred prior to data collection, following leaf-off of the previous year. For example, at the Dog River site, two flood events occurred between leaf off in Fall 2018 and data collection on April 25, 2019; a 4.2 yr and 7.5 yr flood. Thus, we divided the average TP deposition at the site, in g m^{-2} by 11.7 yr.

To build the dataset of site-average $dep_{TP,yr}$, we interpolated between plots to create a spatial average for the study site floodplain. We defined the study area to include the portion of the floodplain that was no greater than 2 channel widths away from the channel bank, and whose morphologic and land cover characteristics were captured by the monitoring plots. Relationships between distance from the channel or relative elevation above the channel (i.e., HAND elevation), and in limited cases *DivAng* (see below for variable definition) and landcover types and $dep_{sed,yr}$ and TP_{conc} were developed for each site (See Appendix D for details on each site). These relationships were then used to create surfaces of $dep_{sed,yr}$ and TP_{conc}, and as a result, $dep_{TP,yr}$ within the study area. Spatially-averaged phosphorus deposition rates were translated to annual floodplain phosphorus deposition, per meter length of stream ($dep_{TP,yr,2ch}$ g P m^{-1} yr^{-1}). To calculate $dep_{TP,yr,2ch}$ we divided $dep_{TP,yr}$ by 2 x channel width, or the one-sided floodplain width (based on the 100-yr flood, see below), whichever was smaller. We also converted $dep_{TP,yr,2ch}$ into an annual efficiency, defined as the proportion of the annual river load of TP captured by the floodplain. We identified a site's TP load per length of stream (kg m^{-1} yr^{-1}) for the associated HUC12 from the VT DEC's Clean Water Roadmap Tool (https://anrweb.vt.gov/DEC/CWR/CWR-tool) and divide the TP load by the length of stream with a drainage area >25 km^2 within the HUC12.

Task 5. Identify variables important for TP deposition

From an examination of the peer-reviewed literature, we identified seventeen variables, associated with eight general physical metrics that may describe variability in TP deposition on floodplains (Table 3). All variables may be calculated using existing geospatial datasets, to enable extrapolation from the existing study sites. For each of the 24 floodplain sites, we calculated eleven variables describing watershed and reach characteristics. At the 170 monitoring plots, we calculated an additional six variables that describe the local physical characteristics. We then identified the importance of the physical metrics on TP deposition by looking for statistical significance in bivariate relationships with $dep_{sed,yr}$, TP_{conc}, $dep_{TP,yr}$, $dep_{TP,yr,2ch}$, and efficiency. See Appendix E for a list of all variables referenced in this report.

Variable Calculations

A shapefile of the watershed upstream of each site was first created in USGS's StreamStats (http://streamstats.usgs.gov) and used to quantify drainage area (km^2) and the land use, land cover, soils, and geology using 2016 Vermont-specific land cover layers (https://geodata.vermont.gov/pages/land-cover) and the soils layer (SSURGO) attributed with the NRCS TOP20 soils data available for the State of Vermont (https://geodata.vermont.gov/datasets/vt-data-nrcs-top20-soils-attributes-and-documentation). Bankfull channel width and channel slope (S_{CH}) were measured from high resolution (1-meter) LiDAR-derived DEMs. An average bankfull channel width was measured along the length of the study site, calculated as the bankfull channel area defined by the extent of the top of banks divided by stream length. Specific stream power (*SSP*) was calculated as the product of the two-year flood peak discharge (m^3 s^{-1}) derived from the USGS's StreamStats application (streamstats.usgs.gov), S_{CH}, and the unit weight of water (9800 N m^{-3}), divided by bankfull channel width. Floodplain width (W_{FP}) was calculated at each transect of plots as the width of the 50th percentile 100-yr map, from Task 2. To identify the ratio between inset floodplain height and bankfull height at each site, or incision ratio (IR), we used the field-measured IR reported in the VTANR Stream Geomorphic Assessment database for streams that have a phase 2 geomorphic assessment (Kline et al., 2009; https://anrweb.vt.gov/DEC/SGA/). Otherwise, we measured IR from profiles taken from the DEMs within the study area. We calculated angle between channel and floodplain flow (*DivAng*) after Czuba et al (2019), where channels that flow straight downvalley are assigned values of zero; negative values are indicative of divergent flow and positive values indicate convergent flow.

Tree cover (X_{tree}), calculated as a percent of canopy coverage, was calculated within a 10m radius of each plot, and for the full floodplain site using 0.5-m resolution land cover datasets from the State of Vermont (geodata.vermont.gov). The distance of the plot to the channel bank (*D*) was measured as the straight-line distance. Relative elevation above the channel (*HAND*) and annual probability of inundation (*Inun*) were identified from probHAND and floodplain maps, respectively, developed in Task 2. To identify a single *Inun* value from the probabilistic maps, we made a single composite map, created by calculating the annual probability of inundation on a cell-by-cell basis. The annual probability of inundation of any given cell was calculated as:

$$Inun_{cell} = \sum_{RI=2}^{500} \frac{\frac{1}{RI} \times Prob_{RI}}{\sum Prob_{RI}}$$

where *RI* is the recurrence interval of a modeled flood (for each of the RI's modeled: 2, 5, 10, 25, 50, 100, 200, and 500) and *ProbRI* is the highest probability that the given cell will be inundated by that associated flood. Because we did not model floods that occur more frequently than once every 2 years (*RI* < 2), and many of our plots were located in areas that are typically inundated every year, we assigned a value of "1.0" to sites that had a 95% probability of being inundated by the 2-year flood.

Table 3. Physical attributes calculated for all sites and plots.

Metrics	Variables		Citations	Study Range		
				median	min.	max.
WATERSHED						
CONTRIBUTING AREA	drainage area (km^2)	*DA*	Church 2002; Macnab et al. 2006	170	4	2745
LAND USE AND LAND COVER	% area watershed in agriculture	WS_{AG}	Mcmillan and Noe 2017; Noe and Hupp 2005; Owens et al 2001; Ross et al 2008	8	0.3	47
	% area watershed impervious cover	WS_{IMP}		1.4	0.5	2.5
	% area watershed wetland	WS_{WET}		7	3	17
SOILS AND GEOLOGY	% area watershed glaciolacustrine	WS_{HSGD}	Gellis et al. 2008; Norton and Fisher 2000	2.4	0.1	62
	% area watershedhydrologic soils group D	WS_{GL}		54	26	84
REACH						
ENERGY REGIME	specific stream power (W m^{-2})	*SSP*	Jain et al. 2008; Swinnen et al. 2020	17	0.4	86
CHANNEL & FLOODPLAIN MORPHOLOGY	floodplain width (m)*	W_{FP}	Czuba et al. 2019; Hupp et al. 2013 and 2015;Mcmillan and Noe 2017; Noe and Hupp 2009; Schenk et al. 2013	151	12	1266
	floodplain width/channel width (m/m)[a]	$W_{FP/CH}$		5.6	0.7	33
	incision measured as ratio of inset bench to bankfull depth (m/m)	*IR*		1.2	1	1.9
	channel slope (m/m)	S_{CH}		0.001	0.00001	0.006
LOCAL						
LAND COVER	% area within 10 m radius with tree canopy[b]	X_{tree}	Gordon et al 2020; Olde Ventenrink et al. 2006	30	4	94
HYDRAULIC CHARACTERISTICS	angle between channel and floodplain flow (degree)	*DivAng*	Asselman and Middlekoop 1995; Bannister et al 2015; Czuba et al. 2019; Hupp and Bazemore 1993; Walling et al., 1999	0	-73	130
	distance from plot to channel bank (m)	*D*		15	0.1	101
	distance from plot to channel bank/channel width (m/m)	D_{CH}		0.5	0.01	4.8
	relative elevation above the channel (m)	*HAND*		1.7	0.1	3.7
HYDROLOGIC CONNECTIVITY	annual probability of inundation	*Inun*	Kleiss 1996; Pizzuto et al 2016; Renshaw et al 2014	0.5	0.01	1

a. calculated average value for site and differentiated values for each plot
b. calculated average around plots and for site

Bivariate Relationships

Bivariate relationships between physical metrics and measures of TP deposition were tested using Spearman's rank correlation. At the plot-scale we tested the importance of local metrics on three response variables: $dep_{sed,yr}$ (kg m^{-2} yr^{-1}), TP_{conc} (mg kg^{-1}), and $dep_{TP,yr}$ (g P m^{-2} yr^{-1}). At the site-scale we tested the importance of watershed and reach metrics on a floodplain's $dep_{TP,yr,2ch}$ (kg P m^{-1} yr^{-1}) and efficiency (% of yield). Correlations were determined to be significant at $\alpha<0.05$, but we also highlight variables with $\alpha < 0.10$.

Task 6. Develop models for prioritizing and quantifying impact of floodplain restoration

We developed a framework to prioritize floodplain restoration sites and assist with Lake Champlain Basin planning using statistical models that describe functional relationships between physical attributes and TP deposition. To build the framework we exploited the strengths of two statistical approaches, generalized linear models and boosted regression tree models. We describe these two modelling approaches, their application to TP deposition at multiple scales, and how they may be used to achieve two goals 1) prioritize where in a watershed to work, referred to as the ***prioritization function*** and 2) approximate the effect of restoration, protection, or enhancement intervention's on TP deposition, referred to as the ***intervention function***.

Generalized Linear Models

Generalized linear models (GLMs) are easy to interpret and provide insight into general trends between multiple predictors and response variables. We use GLMs to describe the magnitude and direction of change in TP deposition rates in response to changes to watershed, reach, and local variables across spatial scales. We build models to describe spatial trends in TP deposition rates 1) through a watershed and 2) across a floodplain.

From site-average values, we identified the best models to describe 1) $dep_{TP,yr,2ch}$ 2) the associated efficiency. We constructed 38 alternative models, using combinations of non-correlated variables (correlation coefficient < 0.4). We tested models for multicollinearity, removing variables with variance inflation factors greater than 10 (Hair et al., 1995). Because geomorphic thresholds are important for determining the production, transport, and storage of sediment (Church, 2002; Jain et al., 2008), we also hypothesize that functional relationships differ based on energy regime. To test this hypothesis, we included specific stream power in our analysis as a categorical variable, differentiating sites based on a specific stream power threshold of 10 W m^{-2} (low energy cohesive floodplains vs medium energy non-cohesive floodplains; Nanson and Croke 1992; Figure 2).

From plot-scale values, we identified the best models to describe $dep_{TP,yr}$. Thirty-five candidate models were constructed from local metrics, using combinations of non-correlated variables (correlation coefficient < 0.4), removing variables with variance inflation factors greater than 10. To account for variability in TP deposition rates as a function of watershed or reach-scale factors we included the site-average $dep_{TP,yr}$ in each candidate model.

Models were ranked based on lowest Akaike Information Criteria (AIC) score and highest Akaike weights. The AIC is a measure of the parsimony of models based on a trade-off between deviance reduction and the number of parameters fitted in the model. The model with the lowest AIC value and those with $\Delta AIC < 2$, are considered to have substantial empirical support (Burnham and Anderson, 2002). In selecting models for use in the restoration framework, we also considered other factors including the applicability of the model to certain settings. For reference we also report on the top model's R^2 value, but do not use this value for model selection.

Boosted Regression Tree Models

We use boosted regression trees (BRT) to evaluate $dep_{TP,yr}$ at the plot scale. These types of models can estimate complex nonlinear relationships and inherently consider interactions among predictors (Elith et al., 2008). Additionally, BRTs provide a platform to evaluate the importance of physical attributes over multiple scales on TP deposition rates within one model.

Boosted regression trees combine regression trees with boosted machine learning to adaptively improve model performance (Elith et al., 2008). The boosting technique builds hundreds to thousands of statistical trees that iteratively fit the residuals of prior trees. As a result, BRTs provide an estimate of the relative importance of each predictor variable to explain variation in the dependent variable and partial dependence plots that visualize the effect of each predictor variable after accounting for the average effects of all other variables in the model. The relative influence of predictor variables is based on the number of times that variable is selected for splitting (e.g., added to the model), weighted by the squared improvement to the model resulting from each split, and averaged over all trees.

We evaluated the best predictors of TP deposition rate using the DISMO package in R (Hijmans et al., 2015) following the guidelines of Elith et al. (2008). Because of a relatively low sample size (n = 126), we lowered the default bag fraction of 0.5 to 0.65, where 65% of the sample drawn at random, without replacement, from the full training set at each iteration. Tree complexity and learning rate were optimized based on model predictive performance during validation using cross-validation. After initial model calibration with all predictors (Table 3), subsequent model simplification successively dropped those parameters that contributed the least to total error prediction. Once all predictors had more than 3% relative influence, we then removed the correlated predictors (correlation coefficient>0.4) with the lower influence to prevent over-fitting of the model. As an exception, we chose the relative distance from the channel (D_{ch}) over the absolute distance (D) so that the model was more informative of processes that occur across a range of spatial scales.

Application of Floodplain Restoration Framework

The resulting statistical models were used to define the floodplain restoration framework for the Lake Champlain Basin. We use evidence from both the GLM and BRT models to identify watershed-scale trends for prioritization, termed the prioritization function, and local relationships to evaluate the impact of interventions, termed the intervention function, on phosphorus deposition.

To determine where in the watershed stakeholders should prioritize efforts, the framework considers predictions from the top GLMs for $dep_{TP,yr,2ch}$. To calculate phosphorus deposition rates through the Mad River Watershed, we applied top site-scale GLMs to segments of river defined by stream geomorphic assessment (SGA) reach breaks The model is applied to segments of river defined by stream geomorphic assessment (SGA) reach breaks (http://anrgeodata.vermont.gov/datasets) with a drainage area greater than 25 km^2 (21 reaches; 55 km) and with slope-drainage area values that fall within the “likely depositional” range (Figure 2). Predicted values are classified based on quartiles of the resulting range of values. We demonstrate application of the prioritization function of the floodplain restoration framework in the Mad River Watershed (DA = 373 km^2; median slope = 0.007) in the headwaters of the Winooski River Basin (Figure 1).

To evaluate the impact of restoration interventions on phosphorus deposition, the framework considers predictions from the top GLMs and BRT model for $dep_{TP,yr}$ applied to both existing and proposed topographic and land cover conditions. Because the GLM includes $dep_{TP,yr,2ch}$ as an input, we use output from the $dep_{TP,yr,2ch}$ GLM. We demonstrated application of the intervention function of the floodplain restoration framework at two floodplains in the Lake Champlain Basin;

Potash Brook and the Mad River (Figure 1) and report on total site TP deposition for existing and proposed conditions.

An approximately 0.5-acre area of floodplain along Potash Brook, south of Burlington, Vermont is under consideration for restoration. Reducing floodplain elevations by ~0.5 meter will increase the sites hydrologic connectivity, increasing its frequency of inundation from once every 100-years to once every 2-years (Fitzgerald 2020). We used the Potash Brook floodplain as a test of the application of our framework to settings that are likely to store sediment over the long term, but for which some physical attributes are out of the range of those measured in our study. In particular, Potash Brook has a relatively steep channel slope (0.012 m/m) through the study area and is located within a highly urbanized watershed; impervious surfaces comprise 22% of the contributing area. We also explored the impact of creating a floodplain bench along ~340 m of the Mad River, in Waitsfield, Vermont. Lowering a 2.7-acre area of hydrologically-disconnected floodplain in Couples Field by an average of 1.5 meters would increase the frequency of inundation from an average of once every 25 years to once every 4 years at the floodplain bench. For both scenarios, we also evaluated the additional impact of revegetation, resulting in 100% canopy cover, on phosphorus deposition rates.

4 Quality Assurance Tasks Completed

All data presented in this report were reviewed by the UVM Project and UVM QA Managers for logical consistency and coding errors. Quality assurance protocols, as described in the project QAPP, were followed including: (1) sample documentation and handling, (2) quality acceptance criteria for field samples, (3) quality acceptance criteria for laboratory samples, (4) inspection and correction, where necessary, of digital data files, (5) proper data archiving and back up, and (6) documentation of secondary data used for analysis. Details on these measures are described below. Dr. Beverley Wemple served as the Quality Assurance manager with primary responsibility of oversight of sample handling and along with Dr. Don Ross, oversight of laboratory procedures. Dr. Rebecca Diehl served as Project Manager and maintained oversight of collection and archiving of floodplain mapping and deposition data and secondary data.

1. Sample Documentation and Handling

Sediment samples collected from turf pads and cores were placed in a polyethylene bags and labelled with the date, site, plot (or core) number, and measured depths. At the time of collection, notes were entered into ESRI's Collector for ArcGIS (referred to as Collector) using pre-made forms. Creation of a new observation automatically associates field notes with a GPS location. Photos were taken in Collector and automatically attached to the appropriate entry. For the few instances where access to Collector was not possible, we entered data into a field notebook and used a handheld GPS. Data in Collector is automatically backed up through the cellular network. In the office, we downloaded all features from Collector and manually entered values from field notebooks.

Field samples were delivered either to the Wemple Lab or to the Agricultural and Environmental Testing Laboratory (AETL) at the University of Vermont and organized and stored in boxes. A unique sample number was assigned to each sample bag and entered into a master spreadsheet stored on Microsoft Teams. Within 90 days of collection, most samples were dried and weighed, and values were recorded. If they were stored in the Wemple Lab, they were transferred to the AETL for sample preparation and analysis of total phosphorus. Field work restrictions and limited access to the AETL laboratory between March and June 2020, associated with COVID restrictions, limited processing of data collected at all pads. Initially, we prioritized processing two pads from each plot, and in the end were able to dry and weigh 97% of the pads, with TP analysis conducted on two pads per plot as described above (Task 4).

2. Quality Acceptance Criteria for Field Samples

High spatial variability in deposition depths prevents us from evaluating field sample collection precision. Four duplicate turf mats placed in a single plot allows for measurement of spatial variability within a single sampling location. Individual turf pad and averaged plot measurements are provided in Appendix B.

Cores collected within monitoring plots following floods in the summer and fall 2019, provide estimates of differences between the two methods (Table 4). Depth estimates from cores are as much as 90% less (average of 26% less) than those measured from turf pads. Translated to mass, cores overestimated sediment deposition rates by an average of 20% (using turf pad dataset average of 1.23 g m^{-3}). For the majority of comparisons, total phosphorus concentrations measured from cores were within 10% of that measured from turf pads; 3 cores underestimated TP concentrations by an average of 23%. As a result, phosphorus deposition measured from cores was overestimated by 12% on average (-32% to 34%) compared to estimates from turf pads, because of uncertainties in bulk densities and spatial variability in depths not adequately captured by cores. We determined that the uncertainties in translating cores to phosphorus deposition rates were too great to combine cores and turf pads in the same plot-scale dataset. However, as described in Section 3, at two sites with high confidence in the core's contact, we calculated spatial averages of phosphorus deposition, correcting site-average values by 12%.

Table 4. Comparison of results for samples collected concurrently from turf pads and cores.

Site	Plot	Flood Date	Core				Turf Pads				% Difference Core			
			Depth (cm)	dep_{sed} (g cm^{-2})	TP_{conc} (mg kg^{-1})	dep_{TP} (g P m^{-2})	Depth (cm)	dep_{sed} (g cm^{-2})	TP_{conc} (mg kg^{-1})	dep_{TP} (g P m^{-2})	Depth	dep_{sed}	TP_{conc}	dep_{TP}
Cota	Plot 6	2019-Nov-01	5.1	6.2	725.4	45.2	4.7	4.4	759.2	33.7	7%	29%	-5%	25%
Idletyme	Plot 2	2019-Nov-01	2.1	2.6	766.4	19.8	2.3	2.1	730.8	15.3	-11%	19%	5%	23%
Jericho Settlers Farm	Plot 2	2019-Nov-01	1.8	2.3	804.4	18.1	2.2	1.6	754.4	11.9	-20%	30%	6%	34%
Lareau	Plot 2	2019-Nov-01	3.0	3.6	822.4	30.0	4.0	3.5	984.7	34.2	-34%	5%	-20%	-14%
Saunders	Plot 5	2019-Nov-01	1.7	2.1	575.7	12.3	3.3	2.2	732.6	16.2	-90%	-4%	-27%	-32%
Saunders	Plot 3	2019-Oct-22	2.5	3.0	575.8	17.5	2.3	1.7	699.2	11.8	6%	44%	-21%	32%
Wolcott	Plot 1	2019-Nov-01	1.7	2.1	511.1	10.5	2.4	1.7	510.3	8.8	-42%	16%	0%	16%

3. Quality Acceptance Criteria for Laboratory Samples

Quality acceptance for all samples processed in the laboratory for TP concentration was assessed through review of quality control standards, recovery of a reference sample, and results of duplicates processed with each run (Appendix F). QC standards fell within acceptable limits (5-10% or less of known values) when averaged for each run, and all laboratory blanks were below the 0.1 mg/L minimum detection level. Recovery of the NAPT reference soil averaged 95.8% across all runs. For the 36 samples run in duplicate, percent error ranged from 0.2 to 6.5 with an average of 2.6% across all duplicates. Based on these outcomes, we accepted all laboratory results and used them in the analysis provided in this report.

4. Inspection and Correction of Digital Files

Floodplain maps created with the probHAND model were compared to those generated from the calibrated and FEMA-approved 1D HEC-RAS model for the Mad River Valley (DuBois and King, 2017). For the 50th percentile maps, F-statistics (% conforming wet cells between models) ranged from 0.61 to 0.82, averaging 0.74 for the 3 HUC12's of the Mad River. The F-statistic is a more robust measure of model agreement than the kappa statistic, which is very sensitive to the choice of the model domain extent (Afshari et al., 2018). Our F-statistic values exceed those calculated by Afshari et al. (2018) in a similar study, whose kappa statistics ranged between 0.91 and 0.95. Thus, we deemed our floodplain mapping approach to be well-calibrated.

Sediment depths and plot and site names for sediment samples in the master database were checked against field notes and sample bags multiple times during sample handling, processing, and analysis. Inconsistencies among the data sources were noted and immediately corrected. The deposition datasets were scanned for completeness and accuracy.

GPS point plot locations were inspected for spatial accuracy relative to other plots and location on floodplain using air photos and LiDAR-derived DEMs available through the Vermont Center for Geographic Information. All data points were deemed acceptable (at least a horizontal position error of 5 meters and most less than 1 meter) and are archived as part of this dataset.

5. Data Archiving and Backup

Field and laboratory data files were created and shared on mobile platforms (ArcGIS online and Microsoft Teams) and downloaded regularly to a shared network drive on the UVM central computing network. UVM maintains a weekly network backup. Upon completion of this project and delivery of the final report, all project data files will be maintained on the UVM network for a period of no less than two years.

A copy of primary data files generated for this project will be delivered with the final report and will include metadata files with variable descriptions. All spatial data files will be provided in Vermont State Plane coordinates. Northing and easting coordinates of plots, cores, and sites are provided in Appendix B.

6. Documentation of Secondary Data

Four types of secondary data were used in the analysis completed for this report: 1) spatial data accessed from the Vermont Center for Geographic Information (VCGI), 2) USGS StreamStats data, 3) stream flow data from the US Geological Survey gaging stations in the Lake Champlain Basin, 4) precipitation records from the National Weather Service, 5) Vermont DEC Data, and 6) additional geospatial datasets from Milone & MacBroom, Inc. and Fitzgerald Environmental. Associates, LLC.

Within the text, we indicate which spatial datasets were downloaded from VCGI, and provide a link. The USGS's StreamStats application is well-documented (streamstats.usgs.gov). For Vermont, regional flood frequency regressions are based on Olson (2014). Peak stream flow values for each flood event were identified for gages in the study area. We provide gage names, links to gage websites, and flood frequency relationships in Appendix C. The data access link for precipitation data from the National Weather Service is provided in the text.

Vermont ANR data sources are documented within the text. We provide links to the SGA data as well as the Vermont Clean Water Roadmap tool within the text. For the additional geospatial datasets, we provide links to documents describing the data.

5 Deliverables Completed

Task 2. Develop and execute procedure that identifies floodplains, and their level of hydrologic connectivity.

Application of the probHAND model to the Vermont's Lake Champlain Basin HUC12 watersheds resulted in probabilistic floodplain maps for floods with 2-, 5-, 10-, 25-, 50-, 100-, 200-, and 500-year recurrence intervals along more than 2,000 km of stream. These maps will be available for public download.

Task 3. Establish floodplain monitoring network.

We determined that 82% of the streams in the Vermont portion of the Lake Champlain Basin whose drainage area is greater than 25 km^2 (10 mi^2) are likely to be depositional over the long-term (i.e., below the gray line in Figure 2). Along these streams, we identified 24 floodplain monitoring sites that had a total of 170 monitoring plots. We note that one site, EPSCoR is on a stream with a drainage area less than 25 km^2. We chose this site because it is a long-term study site for EPSCoR-focused research activities at UVM. Additionally, we collected floodplain cores from 9 floodplain sites (8 also had monitoring plots), two of which were of sufficient quality and coverage, and provided new information to the dataset, to provide for site-average values. The 24 study sites ranged in slope from 0.00001 to 0.006 m/m with drainage areas between 11 and 2750 km^2, corresponding to channel-adjacent specific stream power values between 0.8 and 137 W m^{-2} (Table 3; Figure 2).

Task 4. Collect and process field data to develop floodplain deposition dataset.

In 2019, we documented floodplain deposition on monitoring plots from three discrete flood events, whose recurrence interval ranged from 1.5-yr to 130-yr recurrence (

Table 5). No inundating flood events occurred in 2020. Of the 170 plots established, 152 were inundated by one or more floods, and sediment was deposited on 123. Of the remaining inundated plots, we noted erosion around 3, 6 were not recovered because of scour or excessive deposition, and 20 had no evidence of deposition or scour. All 123 plots collected for sediment had floodplain deposition measurements collected following widespread flooding on November 1, 2019; 13 of the plots have additional observations from June 22 and/or October 17, 2019. We note that we included the three erosional plots in the dataset, assigning "0" to their deposition rate. We also documented floodplain deposition from an additional two to three floods, which occurred in the winter and spring of 2018/2019 identified as a composite layer from floodplain cores. Following snowmelt floods that peaked around April 15, 2019, we collected 59 cores from 9 sites. Most crest gages performed poorly and uncertainties in cork strand line interpretation prevented us from adopting their observations into our analyses. We provide the full dataset of measurements collected at each turf pad, within each plot, and for cores (Appendix B).

Table 5. Site-averaged phosphorus deposition rate and efficiency.

Site	TP Deposition ($g\ m^{-1}\ yr^{-1}$)	Efficiency[a]	RI of Documented Floods (yrs)[b]
EPSCoR	3.4	2.4%	26
Black Creek #1	6.2	2.5%	31
Black Creek #2	14.3	2.9%	31
Trout River	31.5	32.2%	79
North Troy	3.8	2.1%	130
Richford Farm	58.3	9.5%	29
Enosburg Falls Farm	56.7	22.3%	28
Atlas	0.6	0.8%	126
Browns	161.4	163.9%	8.8
Wolcott	7.9	9.9%	21
Ryder	7.1	4.7%	30
Idletyme	15.0	7.0%	9.1
Dog River[e]	63.1	16.1%	*4.2, 7.5*
Lareau	135.6	42.0%	6.7
Jericho Settlers Farm	83.8	82.0%	6.3
McKenzie	95.0	110.4%	6.5
Cota[c]	73.7	62.4%	1.7, 7.6
Otter Creek WMA	79.7	52.2%	1.6
Lemon Fair	24.9	6.2%	3.7
Saunders[d]	130.7	44.2%	3.4, 8.1, 21.3
Desmarais[e]	59.7	54.2%	*2.3, 3.5, 9.6*, 1.5
Green Mountain College	59.0	49.2%	1.4

a. Relative to annual loads in the associated HUC12
b. Italicized values represent flood events captured by floodplain cores
c. Measured deposition following two flood events; values are average rates
d. Measured deposition following three flood events; values are average rates
e. Measured values; not adjusted by 12% to account for differences in methodology

Deposition depths in the turf pad dataset averaged 2.4 cm (median 1.2 cm) and translated to average dep_{sed} of 1.63 g cm^{-2} (median 1.03 g cm^{-2}). Samples from pads had average TP_{conc} values of 752 mg kg^{-1} (median 724 mg kf^{-1}). Deposition depths in the core dataset averaged 2.6 cm (median 2.1 cm) and translated to average dep_{sed} of 3.25 g cm^{-2} (median 2.6 g cm^{-2}). Samples from cores had average TP_{conc} of 620 mg kg^{-1} (median 572 mg kg^{-1}). Comparison of samples concurrently collected using the two methods (turf pads and cores) indicated that dep_{sed} is greater when measured by cores (average of 20% greater than plot-derived values), and TP_{conc} are less (average 9% less than plot-derived values; Table 4). We attribute this over-estimation of dep_{sed} by cores to a variety of factors including the imprecision of depth measurements, selective sampling of cores typically targeting thicker deposits, and uncertainties with identification of contacts. Under-estimation of TP_{conc} in core samples may result, in part, from more regular inclusion of organic matter in plot-derived data than from cores, as TP has been found to be positively correlated to percent organics (Burt et al., 2002).

Deposition rates were highly variable among turf pads within a given plot. Differences in deposition rates were, on average, 3 to 4 times greater between the pad with the most and least amount of sediment. However, the median is closer to 1 to 2 times greater, skewed by plots with extremely high local variability. We documented as much as a two order of magnitude difference in deposition rates at two plots, where sand waves travelled through (Appendix B).

Spatially-averaged $dep_{sed,yr}$ for each site described most of the variability (94%) in spatially-averaged $dep_{TP,yr}$ (Figure 4). Slight differences in the trend may be attributed to TP_{conc} that are much larger (i.e., > 1000 mg kg^{-1}; Lemon Fair and EpSCOR) or much smaller (i.e., < 500 mg kg^{-1};

Dog River). Spatially-averaged $dep_{TP,yr}$ are, on average 14% less than averages of plots for a site (range from -68% to 40%), suggesting that at some sites, the placement of our plots was not fully representative of the topographic or hydraulic variability.

Annual floodplain phosphorus deposition within 2 channel widths ($dep_{TP,yr,2ch}$) varied greatly amongst the 22 sites included in the deposition dataset ranging from less than 1.0 g P m^{-1} yr^{-1} to more than 100 g P m^{-1} yr^{-1} (

Table 5). Floodplain deposition generally scaled with efficiencies; where deposition was less than 1.0 g P m^{-1} yr^{-1}, the floodplain was less than 1% efficient at capturing the annual phosphorus load and where deposition was greatest (161 g P m^{-1} yr^{-1}), efficiency exceeded 100%. Low efficiencies compared to deposition rates (e.g., Lareau and Richford Farm) indicated high TP loads within the HUC12, per meter of stream.

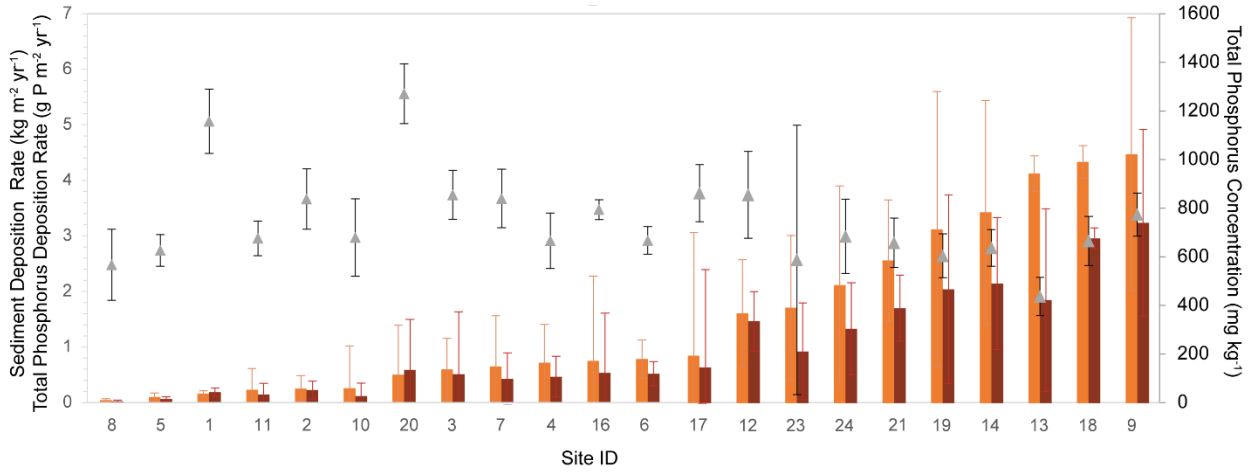

Figure 4. Spatially averaged deposition for 22 sites. Phosphorus deposition rates (red bars) scale to sediment deposition rates (orange bars), and only vary where TP concentrations (gray triangles) are very high or very low. Sites listed in order of increasing sediment deposition rates and are associated with their ID (see Table 2).

Task 5. Identify variables important for TP deposition

Values associated with each of the 22 sites in the dataset (for watershed- and reach-scale metrics) or 126 plots (local-scale metrics) capture large environmental gradients and are representative of many of types of depositional settings in the Lake Champlain Basin (Table 3). We note, however, that some physical attributes associated with depositional floodplains in the Lake Champlain Basin do fall outside the range of values calculated. Our sites are located in watersheds with relatively low percentage of impervious surfaces; all sites have less than 2.5% impervious cover. Undeveloped watersheds are common in the Lake Champlain Basin, VT (median HUC12 % impervious is 2.1), but in urban settings, these values can exceed 10%. Additionally, to assure inundation during the short study period, our plots are located relatively close to the channel, (the majority of plots within a half of a channel width), have high probabilities of inundation (more than half are inundated at least once every 2 years), and relatively low incision ratios. Yet many floodplains in the Lake Champlain Basin are much less frequently inundated (Kline and Cahoon, 2010).

From the site-scale dataset, we found that the percent watershed impervious area (WS_{IMP}) and the *SSP* were positively correlated with $dep_{TP,yr,2ch}$ while percent watershed in wetland (WS_{WET})

was negatively correlated (Table 6). Efficiency was positively correlated with drainage area (DA), WSI_{MP}, and floodplain width (W_{FP}), and negatively with percent watershed glaciolacustrine (WS_{GL}). The plot's distance and its inundation probability *Inun*, were correlated with $dep_{sed,yr}$ and $dep_{TP,yr}$ (Table 7). Deposition rates decreased with increasing distance from the channel and increased with increasing probability.

Table 6. Correlations between watershed and reach attributes and site-scale phosphorus deposition. Shown are Spearman rank correlation coefficients; bold values indicate significant correlation at $\alpha = 0.05$, italicised values are significant at $\alpha = 0.10$.

	TP Deposition ($g\ P\ m^{-1}\ yr^{-1}$)	Efficiency
WATERSHED		
Drainage Area (km2)	0.31	*0.38*
Impervious Cover (%)	*0.36*	*0.37*
Agriculture (%)	-0.35	-0.28
Wetland (%)	*-0.37*	-0.25
Hydrologic Soils Group D (%)	-0.06	-0.18
Glaciolacustrine (%)	-0.34	*-0.38*
REACH		
Specific Stream Power ($W\ m^{-2}$)	*0.38*	0.31
Floodplain Width (m)	0.28	*0.38*
Floodplain Width/Channel Width (m/m)	0.05	0.18
Tree Cover (%)	0.03	0.03
Channel Slope (m/m)	0.23	0.14
Incision Ratio (m/m)	0.04	-0.08

Table 7. Correlations between local attributes and plot-scale TP concentration and sediment and phosphorus deposition rates. Shown are Spearman rank correlation coefficients; bold values indicate significant correlation at $\alpha = 0.05$, italicised values are significant at $\alpha = 0.10$.

	TP Concentration ($mg\ kg^{-1}$)	Sediment Deposition Rate ($kg\ m^{-2}\ yr^{-1}$)	TP Deposition Rate ($g\ P\ m^{-2}\ yr^{-1}$)
LOCAL			
Floodplain Width (m)	-0.03	0.13	0.12
Floodplain Width/Channel Width (m/m)	0.11	0.13	0.14
Tree Cover (%)	-0.08	0.00	-0.02
Flow Divergence Angle (degrees)	*0.16*	0.10	0.12
Distance from channel (m)	0.11	**-0.24**	**-0.23**
Distance from Channel/Channel Width (m/m)	0.14	**-0.29**	**-0.26**
Elevation above the Channel (m)	-0.09	-0.08	-0.10
Inundation Probability	0.15	**0.24**	**0.27**

Task 6. Develop models for prioritizing and quantifying impact of floodplain restoration

Results and Interpretation of Statistical Models

The best GLMs predicting $dep_{TP,yr,2ch}$ and efficiency through the watershed have drainage area (*DA*), incision ratio (*IR*), % watershed impervious (WS_{IMP}), floodplain width divided by channel width ($W_{FP/CH}$), % watershed wetland (WS_{WET}),% watershed glaciolacustrine (WS_{GL}), or % watershed agriculture (WS_{AG}) (Table 8; see Appendix G for all models). The relationship between

DA and TP deposition rates differs for low and medium energy settings (*SSP*), and the intercept is more than three times greater for medium energy floodplains than low energy floodplains. The top five models for efficiency and seven of the top nine models for $dep_{TP,yr,2ch}$, comprising 51% and 71% of the cumulative weight of evidence, respectively, all contained the variables *DA*, WS_{IMP}, and *SSP*, indicating overwhelming support for these factors. Additionally, IR was in all top models for efficiency and six of the top nine for $dep_{TP,yr,2ch.}$ All site-scale models listed in Table 8 are within ΔAIC<2, and therefore have considerable empirical support. The location of the plot away from the channel (*D*), the inundation frequency (*Inun*), percentage of tree cover (X_{tree}), elevation above the channel (*HAND*), floodplain width relative to channel width ($W_{FP/CH}$), along with the classification of floodplain deposition setting based on *SSP* (e.g., low vs medium energy) are in the top GLMs for predicting local $dep_{TP,yr}$. We also consider the sixth ranked model for $dep_{TP,yr}$ (ΔAIC =5.04), which includes D_{CH}, which is more generalizable than *D* across scales. Top GLMs described 45-69% of the variability at the watershed scale, and 45-46% at the local scale. At the local scale, 25% of the variability may be described by site-scale variability, as shown by the plot-scale model that only includes $dep_{TP,yr,2ch}$.

The BRT model of $dep_{TP,yr}$ at the plot-scale explained a large amount of variability (68% of deviance; calibration dataset) and was moderately predictive (0.63 CV correlation; validation dataset). TP deposition rate at the plot-scale was most strongly influenced by WS_{AG} (22%), $W_{FP/CH}$ (19%), *HAND* (16%), and D_{CH} (13%) followed by X_{tree} , WS_{IMP}, *Inun* and floodplain energy setting classified by SSP, all <10% influence on $dep_{TP,yr}$ (Figure 5). Non-linearities in the data are apparent in the partial dependence plots, which display the response of $dep_{TP,yr}$ (normalized to a mean of zero) to individual predictor variables with the effects of other predictors removed.

At the watershed-scale, phosphorus deposition was greatest in wide valleys ($W_{FP/CH}$ > 25 in particular), with high WS_{IMP}, low incision ratios, and with SSP greater than 10 W m^{-2} (Table 8; Figure 5). Through a watershed (i.e., with increasing DA), phosphorus deposition depended on the energy regime. In medium energy settings, $dep_{TP,yr,2ch}$ decreased with increasing *DA* and in low energy settings, $dep_{TP,yr,2ch}$ increased with increasing *DA* at a much greater rate. Phosphorus deposition also increased with increasing upstream WS_{GL} and decreasing upstream $WS_{Wetland}$. The impact of upstream WS_{AG} differed, depending on the metric. For $dep_{TP,yr,}$ deposition rates were greatest for low WS_{AG}, notably if the proportion of the upstream watershed was less than 10% (Figure 5). For $dep_{TP,yr,2ch,}$ total deposition increased with increasing WS_{AG} (Table 8).

Locally, phosphorus deposition was greatest close to the channel in both the horizontal (i.e., within 1 channel width) and vertical direction (< 1.5 m vertical distance) and decreased rapidly with increasing distance (Figure 5). For increasing frequency of inundation, $dep_{TP,yr}$ increased. Phosphorus deposition rates were highest where trees are essentially absent (cover < 20%) (Figure 5). Often herbaceous plant communities are associated with greater deposition rates, at least in the short term, in part, because of their proximity to the channel and association with high rates of disturbance (Steiger and Gurnell, 2003; Diehl et al., 2017b).

Table 8. Summary of top GLMs. Model selection criteria used in ranking generalised linear models predicting phosphorus deposition rate and efficiency at the site-scale and phosphorus deposition rate at the plot scale. The full list of candidate models can be found in the Appendix.

Response Variable		df	delta AIC	AIC weight	R^2	Intercept		Coefficients of Predictors						
SITE-SCALE														
						low energy	medium energy	*IR*	*WS IMP*	*WS GL*	*WS WET*	*WS AG*	*W FP/CH*	*DA* [a] low energy	*DA* [a] medium energy
$dep_{TP,yr,2ch}$	1	5	0.00	0.13	0.57	24.8	108.8	-46.0	2217					0.026	-0.011
	2	4	0.27	0.11	0.52	-26.0	45.4		2239					0.026	-0.007
	3	4	1.30	0.07	0.50	55.3	140.9	-46.6						0.034	-0.007
	4	3	1.32	0.07	0.45	4.08	76.87							0.034	-0.004
	5	5	1.42	0.06	0.54	-39.01	36.68		2241				0.86	0.020	-0.008
	6	6	1.65	0.06	0.58	22.97	112.64	-48.7	2171	34.0				0.028	-0.011
	7	6	1.94	0.05	0.57	16.65	100.79	-42.0	2220				0.25	0.025	-0.011
	8	6	1.95	0.05	0.57	29.09	111.12	-45.3	2192		-43.7			0.026	-0.010
	9	6	2.00	0.05	0.57	24.43	109.0437	-46.2	2201.8			4.53		0.027	-0.011
efficiency	1	5	0.00	0.27	0.68	0.58	1.28	-0.84	23.7					0.00028	-0.00006
	2	6	1.37	0.13	0.69	0.47	1.22	-0.86	24.3		1.13			0.00029	-0.00007
	3	6	1.89	0.10	0.68	0.57	1.29	-0.86	23.5	0.15				0.00029	-0.00006
	4	6	1.91	0.10	0.68	0.50	1.20	-0.81	23.7				0.002	0.00027	-0.00006
	5	6	1.97	0.10	0.68	0.59	1.27	-0.84	24.1			-0.109		0.00028	-0.00006
PLOT-SCALE															
						low energy	medium energy	*D* [b]	*D CH* [b]	*Inun*	*HAND*	*X tree*	*W FP/CH*	*depTP,yr,2ch*	
$dep_{TP,yr}$	1	7	0.00	0.45	0.45	0.61	1.31	-0.46		0.37		-0.69	0.048	0.014	
	2	8	0.76	0.31	0.46	0.92	1.61	-0.46		0.23	-0.14	-0.54	0.048	0.014	
	6	8	5.04	0.04	0.44	-0.11	0.71		-0.39	-0.03	-0.32	-0.67	0.052	0.012	
	33	2	53.4	0.00	0.25	0.22								0.017	

a. Interaction with floodplain type (as defined by threshold in SSP)

b. Natural log of distance from channel and distance from channel/channel width

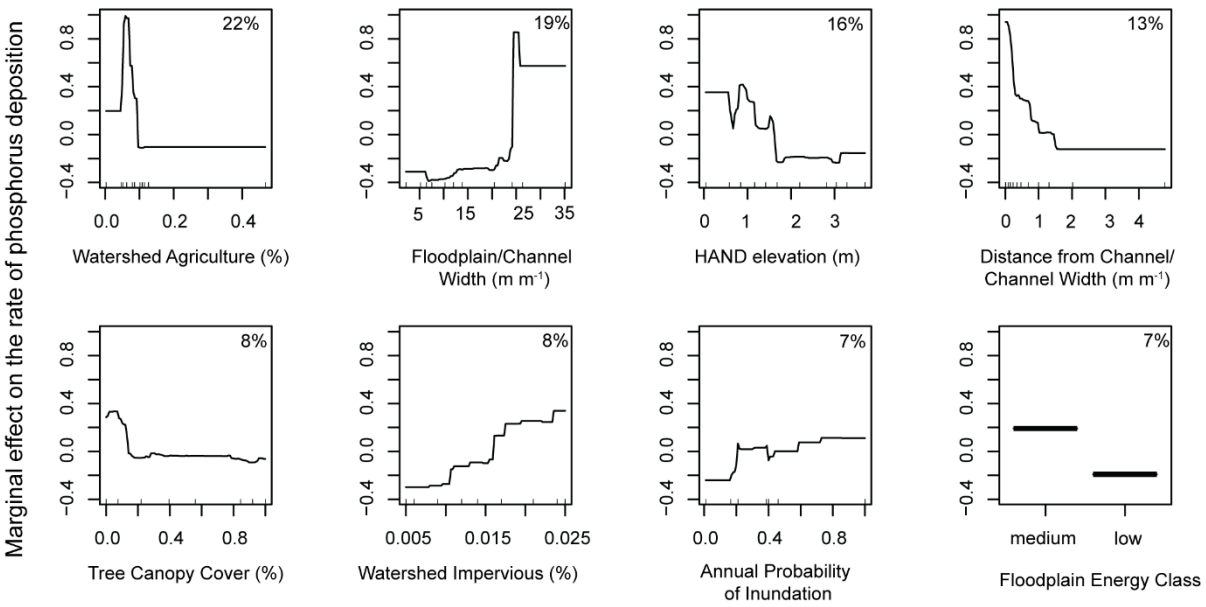

Figure 5. Partial dependence plots for the BRT model. Plots show phosphorus deposition rate ($dep_{TP,yr}$) depends on each predictor variable after accounting for the average effects of other predictors. The relative contribution of each predictor to the overall error reduction is indicated as a percentage in the upper right corner of each plot. Rugs at the bottom of each plot show the distribution of data in deciles.

Application of Framework: Prediction Function

For the Mad River Watershed, we created a map of those areas with the greatest likelihood to capture sediment-bound phosphorus based on 1) existing conditions and 2) the potential gain in phosphorus deposition with floodplain or channel intervention (i.e., gain = potential-existing). For potential conditions we lowered IR values to "1.0", indicative of floodplain that is well connected to its river channel, receiving regular inputs of flood water, sediment, and nutrients.

To calculate phosphorus deposition rates through the Mad River Watershed, we applied top site-scale GLMs to segments of river defined by stream geomorphic assessment (SGA) reach breaks (anrgeodata.vermont.gov/datasets) with a drainage area greater than 25 km^2 (21 reaches; 55 km). We first calculated watershed characteristics for each reach (e.g., WS_{IMP}, WS_{GL}, WS_{AG}, WS_{WET}) using a methodology similar to that descried in Section 3. Incision ratios were field assessed for 76% of the reaches and reported in the SGA dataset. For the remaining reaches, IR values were measured from profiles taken from the DEMs within the study area based on methods modified from Pataseanu-Lovejoy et al (2016), relying on datasets derived under the Functioning Floodplain Initiative. To identify if the reach was low or medium energy, we referenced specific stream power values calculated as part of the Vermont River Sensitivity Coarse Screen by Milone & MacBroom (https://extension.umass.edu/riversmart/sites/extension.umass.edu.riversmart/files/pdf-doc-ppt/MA%20FGM%20Coarse%20Screen%202014.pdf).

Sixty-six percent of the stream reaches in the Mad River have floodplains that are likely to be depositional (e.g., below gray line in Figure 2), and all have *SSP* greater than 10 W m^{-2}. Because nearly all % watershed impervious values fall within the study range (one reach WS_{IMP} is 4.7%), we apply the first model (Table 8). Existing deposition rates ranged from 0 to 99 g P m^{-1} yr^{-1} are greatest in reaches located throughout the watershed and are often those areas with the least to

gain (existing-potential; Figure 6). Potential gains range from no increase in phosphorus deposition (i.e., where IR=1 for existing conditions) to an order of magnitude greater deposition under potential conditions compared to the existing IR. A step-by-step guide to adopting the prioritization function can be found in Appendix H.

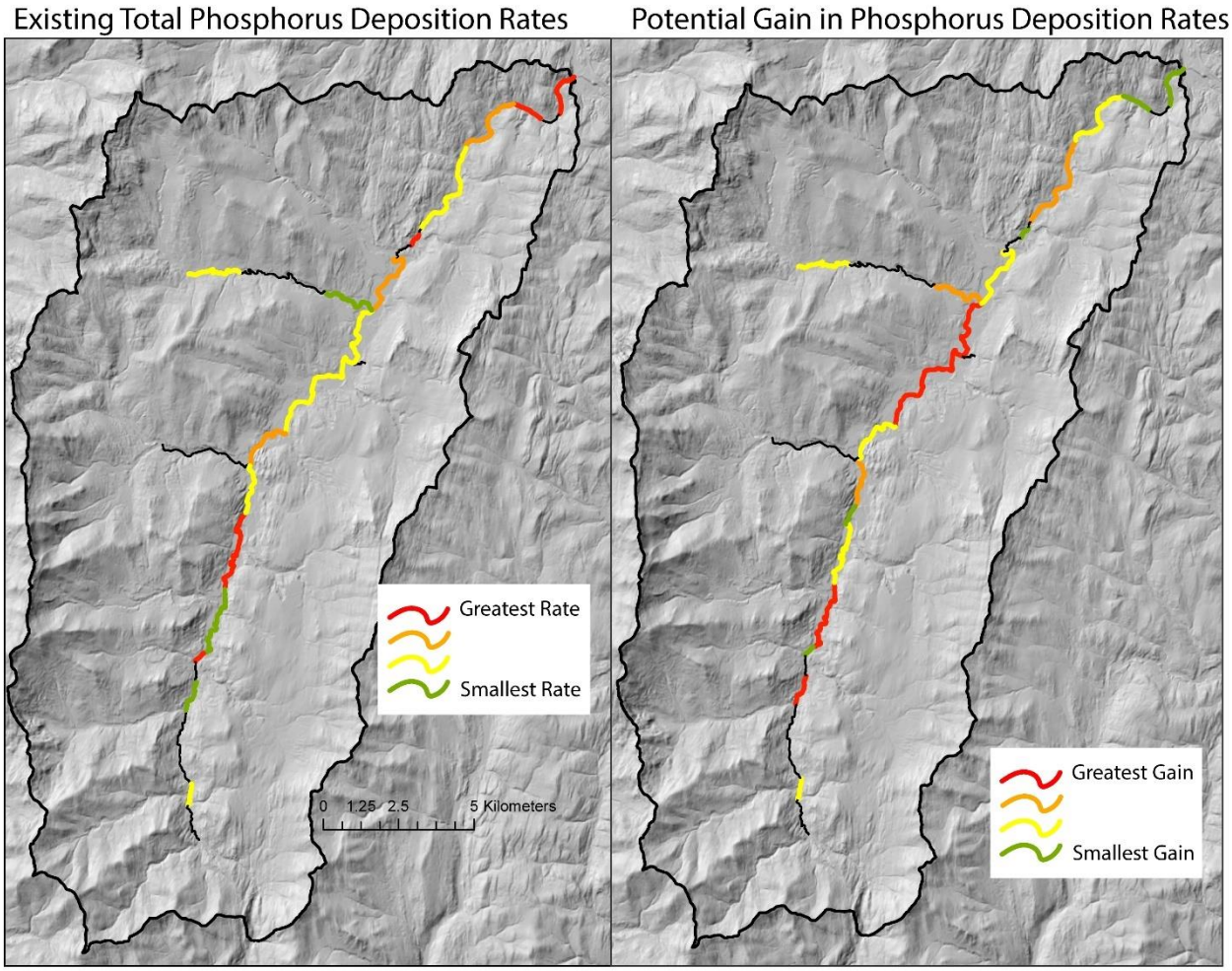

Figure 6. Example application of the prioritization function to the Mad River Watershed.

Application of Framework: Intervention Function

We evaluated the impact of floodplain lowering with and without revegetation at the Potash Brook and Mad River sites predicted from the two statistical models: 1) GLMs and 2) BRT (

Table 9; **Error! Reference source not found.** and **Error! Reference source not found.**). To apply the GLMs, we first calculated the site-averaged $dep_{TP,yr,2ch}$ as an input into the plot-scale models. To be sure that we did not extend our predictions outside of the range of modeled predictors, we chose the top model for which all site parameters fell within the range of watershed characteristics (Table 3 and Table 8). For Potash Brook, we therefore used the third ranked model, because it did not include WS_{IMP}, for which values in the watershed greatly exceed the range included in the model. At the plot-scale we used the sixth-best model, because it includes D_{CH}. Negative values predicted by the model are assigned a value of "0" to indicate a lack of deposition. A step-by-step guide is provided in Appendix H.

Based on the statistical models, hydrologic reconnection through floodplain lowering altered phosphorus deposition rates between 17% and 55% at Potash Brook and 19% and 77% at Couples Field, Mad River (

Table 9; Figure 7 and Figure 8). The additional consideration of revegetation reduced deposition rates by an average of 16% compared to no revegetation. The two models were inconsistent in describing which site had the greater deposition rate. The BRT model consistently predicted smaller changes with restoration interventions than did the GLM, which is more sensitive to local changes. Although the two test floodplains differed in many attributes, they were similar in others, notably $W_{FP/CH} < 5$ and medium energy regime. As such, we would expect that model predictions will differ for other types of settings (Table 8).

Differences between results may be attributed to model structure, and the complexity of understanding and predicting deposition rates on floodplains. Because GLMs are linear, they can be more responsive to shifts in values along a continuum than BRT models which are often non-linear and whose shape may be sensitive to idiosyncrasies in the dataset (e.g., Figure 5) which may contribute to spurious predictions. Additionally, the BRT model incorporates physical attributes over all spatial scales (watershed, reach, and local) and watershed or reach variables account for more than half of the overall error reduction. Predictions of $dep_{TP,yr}$ with shifts to local variables only are not as large as they are in the GLMs which incorporate the different scales in two consecutively applied models.

Based on these considerations, we propose adoption of both models into the intervention function. The set of predictions may provide an understanding of the range of phosphorus deposition rates a site can support.

Table 9. Results from application of intervention function. Both sites are currently hydrologically disconnected (Inun < 0.5) and their channel is incised (IR > 1.3). We predict phosphorus deposition within targeted areas as a result of floodplain lowering, and floodplain lowering with revegetation, from two types of statistical models (GLM and BRT)

		Potash Brook		Couples Field at Mad River	
Site Area (m^2)		1740		11000	
Elevation Change (m)		0.5		1.5	
Drainage Area (km^2)		18.4		124	
Slope		0.012		0.004	
Existing IR		1.80		1.56	
Floodplain width/Channel Width (m)		2.54		4.40	
% Tree Cover		75%		19%	
% Impervious		22.4%		2.0%	
		GLM, no WS_{IMP}	BRT	GLM, with WS_{IMP}	BRT
Existing	**TP Deposition within 2 channel widths (g P m^{-1} yr^{-1})**	56.9		79.2	
	TP Deposition Rate (g P m^{-2} yr^{-1})	1.03	1.51	1.06	1.02
Proposed	**TP Deposition within 2 channel widths (g P m^{-1} yr^{-1})**	94.2		105.0	
	TP Deposition Rate (g P m^{-2} yr^{-1}) *Floodplain Lowering*	1.59	1.62	1.88	1.22
	TP Deposition Rate (g P m^{-2} yr^{-1}) *Floodplain Lowering & Revegetation**	1.42	1.55	1.34	1.27
% Change with Intervention	**Floodplain Lowering**	55%	17%	77%	19%
	Floodplain Lowering & Revegetation	38%	14%	26%	25%

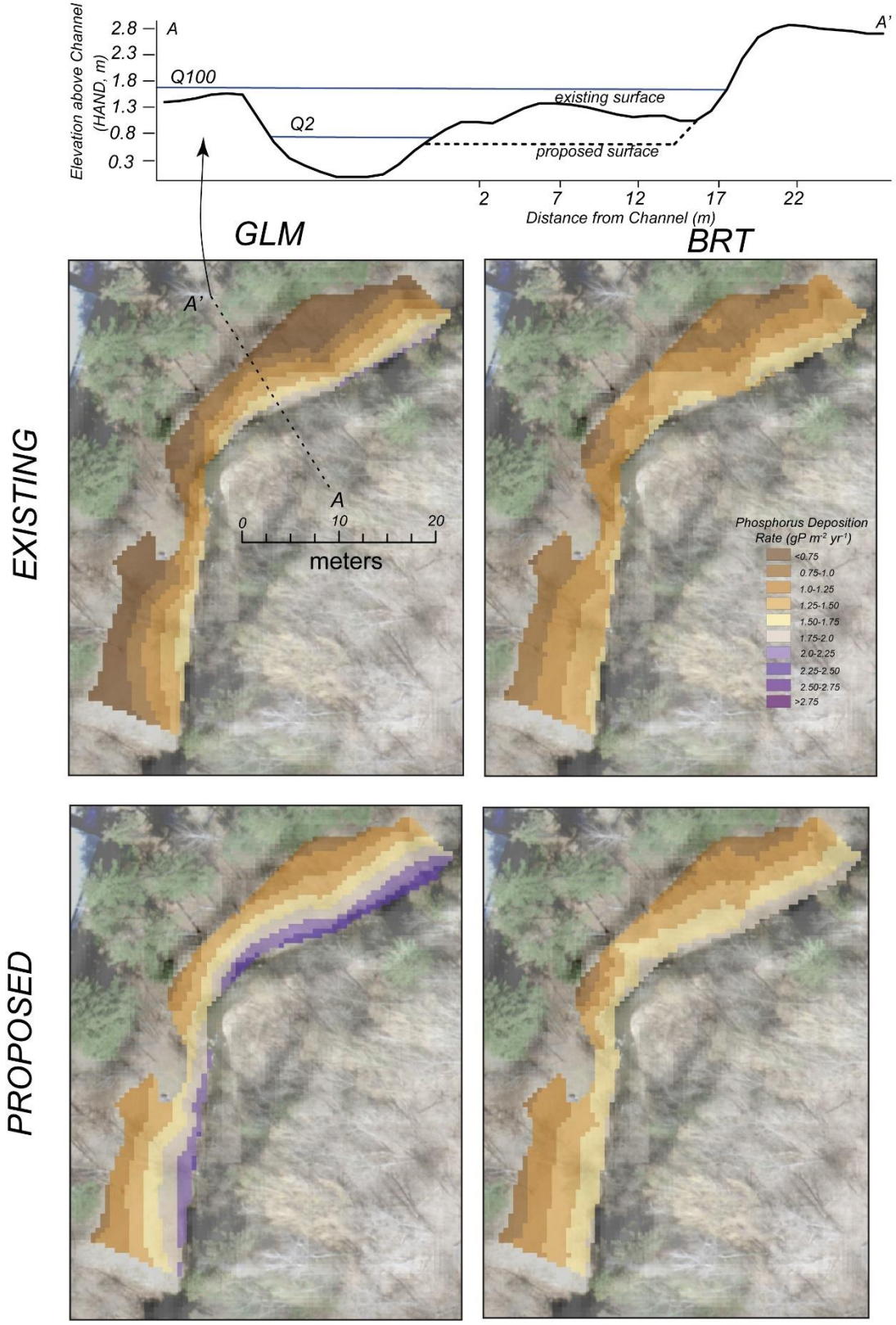

Figure 7. Example application of the intervention function to Potash Brook. We show predicted phosphorus deposition rates for existing conditions (top panel) and proposed conditions with floodplain lowering only (bottom panel).

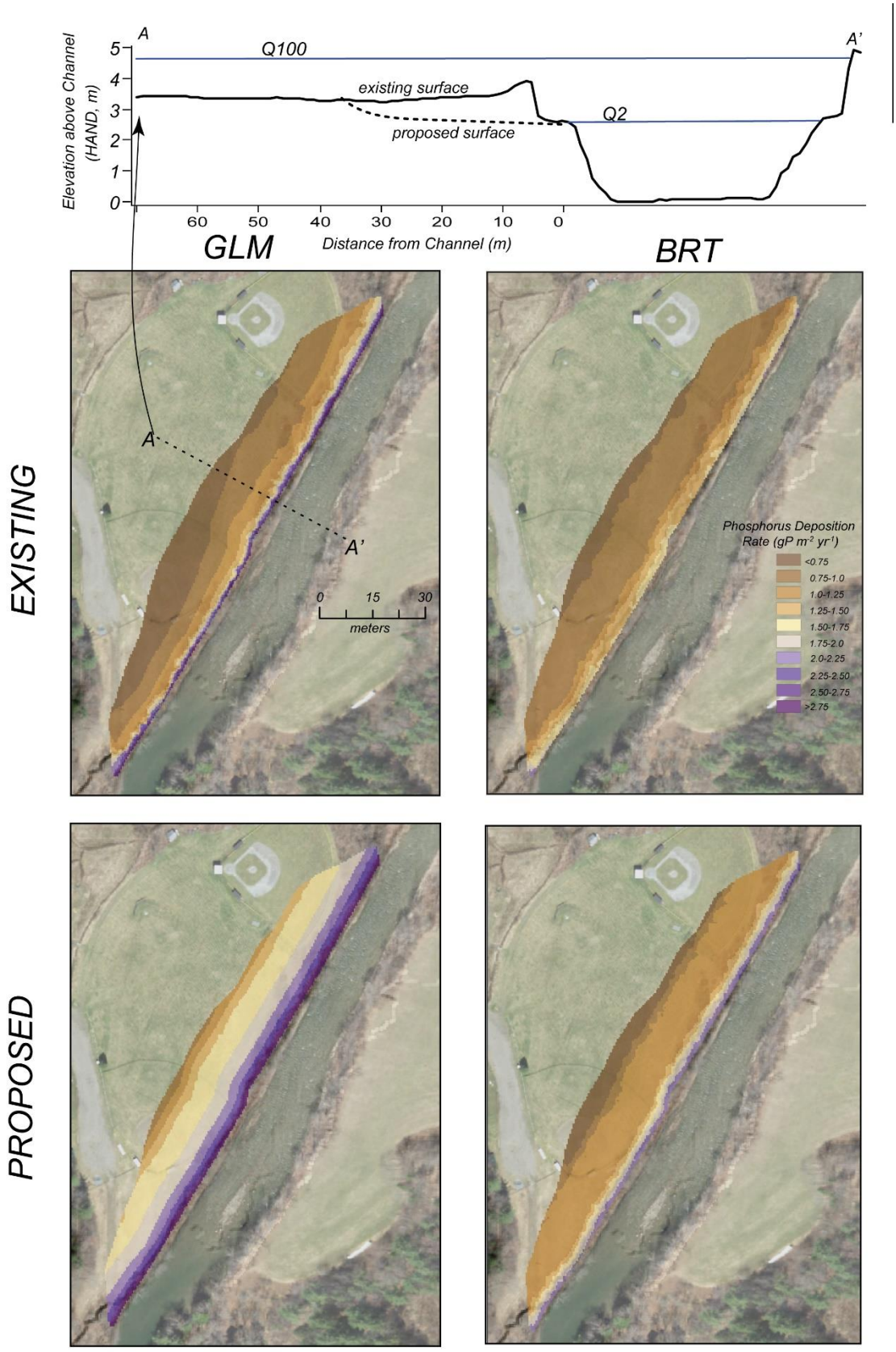

Figure 8. Example application of the intervention function to Couples Field, Mad River. We show predicted phosphorus deposition rates for existing conditions (top panel) and proposed conditions with floodplain lowering only (bottom panel).

6 Conclusions

The work described in this report represents an initial attempt at documenting the distribution of floodplains in the Lake Champlain Basin and quantifying their capacity to store sediment-bound phosphorus, with expected attenuation of the downstream movement of sediment and phosphorous. Results from this work suggest that during floods, floodplains in the Lake Champlain Basin experience sediment deposition rates between 0.04 and 4.48 kg m^{-2} yr^{-1}. Flood-derived sediment captured during this study had an average total phosphorus concentration of 744 mg kg^{-1}, consistent with other regional datasets of streambank sediments (e.g., 678 mg kg^{-1}, Young et al., 2012; 710 mg kg^{-1}, Perillo et al., 2019). As a result, floodplains represented by the range of conditions in our study, may capture as much as 3.3 g P m^{-2} yr^{-1}, or as little as 0.02 g P m^{-2} yr^{-1} (average of 0.94 g P m^{-2} yr^{-1}), corresponding to 0.18 to 29.4 lb ac^{-1} yr^{-1}, or 0.8 to 164% of annual loads transported. The variability in phosphorus floodplain deposition may be governed, in part, by a floodplain's location within a watershed, upstream geology and land use/land cover, and channel and floodplain morphology. The highest rates of phosphorus deposition were associated with wide valleys (floodplain width is at least 25 times greater than channel width), in watersheds with relatively high impervious surfaces, where the degree of channel incision is low, and the channel-adjacent specific stream power is greater than 10 W m^{-2} (but less than 300 W m^{-2}) during a discharge with 2-year recurrence interval. Additionally, phosphorus deposition was greatest close to the channel (i.e., within 1 channel width), and where surfaces were regularly inundated. Multiple statistical models were developed to describe these functional relationships between physical attributes and phosphorus deposition, describing 45-69% of the variability at the plot scale, and through a watershed. We adopted these models into a restoration planning framework to provide a mechanism to 1) prioritize where in a watershed phosphorus deposition rates are likely to be greatest and 2) evaluate the impact of restoration interventions at a floodplain site.

While the results from this project have made good progress in understanding the controls on spatial variability in deposition rates, these conclusions are drawn from a dataset of sediment and phosphorus deposition collected for one year, predominately from one flood. Deposition rates can vary among flood events, depending on the season (i.e, spring snowmelt vs summer thunderstorm), antecedent conditions, land management practices, and size and shape of the hydrograph (Noe et al., 2020). And sediment deposited during one flood may scour following subsequent events (Walling and Bradley, 1989). Unlike the other sites, Saunders on the New Haven River in the Otter Creek watershed experienced three flood events in the summer and fall of 2019. Deposition patterns were spatially consistent from one flood to the next, but the magnitudes varied, even when accounting for the flood's recurrence interval (Figure 9**Error! Reference source not found.**). Over longer timescales, climatic signals, upstream land use changes, and the adjustment of channel and floodplain form (along with hydrologic connectivity) will also influence sediment and phosphorus deposition patterns. Integrated over multiple decades, deposition rates are typically less (~50%) than those measured annually (Hupp and Bazemore, 1993; Kleiss, 1996; Heimann and Roell, 2000; Gellis et al., 2008). Additional data collection over longer timescales is needed to better constrain sediment and phosphorus deposition rates. When placed in the context of export from bank erosion, scour, or from the dissolved release of phosphorus, depositional rates such as those presented in this work may then be used to understand the retentive capacity of floodplains for storing and transforming phosphorus (Noe et al., 2019).

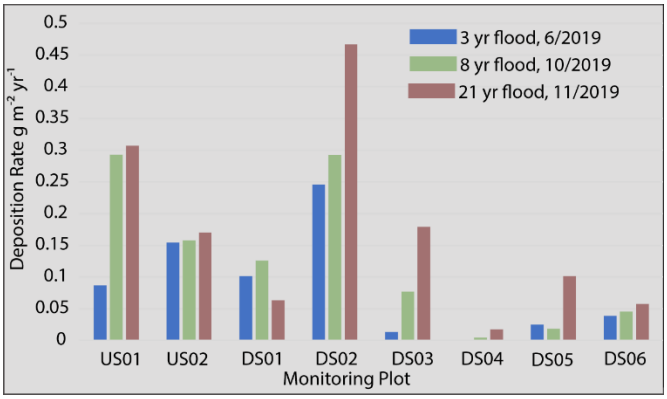

Figure 9. Variability in deposition rates among floods at the Saunders site on the New Haven River.

From the initial assessment of the role of floodplains in capturing flood-transported sediment and phosphorus, we developed a management framework to assist stakeholders with planning for floodplain restoration, protection, or enhancement actions in the Lake Champlain Basin. This framework is the first of its kind in the Lake Champlain Region and Vermont to provide evidence-based, spatially explicit guidance on where and how to improve the functioning of floodplains. It can be used to generally assess where within a region of interest, phosphorus deposition rates should be greatest, and therefore, efforts to either protect or restore floodplain processes may be most beneficial. Additionally, the framework may be used to quantify and evaluate the impact of floodplain interventions that alter channel or floodplain topography or change the tree canopy.

Limitations exist in the management framework, which must be understood and acknowledged in its application. As discussed above, the data used to build the statistical models that serve as the foundation of the framework were collected over a narrow window in time, and while they capture large environmental gradients, there are settings (e.g., urban floodplains) that are not well represented. Because of this, predictions from the models have high uncertainties, notably over longer timescales, and when extrapolated beyond the measured data. Additionally, without understanding the full set of processes that determine a floodplain's net sediment and phosphorus budget, we may misjudge the best settings to target. For example, our model indicates that deposition is greatest in valleys with medium energy rivers, but these settings may be more dynamic than their low-energy counterparts, with higher rates of (natural) streambank erosion to match high rates of vertical accretion. Our focus on low to medium energy settings, which are likely to be sites of significant sediment and sediment-bound phosphorus storage, disregards settings that are higher energy. While sediment storage in such valleys is typically limited to small pockets, the large number of smaller streams, would suggest a potential cumulative importance of these settings (Scott et al., 2019)

Our models were also not highly sensitive to tree cover but did indicate that the highest rates of deposition are in areas with < 20% tree canopy. Sediment deposition can be great where herbaceous communities dominate (Olde Venterink et al., 2006) and where woody stem density is low (Manners et al., 2013; Perignon et al., 2013). However, these results overlook the role of riparian trees in stabilizing stream banks and slowing flood waters, adding to the overall reduction in sediment export in a reach. Additionally, these results do not adequately capture plant-geomorphic interactions. Future work should emphasize more detailed characterization of vegetation community types in conjunction with deposition rates.

Data development and monitoring initiated with this project have been adopted by Vermont's Functioning Floodplain Initiative (FFI). Through the FFI, we will continue to develop the *probHAND* model to improve the accuracy of floodplain maps and collect flood deposition observations from the floodplain monitoring network for an additional year. Collaborations with

Eric Roy (UVM RSENR faculty member) and Kristen Underwood (UVM CEMS faculty member) will contextualize the magnitude of particulate phosphorus deposition relative to other forms of phosphorus flux on floodplains and wetlands in the Basin and provide an understanding of in-channel processes important for determining the net phosphorus budget. The framework presented in this project will be adjusted with additional deposition observations and an improved understanding of sediment and phosphorus fluxes and incorporated into a larger floodplain mapping, floodplain restoration prioritization, and project tracking application. This application may be used to evaluate not only where interventions will have the largest impact on capturing sediment and phosphorus, but also place these processes in the context of social constraints, and other co-benefits of floodplain restoration such as habitat creation and flood damage reduction.

With the floodplain monitoring network established as part of this project, opportunities exist to develop a long-term dataset of sediment and phosphorus deposition in the Lake Champlain Basin. Initial observations derived from event-scale turf pad measurements and associated data analyses can provide a platform to launch a more nimble monitoring program, reliant on synergies between detail-oriented work by UVM researchers and observations by citizen scientists. Engaging community members in the collection of floodplain deposition data will not only create a more sustainable model of floodplain monitoring but also help to increase citizen awareness of the functioning of floodplains in the Lake Champlain Basin.

7 References

Afshari, S., Tavakoly, A.A., Rajib, M.A., Zheng, X., Follum, M.L., Omranian, E., and Fekete, B.M., 2018, Comparison of new generation low-complexity flood inundation mapping tools with a hydrodynamic model: Journal of Hydrology, v. 556, p. 539–556, doi:10.1016/j.jhydrol.2017.11.036.

Asselman, N.E.M., and Middelkoop, H., 1995, Earth Surface Processes a N D Landforms Floodplain Sedimentation: Quantities, Patterns and Processes: Earth Surface Processes a N D Landforms, v. 20, p. 481–499.

Burnham, K.P., and Anderson, D.R., 2002, Model Selection and Multimodel Inference: a Practical Information-Theoretic Approach: Verlag, Berlin, Springer.

Burt, R., Mays, M.D., Benham, E.C., and Wilson, M.A., 2002, Phosphorus characterization and correlation with properties of selected benchmark soils of the United States: Communications in Soil Science and Plant Analysis, doi:10.1081/CSS-120002382.

Church, M., 2002, Geomorphic thresholds in riverine landscapes: Freshwater Biology, v. 47, p. 541–557.

Diehl, R.M., Merritt, D.M., Wilcox, A.C., and Scott, M.L., 2017a, Applying functional traits to ecogeomorphic processes in riparian ecosystems: BioScience, v. 67, p. 729–743, doi:10.1093/biosci/bix080.

Diehl, R.M., Wilcox, A.C., Stella, J.C., Kui, L., Sklar, L.S., and Lightbody, A., 2017b, Fluvial sediment supply and pioneer woody seedlings as a control on bar-surface topography: Earth Surface Processes and Landforms, v. 42, p. 724–734, doi:10.1002/esp.4017.

DuBois and King, 2017, Flood Study Mad River Area:, http://centralvtplanning.org/wp-content/uploads/2019/02/Flood-Study-of-the-Mad-River-Area-Report-DK-5.31.17.pdf.

Elith, J., Leathwick, J.R., and Hastie, T., 2008, A working guide to boosted regression trees: Journal of Animal Ecology, v. 77, p. 802–813, doi:10.1111/j.1365-2656.2008.01390.x.

Fitzgerald, E. Potash Brook Floodplain Restoration Concepts and P Crediting, Memo to City of South Burlington. December 16, 2020.

Gellis, A.C., Hupp, C.R., Pavich, M.J., Landwehr, J.M., Banks, W.S.L., Hubbard, B.E., Landgland, M.J., Ritchie, J.C., and Reuter, J.M., 2008, Sources, transport, and storage of sediment in the Chesapeake Bay Watershed: US Geological Survey Scientific Investigations

Report 2008-5186.:
Hair, J.., Anderson, R.E., Tatham, R.L., and Black, W.C., 1995, Multivariate Data Analysis (3rd ed): New York, Macmillan.
Heimann, D.C., and Roell, M.J., 2000, Sediment loads and accumulation in a small Riparian Wetland system in Northern Missouri: Wetlands, v. 20, p. 219–231, doi:10.1672/0277-5212(2000)020[0219:SLAAIA]2.0.CO;2.
Hijmans, R., Phillips, J., Leathwick, J.R., and Elith, J., 2015, dismo: Species distribution modeling, R package version 1.0-12 (The R Foundation for Statistical Computing).:
Hupp, C.R., and Bazemore, D.E., 1993, Temporal and spatial patterns of wetland sedimentation, West Tennessee: Journal of Hydrology, v. 141, p. 179–196, doi:10.1016/0022-1694(93)90049-F.
Hupp, C.R., Schenk, E.R., Kroes, D.E., Willard, D.A., Townsend, P.A., and Peet, R.K., 2015, Geomorphology Patterns of fl oodplain sediment deposition along the regulated lower Roanoke River , North Carolina : Annual , decadal , centennial scales: Geomorphology, v. 228, p. 666–680, doi:10.1016/j.geomorph.2014.10.023.
Ishee, E.R., Ross, D.S., Garvey, K.M., Bourgault, R.R., and Ford, C.R., 2015, Phosphorus Characterization and Contribution from Eroding Streambank Soils of Vermont's Lake Champlain Basin: Journal of Environment Quality, v. 44, p. 1745, doi:10.2134/jeq2015.02.0108.
Jain, V., Fryirs, K., and Brierley, G., 2008, Where do floodplains begin? The role of total stream power and longitudinal profile form on floodplain initiation processes: Bulletin of the Geological Society of America, v. 120, p. 127–141, doi:10.1130/B26092.1.
Jones, K.B., Neale, A.C., Nash, M.S., Van Remortel, R.D., Wickham, J.D., Riitters, K.H., and O'neill, R. V., 2001, Predicting nutrient and sediment loadings to streams from landscape metrics: A multiple watershed study from the United States Mid-Atlantic Region: Landscape Ecology, v. 16, p. 301–312, doi:10.1023/A:1011175013278.
Kaase, C.T., and Kupfer, J.A., 2016, Sedimentation patterns across a Coastal Plain floodplain: The importance of hydrogeomorphic influences and cross-floodplain connectivity: Geomorphology, doi:10.1016/j.geomorph.2016.06.020.
Kleiss, B.A., 1996, Sediment retention in a bottomland hardwood wetland in Eastern Arkansas: Wetlands, doi:10.1007/BF03161323.
Kline, M., Alexander, C., Jaquith, S., Pomeroy, S., and Springston, G., 2009, Vermont ANR Stream Geomorphic Assessment Protocol Handbooks.:
Kline, M., and Cahoon, B., 2010, Protecting river corridors in vermont: Journal of the American Water Resources Association, v. 46, p. 227–236, doi:10.1111/j.1752-1688.2010.00417.x.
Lammers, R.W., and Bledsoe, B.P., 2017, What role does stream restoration play in nutrient management? Critical Reviews in Environmental Science and Technology, v. 47, p. 335–371, doi:10.1080/10643389.2017.1318618.
Langendoen, E.J., Simon, A., Klimetz, L., Bankhead, N., and Ursic, M.E., 2012, Quantifying Sediment Loadings from Streambank Erosion in Selected Agricultural Watersheds Draining to Lake Champlain.:
Manners, R.B., Schmidt, J., and Wheaton, J.M., 2013, Multiscalar model for the determination of spatially explicit riparian vegetation roughness: Journal of Geophysical Research-Earth Surface, v. 118, p. 65–83, doi:10.1029/2011jf002188.
McMillan, S.K., and Noe, G.B., 2017, Increasing floodplain connectivity through urban stream restoration increases nutrient and sediment retention: Ecological Engineering, v. 108, p. 284–295, doi:10.1016/j.ecoleng.2017.08.006.
Noe, G.B. et al., 2020, Sediment dynamics and implications for management: State of the science from long-term research in the Chesapeake Bay watershed, USA: Wiley Interdisciplinary Reviews: Water, v. 7, p. 1–28, doi:10.1002/wat2.1454.
Noe, G.B., Boomer, K., Gillespie, J.L., Hupp, C.R., Martin-Alciati, M., Floro, K., Schenk, E.R., Jacobs, A., and Strano, S., 2019, The effects of restored hydrologic connectivity on floodplain trapping vs. release of phosphorus, nitrogen, and sediment along the Pocomoke

River, Maryland USA: Ecological Engineering, doi:10.1016/j.ecoleng.2019.08.002.
Noe, G.B., and Hupp, C.R., 2009, Retention of riverine sediment and nutrient loads by coastal plain floodplains: Ecosystems, v. 12, p. 728–746, doi:10.1007/s10021-009-9253-5.
Olde Venterink, H., Vermaat, J.E., Pronk, M., Wiegman, F., van der Lee, G.E.M., van den Hoorn, M.W., Higler, L.W.G. (Bert), and Verhoeven, J.T.A., 2006, Importance of sediment deposition and denitrification for nutrient retention in floodplain wetlands: Applied Vegetation Science, v. 9, p. 163, doi:10.1658/1402-2001(2006)9[163:iosdad]2.0.co;2.
Olson, S.A., 2014, Estimation of flood discharges at selected annual exceedance probabilities for unregulated, rural streams in Vermont.:
Palaseanu-lovejoy, M., Danielson, J., Thatcher, C., Foxgrover, A., and Barnard, P., 2016, Automatic Delineation of Seacliff Limits using Lidar-derived High- resolution DEMs in Southern California: Journal of Coastal Research, v. 76, p. 162–173, doi:10.2112/SI76-014.
Perignon, M.C., Tucker, G.E., Griffin, E.R., and Friedman, J.M., 2013, Effects of riparian vegetation on topographic change during a large flood event, Rio Puerco, New Mexico, USA: Journal of Geophysical Research: Earth Surface, v. 118, p. 1193–1209, doi:10.1002/jgrf.20073.
Perillo, V.L., Ross, D.S., Wemple, B.C., Balling, C., and Lemieux, L.E., 2019, Stream Corridor Soil Phosphorus Availability in a Forested-Agricultural Mixed Land Use Watershed: Journal of Environmental Quality, doi:10.2134/jeq2018.05.0186.
Pizzuto, J.E., Moody, J.A., and Meade, R.H., 2008, Anatomy and dynamics of a floodplain, Powder River, Montana, USA: Journal of Sedimentary Research, v. 78, p. 16–28.
Pizzuto, J., Skalak, K., Pearson, A., and Benthem, A., 2016, Active overbank deposition during the last century, South River, Virginia: Geomorphology, doi:10.1016/j.geomorph.2016.01.006.
Records, R.M., Wohl, E., and Arabi, M., 2016, Phosphorus in the river corridor: Earth-Science Reviews, doi:10.1016/j.earscirev.2016.04.010.
Roy, E. 2019. Quantifying phosphorus retention in restored riparian wetlands of the Lake Champlain Basin. proposal submitted to Lake Champlain Basin Program.
Schenk, E.R., Hupp, C.R., Gellis, A., and Noe, G., 2013, Developing a new stream metric for comparing stream function using a bank-floodplain sediment budget: A case study of three Piedmont streams: Earth Surface Processes and Landforms, v. 38, p. 771–784, doi:10.1002/esp.3314.
Scott, D.T., Gomez-Velez, J.D., Jones, C.N., and Harvey, J.W., 2019, Floodplain inundation spectrum across the United States: Nature Communications, v. 10, p. 5194, doi:10.1038/s41467-019-13184-4.
Singh, N.K., Gourevitch, J.D., Wemple, B.C., Watson, K.B., Rizzo, D.M., Polasky, S., and Ricketts, T.H., 2019, Optimizing wetland restoration to improve water quality at a regional scale: Environmental Research Letters, v. 14, p. 064006, doi:10.1088/1748-9326/ab1827.
Steiger, J., and Gurnell, A.M., 2003, Spatial hydrogeomorphological influences on sediment and nutrient deposition in riparian zones: observations from the Garonne River, France: Geomorphology, v. 49, p. 1–23.
Stryker, J., Wemple, B., and Bomblies, A., 2018, Modeling the impacts of changing climatic extremes on streamflow and sediment yield in a northeastern US watershed: Journal of Hydrology: Regional Studies, v. 17, p. 83–94, doi:10.1016/j.ejrh.2018.04.003.
Swinnen, W., Daniëls, T., Maurer, E., Broothaerts, N., and Verstraeten, G., 2020, Geomorphic controls on floodplain sediment and soil organic carbon storage in a Scottish mountain river: Earth Surface Processes and Landforms, v. 45, p. 207–223, doi:10.1002/esp.4729.
U.S. Environmental Protection Agency (2016) Phosphorus TMDLs for Vermont Segments of Lake Champlain. Available at: https://ofmpub.epa.gov/waters10/attains_impaired_waters.show_tmdl_document?p_tmdl_doc_blobs_id=79000
Vidon, P. et al., 2018, In the path of the Hurricane: impact of Hurricane Irene and Tropical Storm

Lee on watershed hydrology and biogeochemistry from North Carolina to Maine, USA: Biogeochemistry, doi:10.1007/s10533-018-0423-4.
Walling, D.E., and Bradley, S.B., 1989, Rates and patterns of contemporary floodplain sedimentation: A case study of the river Culm, Devon, UK: GeoJournal, v. 19, p. 53–62, doi:10.1007/BF00620549.
Walling, D.E., Owens, P.N., and Leeks, G.J.L., 1999, Rates of contemporary overbank sedimentation and sediment storage on the floodplains of the main channel systems of the Yorkshire Ouse and River Tweed, UK: Hydrological Processes, v. 13, p. 993–1009, doi:10.1002/(SICI)1099-1085(199905)13:7<993::AID-HYP786>3.0.CO;2-C.
Young, E.O., Ross, D.S., Alves, C., and Villars, T., 2012, Soil and landscape influences on native riparian phosphorus availability in three Lake Champlain Basin stream corridors: Journal of Soil and Water Conservation, doi:10.2489/jswc.67.1.1.
Zheng, X., Tarboton, D.G., Maidment, D.R., Liu, Y.Y., and Passalacqua, P., 2018, River Channel Geometry and Rating Curve Estimation Using Height above the Nearest Drainage: Journal of the American Water Resources Association, v. 54, p. 785–806, doi:10.1111/1752-1688.12661.

8 Appendices

Appendix A: ProbHAND Manuscript

See attached (*Diehl_probHAND_PLOSONE.pdf*) for manuscript titled “Improving flood hazard datasets using a low-complexity, probabilistic floodplain mapping approach” accepted for publication to PLOS ONE on March 4, 2021.

Appendix B: Deposition Datasets

Tables provided in this appendix (*Appendix B_Deposition Datasets.xls*) document deposition and associated phosphorus concentrations measured at turf pads, cores, and monitoring plots. We also include the coordinates for all monitoring plots and cores in Vermont State Plane.

Appendix C: Flood Recurrence Interval Identification

Tables provided in this appendix provide information on recurrence intervals for observed floods. We associated basin and rain storm characteristics at each site to those characteristics at nearby stream gages with flood frequency relationships to identify the recurrence interval at floodplain sites.

Table C1. Flood events observed at each of the floodplain sites.

Site	HUC12	Flood Date	11/1/19 Storm Total (in m^{-2})	Drainage area (km^2)	Basin outlet vertical location in state plane (feet)	Basin outlet horizontal location in state plane (feet)	% water bodies & wetlands	% of basin at or above 1200 ft	Peak RI	RI notes	Gages referenced
Atlas	LAM_0302	11/1/19	3.00	32.9	250685	489395	8.9	83.9	125.64	percent basin above 1200 relationship from Missisquoi	4292750, 4292810, 4294000, 4293500, 4293000
Browns	LAM_0202	11/1/19	3.20	140.9	222155	459605	0.76	37.5	8.77	storm precipitation total for Winooski gages > 10 mi^2	4287000, 4286000, 4288000, 4290500, 4288225
Cota Field	LKC_0502	11/1/19	3.22	47.9	193895	455015	0.5	62.5	7.59	storm precipitation total for Lewis Creek, Little Otter, and New Haven River gages	4282780, 4282650, 4282525
Desmarais	OTR_0304	11/1/19	1.81	1209.5	142475	451615	5.7	60.8	1.54	storm precipitation total for Otter Basin and Lewis	4282780, 4282500, 4282000, 4280000
Dubois	WIN_0403	11/1/19	1.62	1269.1	195415	490588	2.26	63	3.90	storm precipitation total for Winooski gages > 10 mi^2	4287000, 4286000, 4288000, 4290500, 4288225
EPSCoR Hungerford	MSQ_0602	11/1/19	2.91	10.0	266005	458025	5.26	0	25.52	percent basin above 1200 relationship from Missisquoi	4292750, 4292810, 4294000, 4293500, 4293001
Green Mountain College	MET_0302	11/1/19	1.74	128.7	113215	439535	2.43	45.7	1.40	Poultney River below Fair Haven gage	4280000
Black Creek #1&2	MSQ_0501	11/1/19	3.17	123.3	255025	469755	2.38	9.4	30.51	percent basin above 1200 relationship from Missisquoi	4292750, 4292810, 4294000, 4293500, 4293000
Idletyme	WIN_0602	11/1/19	3.37	60.3	219275	482705	0.12	84.1	9.14	storm precipitation total for Winooski gages > 10 mi^2	4287000, 4286000, 4288000, 4290500, 4288227
Jericho Settlers Farm	WIN_0702	11/1/19	2.26	2553.6	218705	458055	1.67	59	6.27	storm precipitation total for Winooski gages > 10 mi^2	4287000, 4286000, 4288000, 4290500, 4288228
Lareau	WIN_0502	11/1/19	2.40	148.4	186385	473305	0.41	86.9	6.70	storm precipitation total for Winooski gages > 10 mi^2	4287000, 4286000, 4288000, 4290500, 4288226
Lemon Fair	OTR_0402	11/1/19	2.79	176.6	16605	440035	4.92	0	3.70	storm precipitation total for Otter Basin and Lewis	4282780, 4282500, 4282000, 4280000
Mckenzie Park	WIN_0704	11/1/19	2.35	2745.3	223585	443055	1.95	55.1	6.54	storm precipitation total for Winooski gages > 10 mi^2	4287000, 4286000, 4288000, 4290500, 4288229
North Troy	MSQ_0105	11/1/19	2.57	352.2	276815	508025	1.93	60.8	130.24	drainage area for mainstem Missisquoi	4294000, 4293500, 4293000
Otter Creek WMA	OTR_0103	11/1/19	1.83	162.4	95865	460235	4.51	82.6	1.57	storm precipitation total for Otter Basin and Lewis	4282780, 4282500, 4282000, 4280000
Enosburg Falls Farm	MSQ_0402	11/1/19	2.79	1706.7	267825	470885	1.04	34.9	28.36	drainage area for mainstem Missisquoi	4294000, 4293500, 4293000
Ryder	LAM_0106	11/1/19	2.01	600.9	229685	496805	3.92	75.4	29.59	basin outlet vertical coordinates for Lamoille and nearby Winooski gages	4292500, 4292000, 4288230, 4288225

Saunders	OTR_0203	11/1/19	2.91	184.1	178895	452495	2.11	82.2	21.33	New Haven River at Brooksville gage	4282525
Richford Farm	MSQ_0204	11/1/19	2.60	1214.7	276385	484705	0.96	35.9	39.39	drainage area for mainstem Missisquoi	4294000, 4293500, 4293000
Trout River	MSQ_0302	11/1/19	2.99	211.6	269855	484825	0.38	59.7	79.33	percent basin above 1200 relationship from Missisquoi	4292750, 4292810, 4294000, 4293500,4293000
Wolcott	LAM_0104	11/1/19	1.68	401.4	228045	501695	3.54	78.8	21.23	basin outlet vertical coordinates for Lamoille and nearby Winooski gages	4292500, 4292000, 4288230, 4288225
Cota Field	LKC_0502	10/16/19	N/A	47.9	193895	455015	0.5	62.5	1.70	Lewis Creek at North Ferrisburgh gage	4282780
Saunders	OTR_0203	10/16/19	N/A	184.1	178895	452495	2.11	82.2	8.10	New Haven River at Brooksville gage	4282525
Saunders	OTR_0203	6/22/19	N/A	184.1	178895	452495	2.11	82.2	3.40	New Haven River at Brooksville gage	4282525
Desmarais	OTR_0304	4/15/19	N/A	1209.5	142475	451615	5.7	60.8	7.75	drainage area along mainstem of Otter Creek	4282500, 4280000
Dog River	WIN_0401	4/15/19	N/A	157.7	192595	492375	0.93	66.9	7.50	Dog River at Northfield Falls gage	4287000
Desmarais	OTR_0304	1/25/19	N/A	1209.5	142475	451615	5.7	60.8	3.45	drainage area along mainstem of Otter Creek	4282500, 4280000
Desmarais	OTR_0304	12/22/18	N/A	1209.5	142475	451615	5.7	60.8	2.27	drainage area along mainstem of Otter Creek	4282500, 4280000
Dog River	WIN_0401	12/22/18	N/A	157.7	192595	492375	0.93	66.9	4.24	Dog River at Northfield Falls gage	4287000

Table C2. Basin and flood-producing rain storm characteristics for referenced USGS stream gages

Gage Name	Gage Number	Date of Peak	Peak Discharge ($m^3 s^{-1}$)	RI	11/1/19 Storm Total (in m^{-2})	Drainage Area (km^2)	Basin outlet vertical location in state plane (feet)	Basin outlet horizontal location in state plane (feet)	% water bodies/ wetlands	% of basin at or above 1200 ft	Link
POULTNEY RIVER BELOW FAIR HAVEN, VT	4280000	11/1/19	48	1.4	1.71	486.9	125295	434635	9.5	20.7	https://waterdata.usgs.gov/nwis/uv?site_no=04280000
OTTER CREEK AT CENTER RUTLAND, VT	4282000	11/1/19	97	1.6	1.80	797.7	122715	458565	5.3	72.0	https://waterdata.usgs.gov/nwis/uv?site_no=04282000
OTTER CREEK AT MIDDLEBURY, VT	4282500	11/1/19	84	1.6	1.96	1634.2	128137	460082	8.8	54.2	https://waterdata.usgs.gov/nwis/uv?site_no=04282500
NEW HAVEN RIVER @ BROOKSVILLE, NR MIDDLEBURY, VT	4282525	11/1/19	408	21.3	3.02	300.4	173825	446145	2.1	62.8	https://waterdata.usgs.gov/nwis/uv?site_no=04282525
LITTLE OTTER CREEK AT FERRISBURG, VT.	4282650	11/2/19	35	4.4	3.20	151.3	188905	440055	4.7	0.2	https://waterdata.usgs.gov/nwis/uv?site_no=04282650
LEWIS CREEK AT NORTH FERRISBURG, VT.	4282780	11/1/19	119	7.1	3.32	198.1	194565	441835	5.9	22.4	https://waterdata.usgs.gov/nwis/uv?site_no=04282780
LAPLATTE RIVER AT SHELBURNE FALLS, VT.	4282795	11/1/19	87	35.9	3.54	115.0	207985	442875	3.8	1.7	https://waterdata.usgs.gov/nwis/uv?site_no=04282795
NORTH BRANCH WINOOSKI RIVER AT WRIGHTSVILLE, VT	4285500	11/1/19	28	8.4	0.00	182.3	199875	493695	1.4	68.2	https://waterdata.usgs.gov/nwis/uv?site_no=04285500
WINOOSKI RIVER AT MONTPELIER, VT	4286000	11/1/19	175	1.7	1.59	1023.0	195125	492555	2.6	62.7	https://waterdata.usgs.gov/nwis/uv?site_no=04286000
DOG RIVER AT NORTHFIELD FALLS, VT	4287000	11/1/19	151	5.4	1.75	134.9	182045	486665	0.9	81.6	https://waterdata.usgs.gov/nwis/uv?site_no=04287000
MAD RIVER NEAR MORETOWN, VT	4288000	11/1/19	278	8.7	2.58	360.0	197475	480655	0.4	73.4	https://waterdata.usgs.gov/nwis/uv?site_no=04288000
W BRANCH LITTLE R ABV BINGHAM FALLS NEAR STOWE, VT	4288225	11/1/19	35	12.9	6.25	11.8	224955	478115	0.0	100.0	https://waterdata.usgs.gov/nwis/uv?site_no=04288225
RANCH BROOK AT RANCH CAMP, NEAR STOWE, VT	4288230	11/1/19	17	4.6	3.25	9.8	222635	477595	0.0	100.0	https://waterdata.usgs.gov/nwis/uv?site_no=04288230
LITTLE RIVER NEAR WATERBURY, VT	4289000	11/3/19	48	3.2	0.00	287.5	207775	478595	1.3	59.1	https://waterdata.usgs.gov/nwis/uv?site_no=04289000

WINOOSKI RIVER NEAR ESSEX JUNCTION, VT	4290500	11/1/19	765	6.8	2.33	2693.5	220005	449205	1.9	55.9	https://waterdata.usgs.gov/nwis/uv?site_no=04290500
LAMOILLE RIVER AT JOHNSON, VT	4292000	11/1/19	442	65.6	2.25	802.9	235825	485995	3.5	63.6	https://waterdata.usgs.gov/nwis/uv?site_no=04292000
LAMOILLE RIVER AT EAST GEORGIA, VT	4292500	11/1/19	719	106.0	2.73	1784.4	242255	454635	2.7	48.6	https://waterdata.usgs.gov/nwis/uv?site_no=04292500
MILL RIVER AT GEORGIA SHORE RD, NR ST ALBANS, VT	4292750	11/1/19	39	29.1	2.99	58.5	253485	449035	3.9	0.4	https://waterdata.usgs.gov/nwis/uv?site_no=04292750
JEWETT BROOK AT VT 38, NEAR ST. ALBANS, VT	4292810	11/1/19	7	37.5	2.51	9.7	261965	448535	8.1	0.0	https://waterdata.usgs.gov/nwis/uv?site_no=04292810
MISSISQUOI RIVER NEAR NORTH TROY, VT	4293000	11/1/19	345	137.0	2.57	344.5	274735	508985	1.8	65.0	https://waterdata.usgs.gov/nwis/uv?site_no=04293000
MISSISQUOI RIVER NEAR EAST BERKSHIRE, VT	4293500	11/1/19	580	35.2	2.61	1240.6	273295	484425	1.0	35.2	https://waterdata.usgs.gov/nwis/uv?site_no=04293500
MISSISQUOI RIVER AT SWANTON, VT	4294000	11/1/19	1045	23.6	2.82	2206.6	269025	450365	2.2	27.7	https://waterdata.usgs.gov/nwis/uv?site_no=04294000
PIKE RIVER AT EAST FRANKLIN, NR ENOSBURG FALLS, VT	4294300	11/1/19	42	2.0	2.64	89.6	278145	473715	9.7	2.7	https://waterdata.usgs.gov/nwis/uv?site_no=04294300
NEW HAVEN RIVER @ BROOKSVILLE, NR MIDDLEBURY, VT	4282525	6/20/19	179	3.4	N/A	300.4	173825	446145	2.1	62.8	https://waterdata.usgs.gov/nwis/uv?site_no=04282525
NEW HAVEN RIVER @ BROOKSVILLE, NR MIDDLEBURY, VT	4282525	10/17/19	280	8.1	N/A	300.4	173825	446145	2.1	62.8	https://waterdata.usgs.gov/nwis/uv?site_no=04282525
LEWIS CREEK AT NORTH FERRISBURG, VT.	4282780	10/18/19	31	1.7	N/A	198.1	194565	441835	5.9	22.4	https://waterdata.usgs.gov/nwis/uv?site_no=04282780
LITTLE OTTER CREEK AT FERRISBURG, VT.	4282650	10/19/19	14	1.6	N/A	151.3	188905	440055	4.7	0.2	https://waterdata.usgs.gov/nwis/uv?site_no=04282650
OTTER CREEK AT MIDDLEBURY, VT	4282500	10/17/19	74	1.5	N/A	1634.2	128137	460082	8.8	54.2	https://waterdata.usgs.gov/nwis/uv?site_no=04282500
OTTER CREEK AT CENTER RUTLAND, VT	4282000	10/17/19	119	1.8	N/A	797.7	122715	458565	5.3	72.0	https://waterdata.usgs.gov/nwis/uv?site_no=04282000
POULTNEY RIVER BELOW FAIR HAVEN, VT	4280000	10/18/19	35	1.2	N/A	486.9	125295	434635	9.5	20.7	https://waterdata.usgs.gov/nwis/uv?site_no=04280000

Appendix D: Site Summaries

Figures provided in this appendix document the location of turf pad monitoring plots and floodplain cores used to develop the phosphorus deposition datasets. Site locations are provided on the study map and can be associated with the list of sites in Table 2 and Table 5.

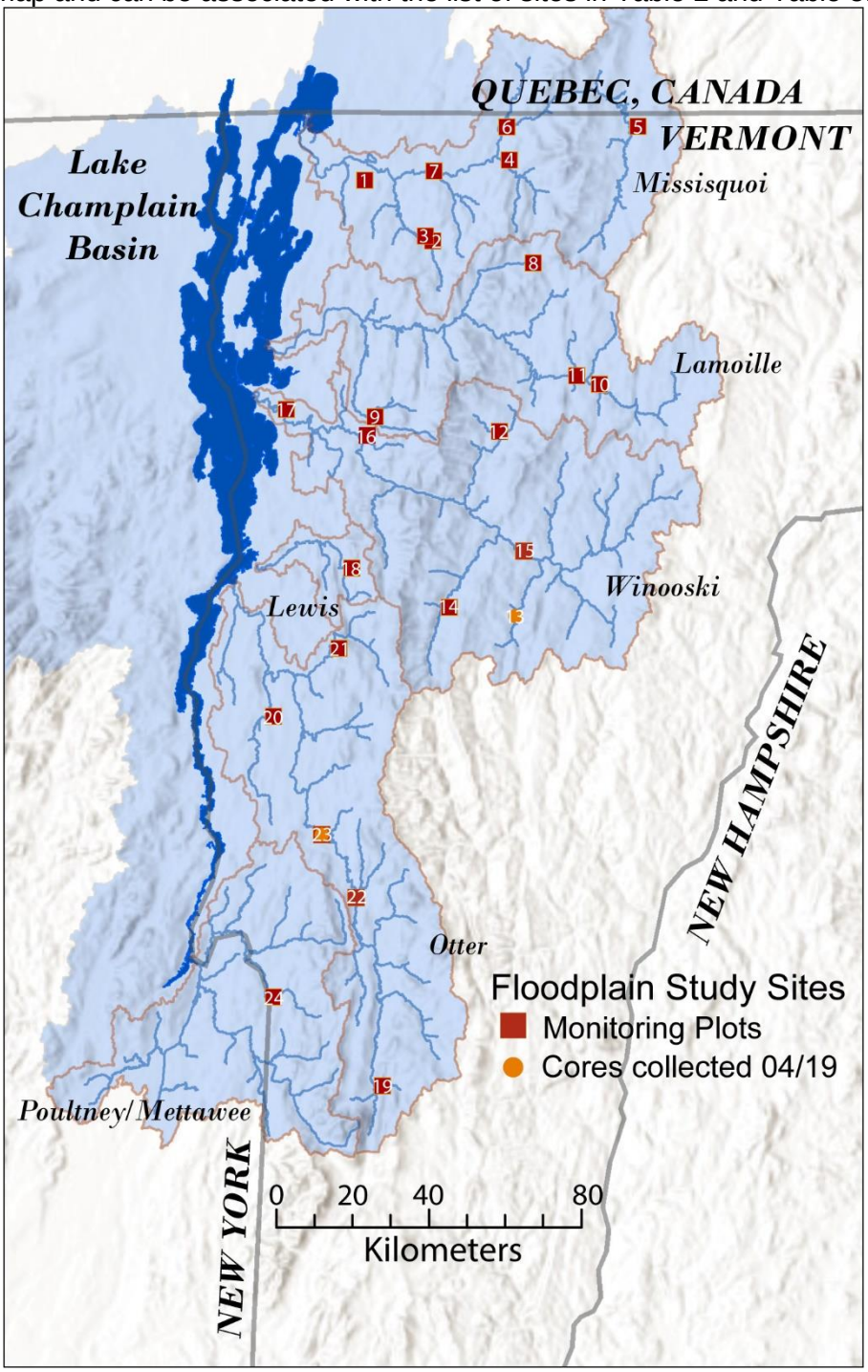

Site (1). EPSCoR on an unnamed tributary to Hungerford Brook

The EPSCoR site is located in a small agricultural watershed (DA = 11 km^2) in a low energy setting (SSP = 5.0 W m^{-2}). Three plots and a crest gage co-located with plot 01 established in 2019 were inundated, with measurable sediment deposited, during the November 1, 2019 flood. For site-average $dep_{sed,yr}$, TP_{conc}, and $dep_{TP,yr}$ values we took the average of the three plots.

Site (2). Black Creek #1 on the Black Creek

The Black Creek #1 site is located in a small agricultural watershed (*DA* = 102 km^2) in a low energy setting (*SSP* = 4.5 W m^{-2}). Two plots and a crest gage (located between the plots) were placed within a riparian buffer on a floodplain that is actively farmed. These two plots were inundated, resulting in measurable deposition, during the November 1, 2019 flood. For site-average $dep_{sed,yr}$, TP_{conc}, and $dep_{TP,yr}$ values we took the average of the two plots.

Site (3). Black Creek #2 on the Black Creek

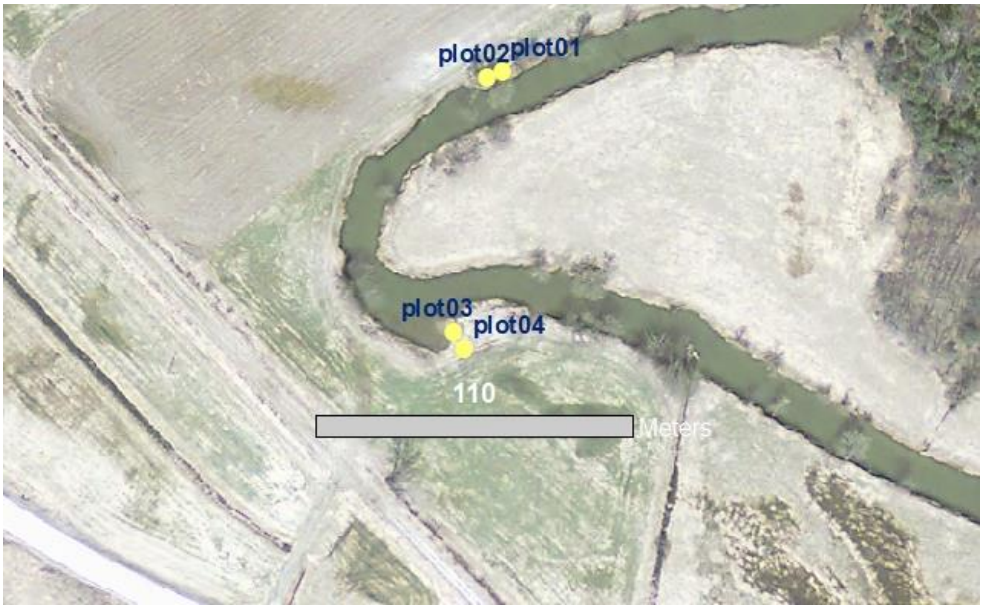

The Black Creek #2 site is located downstream of Black Creek #1 in a small agricultural watershed (DA=129 km^2) in a low energy setting (SSP=8.4 W m^{-2}). Four plots and a crest gage were placed within a riparian buffer on a floodplain that is actively farmed. These four plots were inundated, resulting in measurable deposition, during the November 1, 2019 flood. For site-average $dep_{sed,yr}$, TP_{conc}, and $dep_{TP,yr}$ values we took the average of the four plots.

Site (4). Trout River on the Trout River

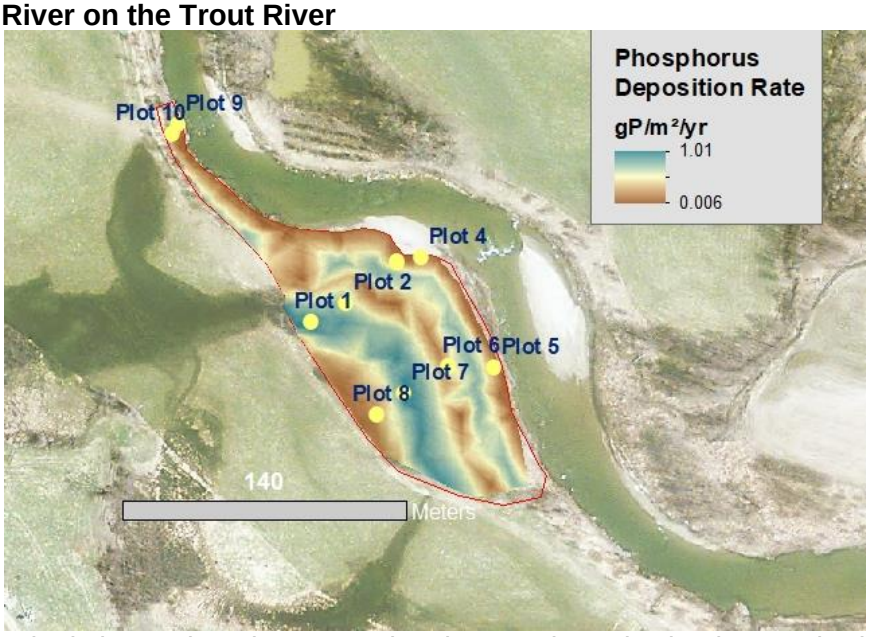

The Trout River site is located on the Trout River in a moderately sized watershed (DA=212 km^2) in a medium energy setting (SSP=67.9 W m^{-2}). Ten plots and a crest gage (co-located with plot04) were placed in transects across ridges and swales on an aggraded point bar and within a riparian buffer. These plots were inundated during the November 1, 2019 flood, resulting in measurable deposition. To determine spatially-averaged $dep_{TP,yr}$ values (see map above), we related distance from the channel bank to $dep_{sed,yr}$ and TP_{conc}, which also corresponded to the topography. Both $dep_{sed,yr}$, TP_{conc} were low close to the channel; $dep_{sed,yr}$ was greatest in swales, while TP_{conc} was greatest along ridges. The resulting spatially-averaged $dep_{TP,yr}$ (0.47 gP m^{-2} yr^{-1}) was 40% greater than the simple average of the plots (0.33 gP m^{-2} yr^{-1}). NOTE: Red outline is the

extent of the floodplain for which topographic and land cover conditions were captured by the plots and is within 2 channel widths from the stream channel.

Site (5). North Troy on the Missisquoi River

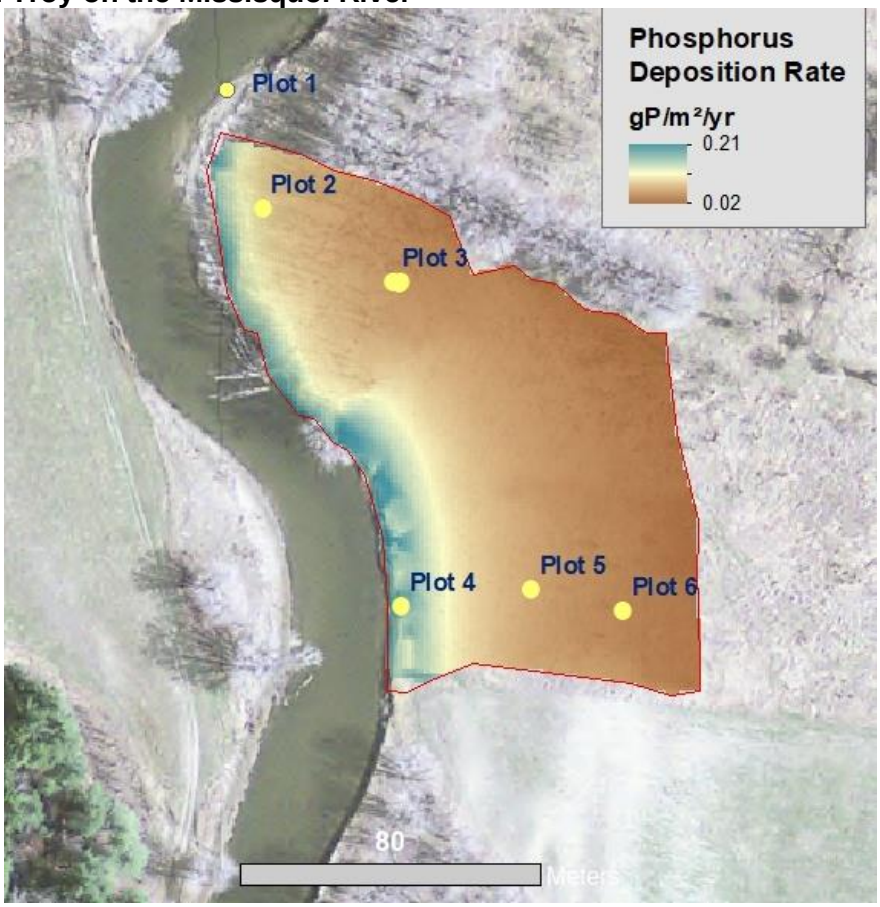

The North Troy site is located on the upper Missisquoi River in a moderately sized watershed (DA=352 km^2) along single-thread channel in a low energy setting (SSP 12.2 W m^{-2}). Six plots and a crest gage (co-located with plot 3) were placed along two transects. These plots were inundated during the November 1, 2019 flood (~130 year RI), resulting in measurable deposition. Turf pads from plot 1 were not recovered because of either excess scour or burial. To determine spatially-averaged $dep_{TP,yr}$ values (see map above), we related distance from the channel bank to $dep_{sed,yr}$ and TP_{conc} dependent on the HAND elevation (for areas less than and greater than 2 m above the channel); $dep_{sed,yr}$ generally decreased with distance from the channel while TP_{conc} generally increased with distance. The resulting spatially-averaged $dep_{TP,yr}$ (0.065 gP m^{-2} yr^{-1}) was within 1% of the simple average of the plots (0.064 gP m^{-2} yr^{-1}). NOTE: Red outline is the extent of the floodplain for which topographic and land cover conditions were captured by the plots and is within 2 channel widths from the stream channel.

Site (6). Richford Farm on the Missisquoi River

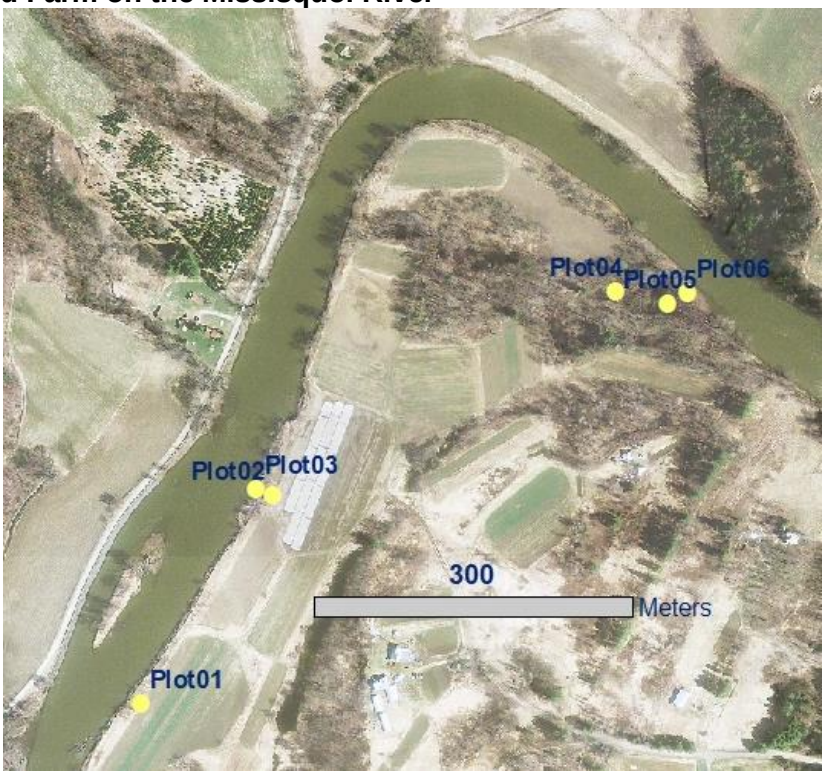

The Richford Farm site is located on the upper Missisquoi River in a large watershed (DA=1215 km^2) in a medium energy setting (SSP 64.6 W m^{-2}). Three plots were placed along a thin riparian buffer (plots 01-03) next to active farm fields, and three plots and a crest gage were placed within a forested riparian wetland (plots04-06). All plots were inundated, resulting in measurable deposition, during the November 1, 2019 flood. Because of large variability in location and land cover, we took averaged the values for the 6 plots to calculate $dep_{sed,yr}$, TP_{conc}, and $dep_{TP,yr}$.

Site (7). Enosburg Falls Farm on the Missisquoi River

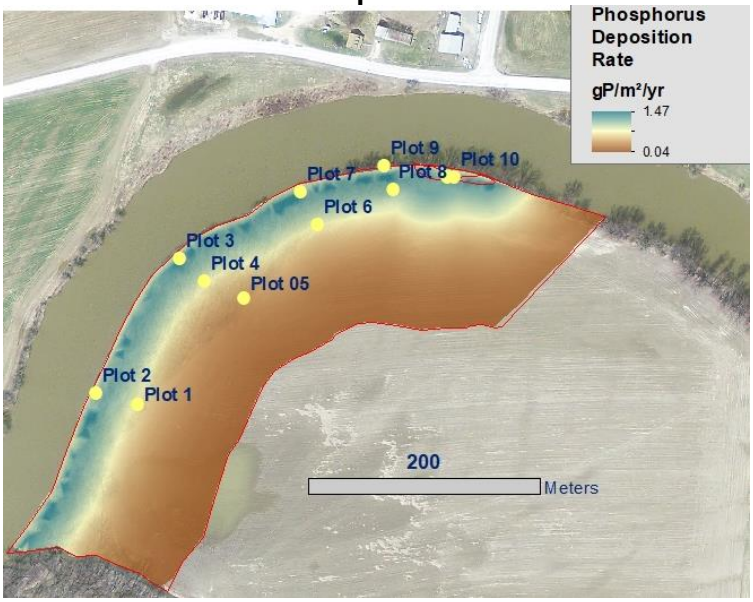

The Enosburg Falls Farm site is located on the mainstem of the Missisquoi River in a large watershed (DA=1707 km^2) along single-thread channel in a low energy setting (SSP 0.8 W m^{-2}). Ten plots and a crest gage (co-located with plot 10) were placed along five transects within the riparian buffer of an actively farmed field. These plots were inundated during the November 1,

2019 flood (~28 year RI), resulting in measurable deposition. To determine spatially-averaged $dep_{TP,yr}$ values (see map above), we related distance from the channel bank to $dep_{sed,yr}$ and TP_{conc}; $dep_{sed,yr}$ initially increased until 10 m from the channel and then decreased, and TP_{conc} generally increased with distance. We extended the sampled area to 2 channel widths, assuming the plots were representative of the full floodplain. The resulting spatially-averaged $dep_{TP,yr}$ (0.43 gP m^{-2} yr^{-1}) was 45% less than the simple average of the plots (0.77 gP m^{-2} yr^{-1}). NOTE: Red outline is the extent of the floodplain for which topographic and land cover conditions were captured by the plots.

Site (8). Atlas on the North Branch Lamoille River

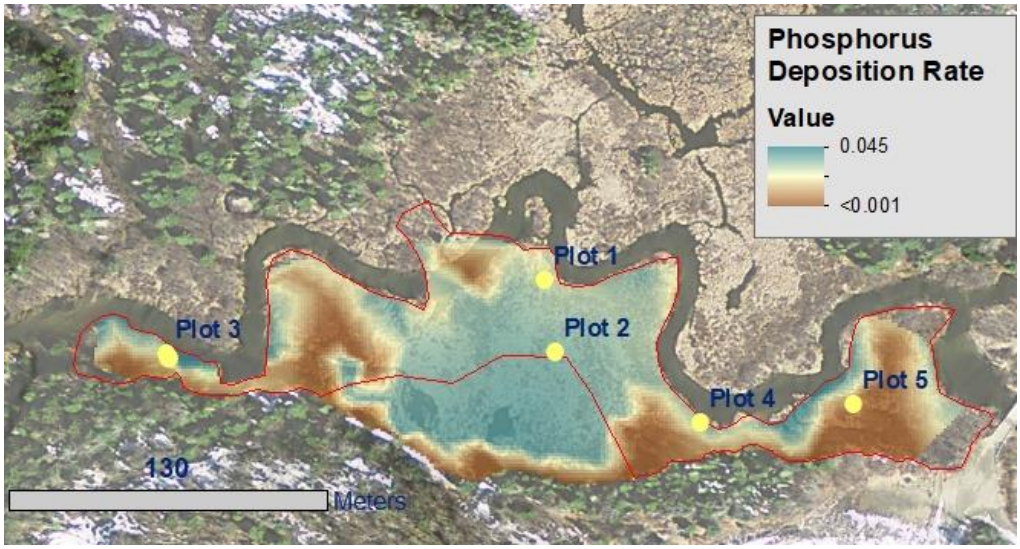

The Atlas site is located on the North Branch Lamoille River in a small watershed (DA=33 km^2) within a riparian wetland in a low energy setting (SSP 1.9 W m^{-2}). Five plots and a crest gage (co-located with plot 3) were placed to capture topographic and land cover variability. These plots were inundated during the November 1, 2019 flood (~126 year RI), resulting in measurable deposition. To determine spatially-averaged $dep_{TP,yr}$ values (see map above), we related distance from the channel bank to $dep_{sed,yr}$ and TP_{conc} based on land cover (scrub/shrub vs emergent wetland from landcover datasets). For both landcover types, $dep_{sed,yr}$ decreased with distance from the channel and TP_{conc} increased with distance; $dep_{sed,yr}$ was greater for scrub/shrub than emergent, but also decreased faster with distance while TP_{conc} was greater for emergent communities. The resulting spatially-averaged $dep_{TP,yr}$ (0.022 gP m^{-2} yr^{-1}) was 6% greater than the simple average of the plots (0.021 gP m^{-2} yr^{-1}). NOTE: Red outline is the extent of the floodplain for which topographic and land cover conditions were captured by the plots that is also within 2 channel widths.

Site (9). Browns on the Browns River

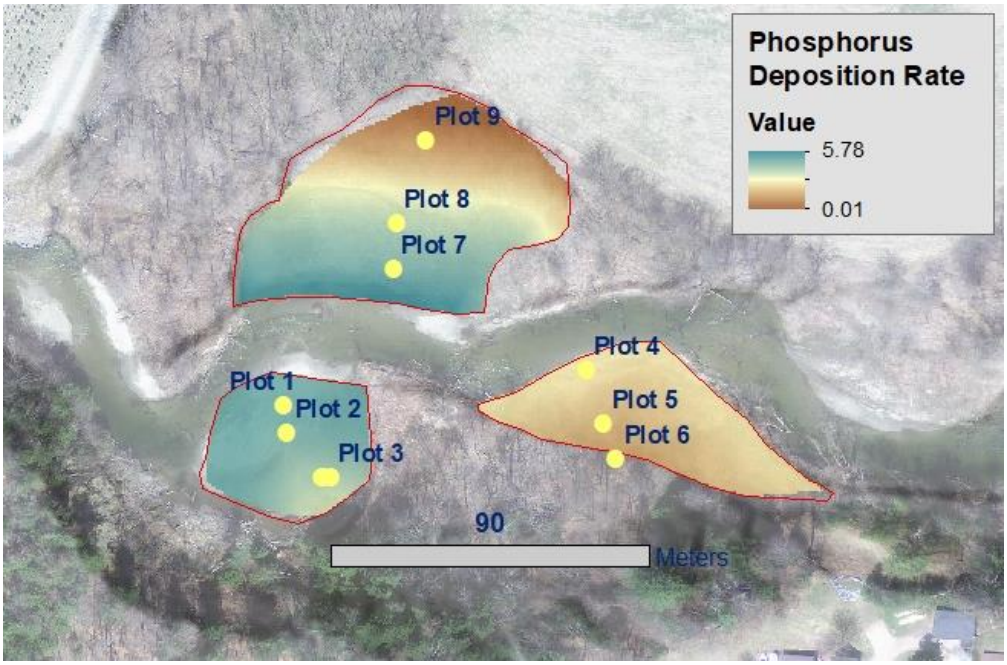

The Browns site is located on the Browns River in a moderately sized watershed (DA=141 km^2) in a medium energy setting (SSP 43.7 W m^{-2}). Five plots and a crest gage (co-located with plot 3) were placed to capture topographic and land cover variability. These plots were inundated during the November 1, 2019 flood (~8.8 year RI), resulting in measurable deposition. To determine spatially-averaged $dep_{TP,yr}$ values (see map above), we related distance from the channel bank to $dep_{sed,yr}$ and TP_{conc} for each isolated floodplain; $dep_{sed,yr}$ decreased with distance from the channel and TP_{conc} increased with distance. The resulting spatially-averaged $dep_{TP,yr}$ (3.25gP m^{-2} yr^{-1}) was 13% greater than the simple average of the plots (2.88 gP m^{-2} yr^{1}). NOTE: Red outline is the extent of the floodplain for which topographic and land cover conditions were captured by the plots that is also within 2 channel widths.

Site (10). Wolcott on the Lamoille River

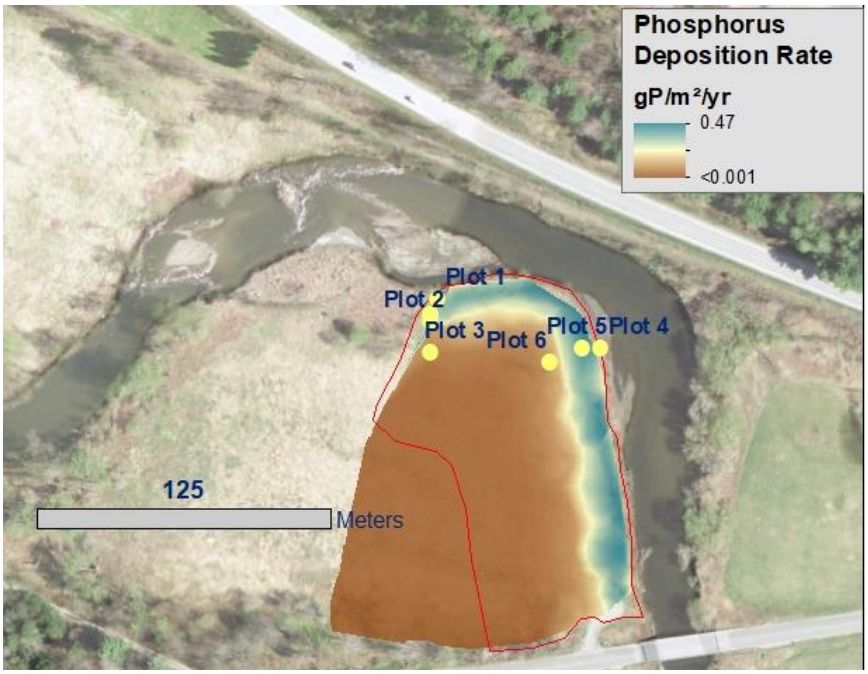

The Wolcott site is located on the Lamoille River in a moderately sized watershed (DA=401 km^2) in a low energy setting (SSP 5.9 W m^{-2}). Six plots and a crest gage (co-located with plot 2) were placed to capture topographic and land cover variability. These plots were inundated during the November 1, 2019 flood (~21 year RI), resulting in measurable deposition. To determine spatially-averaged $dep_{TP,yr}$ values (see map above), we related distance from the channel bank to $dep_{sed,yr}$ and TP_{conc}; $dep_{sed,yr}$ decreased with distance from the channel and TP_{conc} increased with distance. The resulting spatially-averaged $dep_{TP,yr}$ (0.12 gP m^{-2} yr^{-1}) was 55% less than the simple average of the plots (0.27 gP m^{-2} yr^{1}). NOTE: Red outline is the extent of the floodplain for which topographic and land cover conditions were captured by the plots that is also within 2 channel widths.

Site (11). Ryder on the Lamoille River

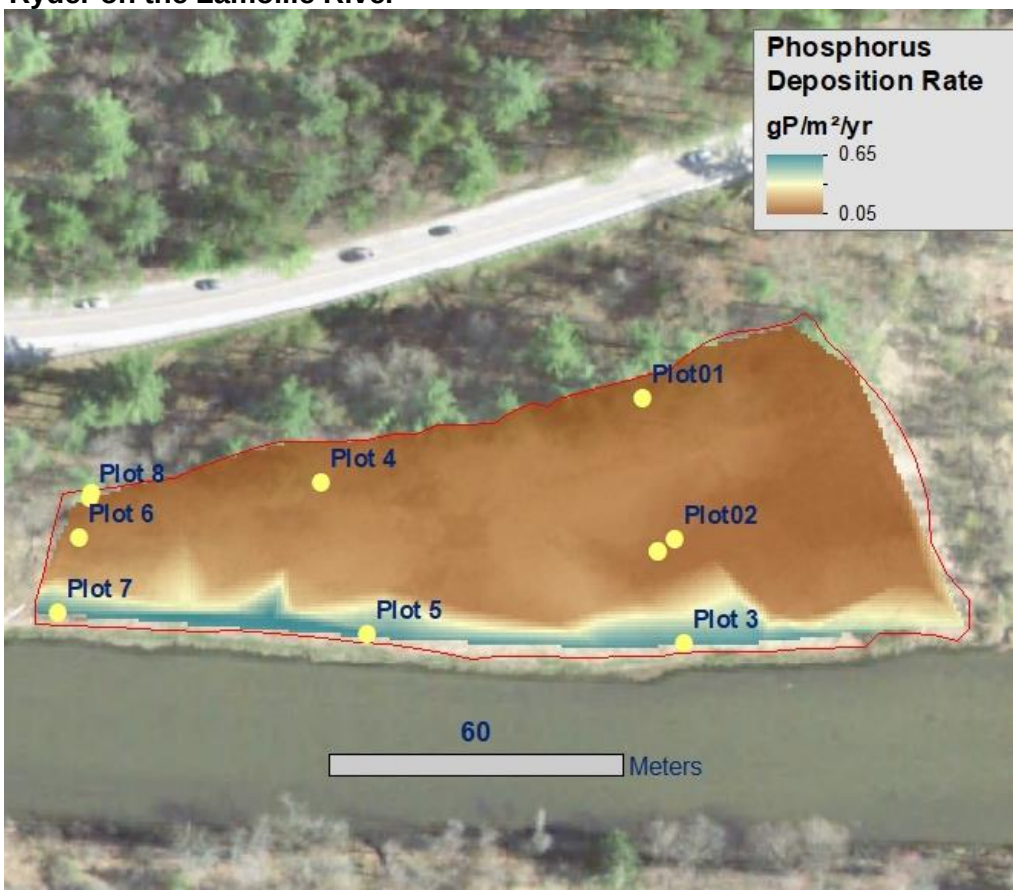

The Ryder site is located on the Lamoille River in a moderately sized watershed (DA=601 km^2) in a medum energy setting (SSP 39.8 W m^{-2}). Eight plots and a crest gage (co-located with plot 2) were placed to capture topographic and land cover variability. These plots were inundated during the November 1, 2019 flood (~30 year RI), resulting in measurable deposition. To determine spatially-averaged $dep_{TP,yr}$ values (see map above), we related elevation above the channel (*HAND*) divided by distance from the channel bank (*D*) to $dep_{sed,yr}$ and TP_{conc}; $dep_{sed,yr}$ increased with *HAND/D* and TP_{conc} decreased with *HAND/D*. The resulting spatially-averaged $dep_{TP,yr}$ (0.15 gP m^{-2} yr^{-1}) was 33% less than the simple average of the plots (0.22 gP m^{-2} yr^{1}). NOTE: Red outline is the extent of the floodplain for which topographic and land cover conditions were captured by the plots that is also within 2 channel widths.

Site (12). Idletyme on the West Branch Little River

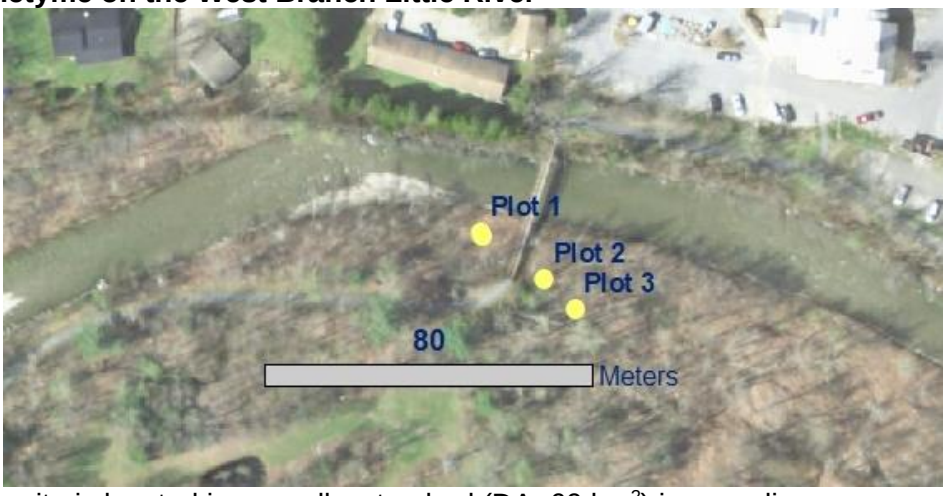

The Idletyme site is located in a small watershed (DA=60 km^2) in a medium energy setting (SSP=137 W m^{-2}). Three plots and a crest gage (co-located with plot 1) were placed on a small floodplain. Plots 1 and 2 were inundated, resulting in measurable deposition, during the November 1, 2019 flood (RI ~ 9.1 yrs). For site-average $dep_{sed,yr}$, TP_{conc}, and $dep_{TP,yr}$ values we took the average of the two plots.

Site (13). Dog River on the Dog River

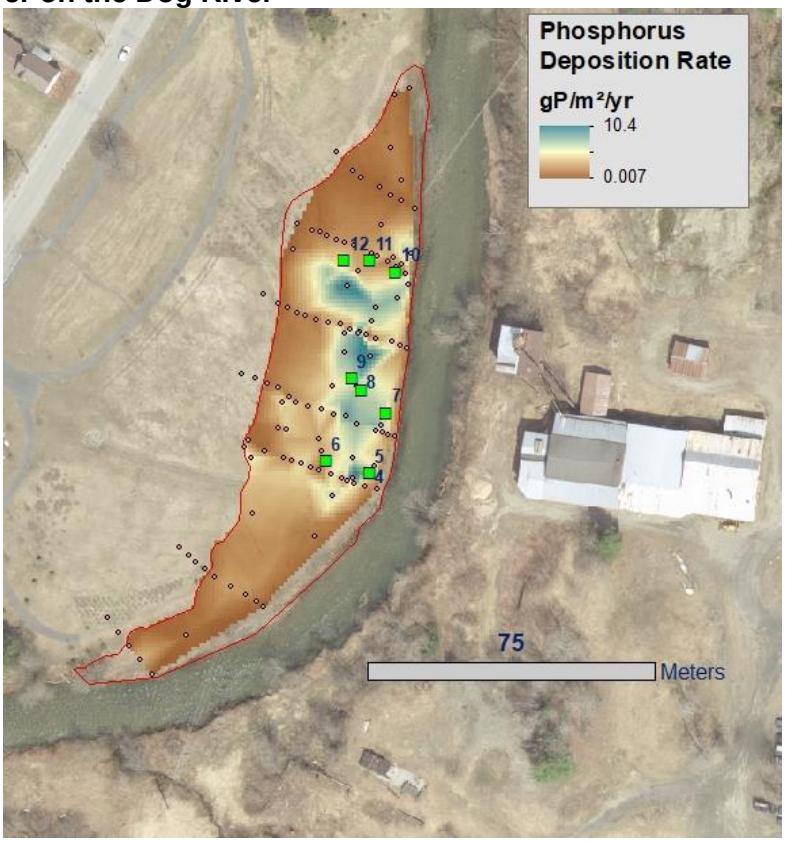

The Dog River site is located in a small watershed (DA=135 km^2) in a medium energy setting (SSP=55.9 W m^{-2}). We visited this site following snowmelt floods in April 2019, and collected 9 cores for analysis of TP, represented by green squares labelled with their sample number (see Table B2 in Appendix B). Because the site is a public park, the ground surface prior to winter and spring floods (2018/19) was well compacted. As a result, the contact between winter/spring flood deposition and the previous surface was easy to identify based on a change in density. An

additional 112 depth measurements were collected, represented by small pink circles. We used this high density network to map $dep_{sed,yr}$ and applied a site-average TP_{conc} value of 439 mg kg^{-1}. Two floods inundated the area between Fall 2018 and April 25, 2019, when we visited the site (RI~4.2 and 7.5 yrs). NOTE: Red outline is the extent of the floodplain for which we identified sediment deposited during winter/spring 2018/19, that is also within 2 channel widths.

Site (14). Lareau on the Mad River

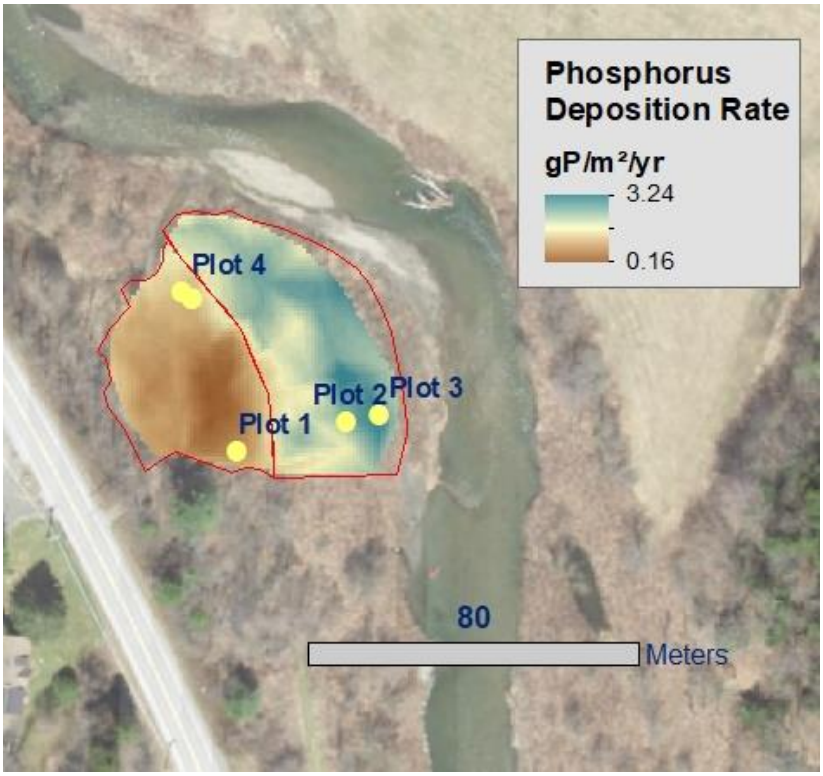

The Lareau site is located on the Mad River in a small watershed (DA=148 km^2) in a medium energy setting (SSP 37.2 W m^{-2}). Four plots and a crest gage (co-located with plot 4) were placed to capture topographic and land cover variability. These plots were inundated during the November 1, 2019 flood (RI ~6.7 yrs), resulting in measurable deposition. To determine spatially-averaged $dep_{TP,yr}$ values (see map above), we related distance from the channel bank $dep_{sed,yr}$ and TP_{conc}; $dep_{sed,yr}$ increased with distance and TP_{conc} decreased with distance. The resulting spatially-averaged $dep_{TP,yr}$ (2.15 gP m^{-2} yr^{-1}) was 7% greater than the simple average of the plots (2.02 gP m^{-2} yr^{1}). NOTE: Red outline is the extent of the floodplain for which topographic and land cover conditions were captured by the plots that is also within 2 channel widths.

Site (15). Dubois on the Winooski River

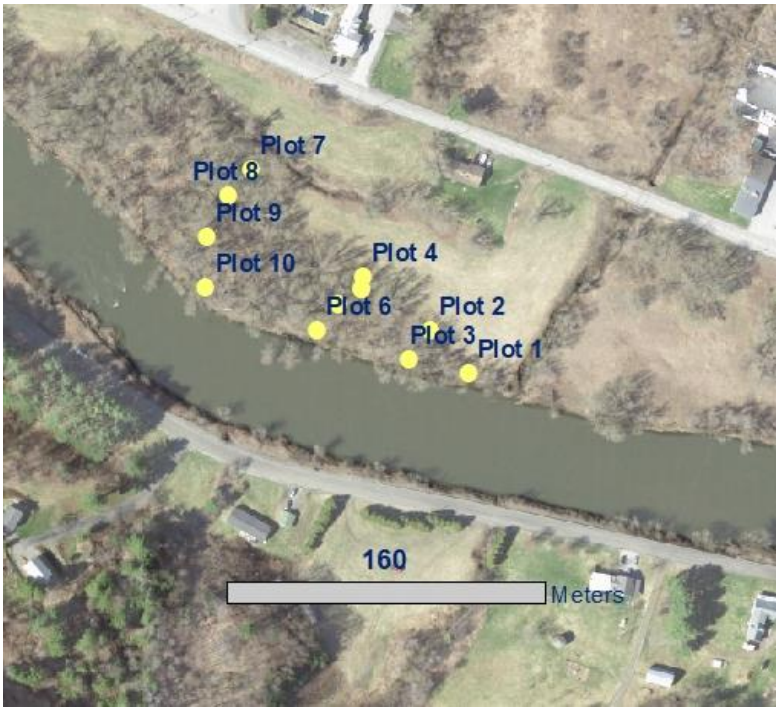

The Dubois site is located on the Winooski River in a large watershed (DA=148 km^2) in a medium energy setting (SSP 35.4 W m^{-2}). Ten plots and a crest gage (co-located with plot 4) were placed to capture topographic and land cover variability. These plots were not inundated during the study period.

Site (16). Jericho Settlers Farm on the Winooski River

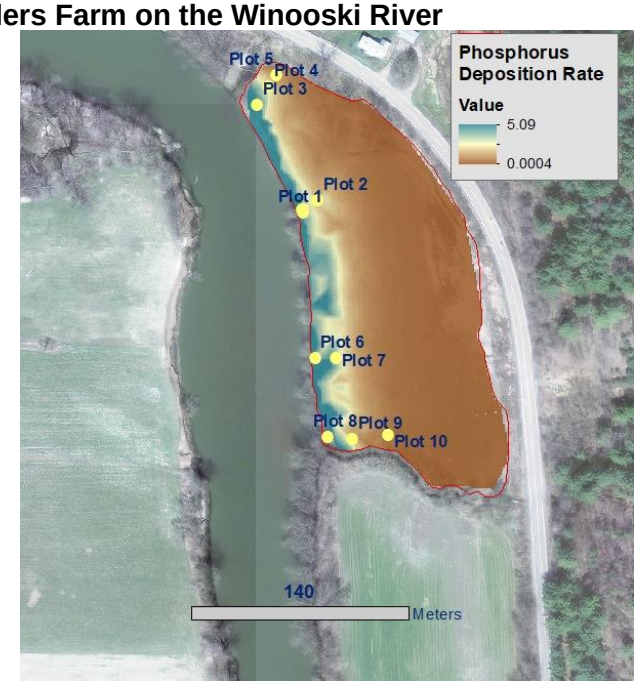

The Jericho Settlers Farm site is located on the Winooski River in a large watershed (DA=2554 km^2) in a medium energy setting (SSP 15.9 W m^{-2}). Ten plots and a crest gage (co-located with plot 1) were placed to capture topographic and land cover variability. These plots were inundated during the November 1, 2019 flood (RI ~6.3 yrs), resulting in measurable deposition. To determine spatially-averaged $dep_{TP,yr}$ values (see map above), we related distance from the channel bank with $dep_{sed,yr}$ and TP_{conc} for HAND elevations that are greater and less than 3.4 m;

$dep_{sed,yr}$ increased with distance and TP_{conc} decreased with distance and $dep_{sed,yr}$ was greater on lower surfaces, whereas TP_{conc} was greater on higher surfaces. The resulting spatially-averaged $dep_{TP,yr}$ (0.54 gP m^{-2} yr^{-1}) was 68% less than the simple average of the plots (1.69 gP m^{-2} yr^{1}). NOTE: Red outline is the extent of the floodplain for which topographic and land cover conditions were captured by the plots that is also within 2 channel widths.

Site (17). McKenzie Park on the Winooski River

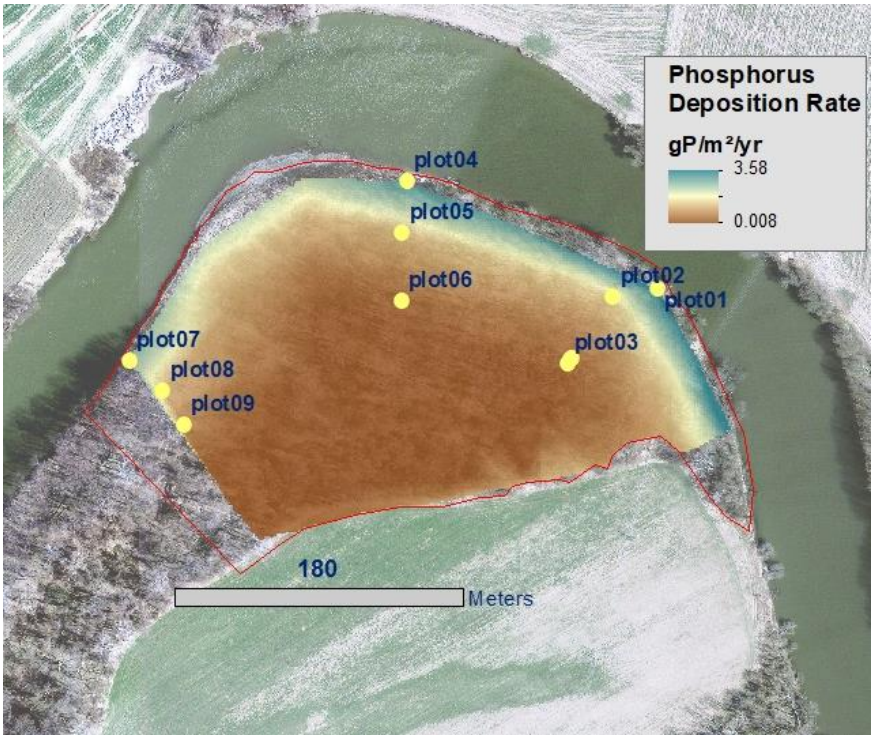

The McKenzie Park site is located on the Winooski River in a large watershed (DA=2745 km^2) in a low energy setting (SSP 3.4 W m^{-2}). Nine plots and a crest gage (co-located with plot 3) were placed in three transects within the riparian forest along the inner bend of the Winooski River. These plots were inundated during the November 1, 2019 flood (RI ~6.5 yrs), resulting in measurable deposition. To determine spatially-averaged $dep_{TP,yr}$ values (see map above), we related distance from the channel bank with $dep_{sed,yr}$ and distance from the channel bank, dependent on *DivAng (*i.e., based on transect location*) for* TP_{conc}; $dep_{sed,yr}$ decreased with distance and TP_{conc} initially increased with distance for high DivAng (i.e., first transect with plots 1-3), and then decreased with distance as DivAng decreased. The resulting spatially-averaged $dep_{TP,yr}$ (0.64 gP m^{-2} yr^{-1}) was 64% less than the simple average of the plots (1.76 gP m^{-2} yr^{1}). NOTE: Red outline is the extent of the floodplain for which topographic and land cover conditions were captured by the plots that is also within 2 channel widths.

Site (18). Cota on Lewis Creek

The Cota site is in a small watershed (DA=48 km2) in a medium energy setting (SSP=48.6 W m^{-2}). Twelve plots and a crest gage (co-located with plot 10) were placed along the floodplain of an actively migrating channel. Six plots were inundated during the October 17, 2019 flood (RI ~1.7 yr), resulting in measurable deposition on five. All plots were inundated during the November 1, 2019 flood (RI ~7.6 yr), resulting in measurable deposition on eleven plots, and erosion around a twelfth. For site-average $dep_{sed,yr}$, TP_{conc}, and $dep_{TP,yr}$ values we found no consistent trends to extrapolate from based on plot-calculated rates, and therefore took the average of all plots.

Site (19). Otter Creek WMA on Otter Creek

The Otter Creek WMA site is in a small watershed (DA=162 km2) in a medium energy setting (SSP=43.8 W m^{-2}). Six plots and a crest gage (co-located with plot 3) were placed in two transects. Three plots were inundated during the November 1, 2019 flood (RI ~1.6 yr), resulting in measurable deposition on two plots, and erosion around a third. For site-average $dep_{sed,yr}$, TP_{conc}, and $dep_{TP,yr}$ value we took the average of the three plots (with a value of "0" assigned to the erosional plot).

Site (20). Lemon Fair on the Lemon Fair River

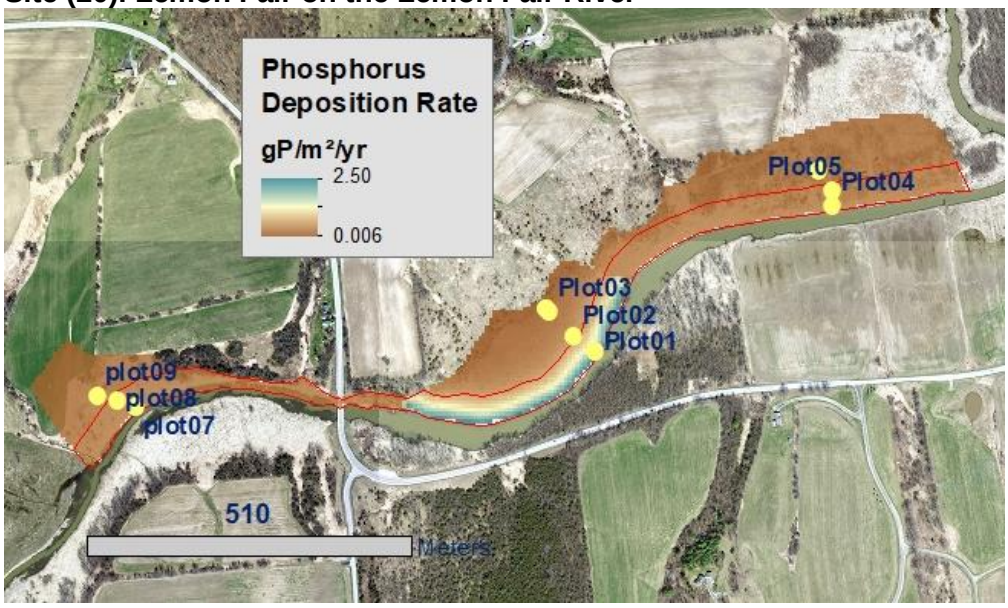

The Lemon Fair site is located on the Lemon Fair River in a moderately sized watershed (DA=177 km^2) in a low energy setting (SSP 0.8 W m^{-2}). Nine plots and a crest gage (co-located with plot 3) were placed in three transects. These plots were inundated during the November 1, 2019 flood (RI ~3.7 yrs), resulting in measurable deposition. Plots 8 and 9 were not re-located likely as a result of scour from ice. To determine spatially-averaged $dep_{TP,yr}$ values (see map above), we related $dep_{sed,yr}$ and TP_{conc} distance from the channel bank, dependent on *DivAng* (i.e., based on divergent vs convergent flow); $dep_{sed,yr}$ decreased with distance and TP_{conc} increased with distance. $dep_{sed,yr}$ values were greater and TP_{conc} less where flow was convergent (i.e., around plots 1-3). The resulting spatially-averaged $dep_{TP,yr}$ (0.59 gP m^{-2} yr^{-1}) was 9% greater than the simple average of the plots (0.54 gP m^{-2} yr^{1}). NOTE: Red outline is the extent of the floodplain for which topographic and land cover conditions were captured by the plots that is also within 2 channel widths.

Site (21). Saunders on the New Haven River

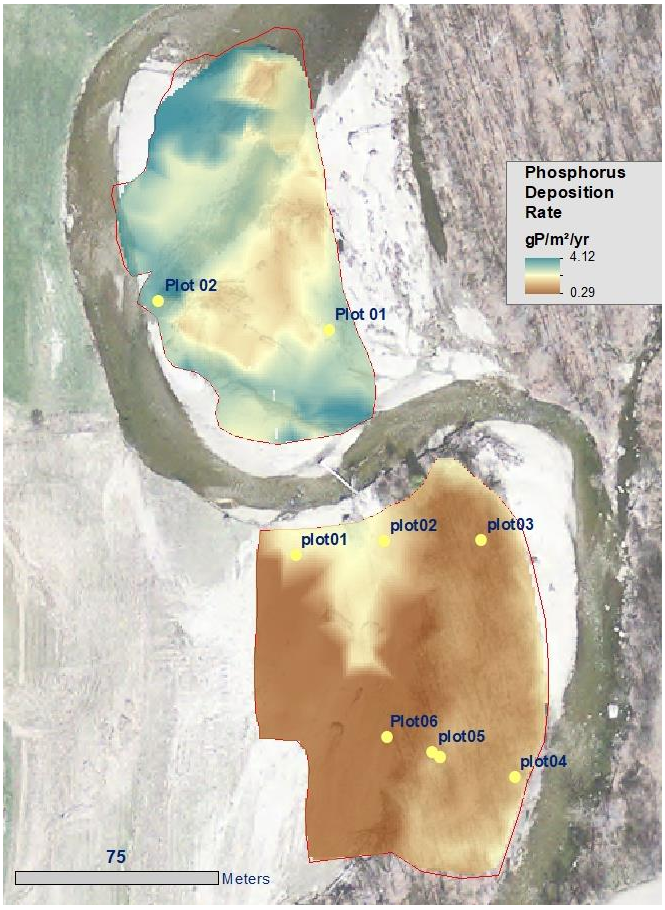

The Saunders site is located on the New Haven River in a moderately sized watershed (DA=184 km^2) in a medium energy setting (SSP 83.4 W m^{-2}). Eight plots and a crest gage (co-located with plot 3) were placed in three transects. All plots were inundated during the June 22, 2019 flood (RI ~3.4 yr), resulting in measurable deposition on seven. All plots were also inundated during the October 17 and November 1, 2019 floods (RI ~8.1 and 21.3 yrs, respectively), resulting in measurable deposition on all plots. To determine spatially-averaged $dep_{TP,yr}$ values (see map above), we related elevation above the channel (*HAND*) to $dep_{sed,yr}$ and distance from the channel (*D*) to TP_{conc}; $dep_{sed,yr}$ generally decreased with *HAND* and TP_{conc} decreased with *D*. The resulting spatially-averaged $dep_{TP,yr}$ (1.71 gP m^{-2} yr^{-1}) was 2% less than the simple average of the plots (1.74 gP m^{-2} yr^{1}). NOTE: Red outline is the extent of the floodplain for which topographic and land cover conditions were captured by the plots that is also within 2 channel widths.

Site (22). Adams on Otter Creek

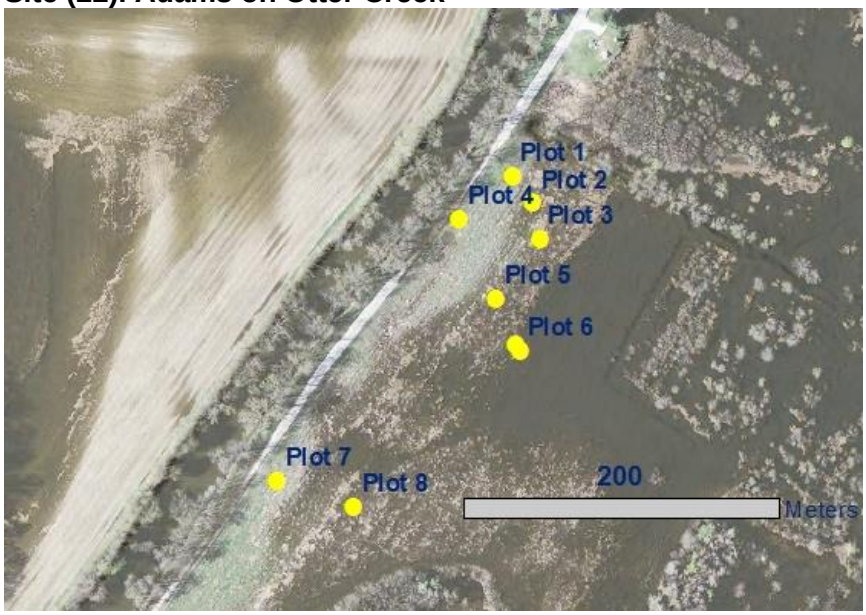

The Adams site is located on Otter Creek in a large watershed (DA=947 km^2) in a low energy setting (SSP 9.1 W m^{-2}). Eight plots and a crest gage (co-located with plot 6) were placed to capture topographic and land cover variability. These plots were inundated during the November 1, 2019 flood (RI ~1.6 yrs) but without any measurable deposition.

Site (23). Desmarais on Otter Creek

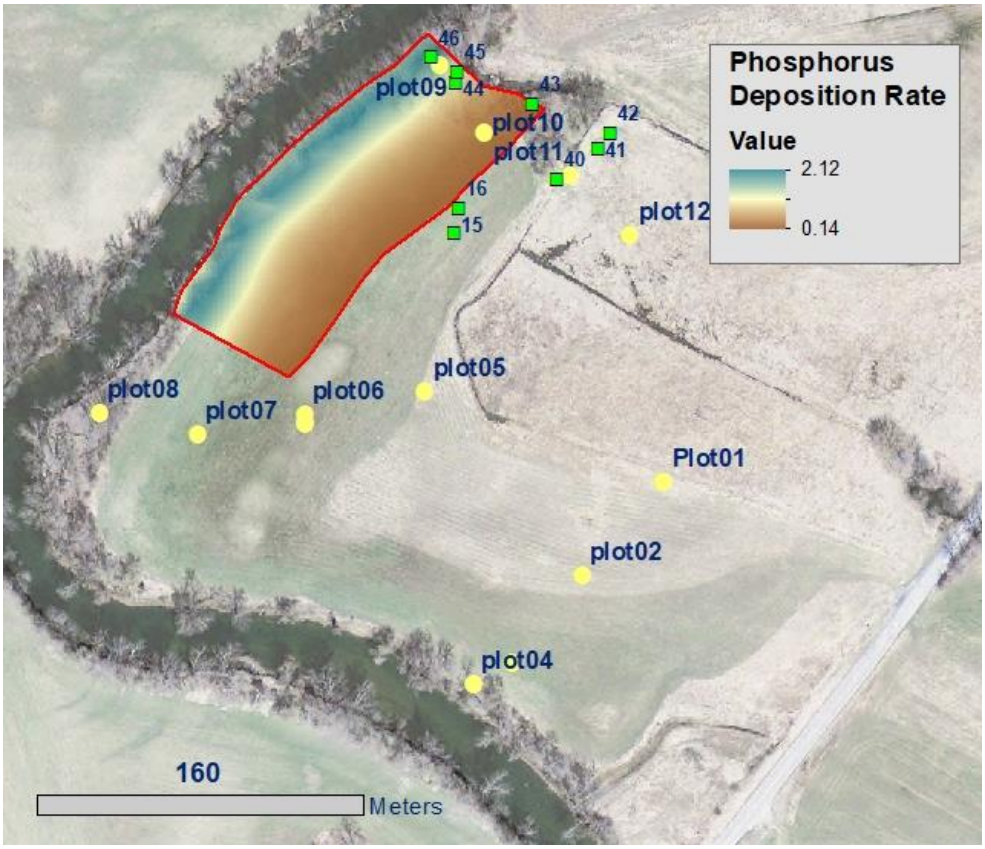

The Desmarais site is located on Otter Creek in a large watershed (DA=1209 km^2) in a low energy setting (SSP 8.6 W m^{-2}). Twelve plots and a crest gage (co-located with plot 6) were placed in three transects. These plots were inundated during the November 1, 2019 flood (RI

~1.6 yrs), but without any measurable deposition. Additionally, we collected nine cores in April 2019 that represented the composite depositional signature of floods that occurred between Fall 2018 and Spring 2019 and included three inundating floods (RI ~2.3, 3.5, and 9.6 yrs). To determine spatially-averaged $dep_{TP,yr}$ values (see map above), we related $dep_{sed,yr}$ and TP_{conc} to distance from the channel bank; $dep_{sed,yr}$ decreased with distance and TP_{conc} increased with distance. The resulting spatially-averaged $dep_{TP,yr}$ (0.93 gP m^{-2} yr^{-1}) was 5% greater than the simple average of the cores and plots (0.89 gP m^{-2} yr^{1}). NOTE: Red outline is the extent of the floodplain for which topographic and land cover conditions were captured by the cores that is also within 2 channel widths.

Site (24). Green Mountain College on the Poultney River

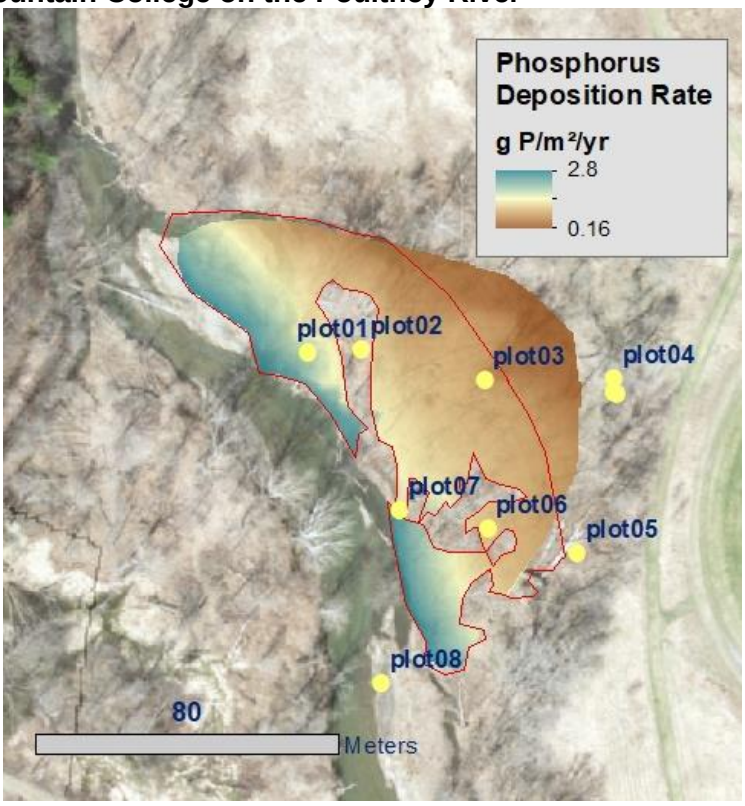

The Green Mountain College site is located on the Poultney River in a moderately sized watershed (DA=129 km^2) in a medium energy setting (SSP 62.5 W m^{-2}). Eight plots and a crest gage (co-located with plot 4) were placed within a riparian forest. Five plots were inundated during the November 1, 2019 flood (RI ~1.4 yrs), with measurable deposition. To determine spatially-averaged $dep_{TP,yr}$ values (see map above), we related $dep_{sed,yr}$ and TP_{conc} to distance from the channel bank; $dep_{sed,yr}$ decreased with distance and TP_{conc} increased with distance. The resulting spatially-averaged $dep_{TP,yr}$ (1.34 gP m^{-2} yr^{-1}) was 6% less than the simple average of the cores and plots (1.42gP m^{-2} yr^{1}). NOTE: Red outline is the extent of the floodplain for which topographic and land cover conditions were captured by the plots that is also within 2 channel widths.

Appendix E: List of Variables

Variable	Unit	Description
D	m	distance from plot to channel bank (m)
DA	km^2	drainage area
D_{CH}	$m\ m^{-1}$	distance from plot to channel bank/channel width
dep_{sed}	$kg\ m^{-2}$	sediment deposition
$dep_{sed,yr}$	$kg\ m^{-2}\ yr^{-1}$	annual sediment deposition rate
dep_{TP}	$g\ P\ m^{-2}$	phosphorus deposition
$dep_{TP,yr}$	$g\ P\ m^{-2}\ yr^{-1}$	annual phosphorus deposition rate
$dep_{TP,yr,2ch}$	$g\ P\ m^{-1}\ yr^{-1}$	annual floodplain phosphorus deposition (for area within 2 channel widths)
$DivAng$	degree	angle between channel and floodplain flow
$HAND$	m	relative elevation above the channel
$Inun$	-	annual probability of inundation
IR	$m\ m^{-1}$	incision measured as ratio of inset bench to bankfull depth
S_{CH}	$m\ m^{-1}$	channel slope
SSP	$W\ m^{-2}$	specific stream power
W_{FP}	m	floodplain width
$W_{FP/CH}$	$m\ m^{-1}$	floodplain width/channel width
WS_{AG}	-	% area watershed in agriculture
WS_{GL}	-	% area watershedhydrologic soils group D
WS_{HSGD}	-	% area watershed glaciolacustrine
WS_{IMP}	-	% area watershed impervious cover
WS_{WET}	-	% area watershed wetland
X_{tree}	-	% area within 10 m radius with tree canopy

Appendix F: ICP Quality Control (QC) Reports

Tables provided in this appendix detail quality control measures documented for laboratory analysis of total phosphorus concentration in sediments collected in this study. The Perkin Elmer Avio 300 ICP-OES was calibrated for each lab run using four calibrations standards (0, 2, 5 and 10 mg/L P) and verified with up to three quality control (QC) samples obtained from a NIST-traceable source and covering the lower 25%, middle 50% and upper 25% of the calibration range (table a). The calibration is deemed acceptable if the middle and upper QC samples are within 5% of their certified value, the lower QC sample is within 10% of its certified value (table b), and the digestion blank (table c, no sediment sample in the digestion solution) is below 0.1 mg/l. For each lab run, composited samples from at least one plot were run in duplicate (table d) to assess reproducibility. A reference soil from the North American Proficiency Testing Program, with a sample of known TP concentration, was processed with each run to assess recovery.

“Sample ID” in section (d) corresponds to “Site” in Table 2. JSF = Jericho Settlers Farm.

Run date: 7/16/2019

a) Calibration QCs--results. Second column is certified value, columns a-i are QC results

QC	actual	a	b	c	d	e	f	g	h	i
	mg/L	mg/L	mg/L	mg/L	mg/L	mg/L	mg/L	mg/L	mg/L	mg/L
1	10.00	10.39	10.67	10.80	10.73	10.66	10.76	10.46	10.74	10.71

b) Calibration QCs--error. Error relative to actual value of each QC

QC		a	b	c	d	e	f	g	h	i
	mg/L	mg/L	mg/L	mg/L	mg/L	mg/L	mg/L	mg/L	mg/L	mg/L
1	error < 5%	3.9%	6.7%	8.0%	7.3%	6.6%	7.6%	4.6%	7.4%	7.1%

c) Laboratory digestion blank

Run ID	Acceptable MDL mg/L	Result mg/L
B1-14	0.10	0.00
B2-14	0.10	-0.02
B4-14	0.10	-0.02
B5-14	0.10	-0.02
B6-14	0.10	-0.01

d) Duplication. 2nd column is first run, 3rd column is duplicate run, 4th column is error between the two

Sample ID	P mg/L	Dup mg/L	error
Dog River_06	510	466	4.5%
Dog River_07	509	467	4.2%
Browns_01	696	782	5.8%
JSF_06	835	848	0.7%
Saunders_02	667	686	1.5%
Saunders_03	869	786	5.1%
Cota_04	824	818	0.4%

e) Reference Soil: Oldham (from North American Proficiency Testing Program)

	mg/kg	recovery
actual	476	
B2-12	481	101.0%
B3-12	471	98.9%
B4-12	463	97.2%
B5-12	448	94.2%

Run date: 7/22/2019

a) Calibration QCs--results. Second column is certified value, columns a-i are QC results

QC	actual	a	b	c	d	e
	mg/L	mg/L	mg/L	mg/L	mg/L	mg/L
1	20.00	20.2	19.8	20.1		
2	5.00	5.19	5.15	5.13	5.11	5.09

b) Calibration QCs--error. Error relative to actual value of each QC

QC	actual	a	b	c	d	e
	mg/L	mg/L	mg/L	mg/L	mg/L	mg/L
	error < 5%	0.9%	0.8%	0.7%		
	error < 5%	3.9%	3.0%	2.7%	2.2%	1.8%

c) Laboratory digestion blank

Run ID	Acceptable MDL mg/L	Result mg/L
B7-14	0.10	-0.04
B8-14	0.10	-0.05
B9-14	0.10	-0.04
B10-14	0.10	-0.06
B11-14	0.10	-0.03

d) Duplication. 2nd column is first run, 3rd column is duplicate run, 4th column is error between the two

Sample ID	P mg/L	Dup mg/L	error
Cota_05	518	587	6.3%
JSF_09	582	596	1.2%
JSF_08	650	610	3.2%
Adams_06	492	529	3.7%
Adams_04	676	698	1.6%

e) Reference Soil: Oldham (from North American Proficiency Testing Program)

	mg/kg	recovery
actual	476	
B7-12	471	98.9%
B8-12	432	90.8%
B9-12	473	99.3%
B10-12	482	101.2%
B11-12	478	100.5%

Run date: 8/3/2020

a) Calibration QCs--results. Second column is certified value, columns a-f are QC results

QC	actual	a	b	c	d	e	f
	mg/L	mg/L	mg/L	mg/L	mg/L	mg/L	mg/L
1	5.00	4.80	4.78	4.82	4.82	4.85	4.86
2	0.20	0.21	0.20	0.20	0.18	0.21	0.21
3	0.00	0.06	0.04	0.05	0.05	0.05	0.05

b) Calibration QCs--error. Error relative to actual value of each QC

QC		a	b	c	d	e	f
1	error < 5%	4.1%	4.4%	3.6%	3.5%	2.9%	2.7%
2	error < 10%	4.6%	0.7%	0.7%	12.0%	4.2%	5.6%
3	MDL=0.1	<MDL	<MDL	<MDL	<MDL	<MDL	<MDL

c) Laboratory digestion blank

Run ID	Acceptable MDL mg/L	Result mg/L
B1-1	0.10	0.098
B2-1	0.10	0.098

d) Duplication. 2nd column is first run, 3rd column is duplicate run, 4th column is error between the two

Sample ID	P mg/L	Dup mg/L	error
JSF_Plot01_TP	722	724	0.2%
JSF_Plot02_TP	785	733	3.5%
JSF_Plot03_TP	721	698	1.6%
JSF_Plot04_TP	789	825	2.2%
JSF_Plot05_TP	789	847	3.5%
JSF_Plot06_TP	669	706	2.6%
JSF_Plot07_TP	781	732	3.2%
JSF_Plot08_TP	713	755	2.9%
JSF_Plot09_TP	727	696	2.2%
JSF_Plot10_TP	761	782	1.4%
BlackCreek1_Plot01_TP	763	777	0.9%
BlackCreek1_Plot02_TP	952	899	2.9%
Trout_10_TP	588	609	1.8%

e) Reference Soil: Oldham (from North American Proficiency Testing Program)

	mg/kg	recovery
actual	476	
B4-2	442	92.9%

Run date: 8/14/2020, Run 2

a) Calibration QCs--results. Second column is certified value, columns a-f are QC results

QC	actual	a	b	c	d	e	f
	mg/L	mg/L	mg/L	mg/L	mg/L	mg/L	mg/L
1	5.00	5.07	4.88	5.05	4.66	5.00	5.06
2	0.20	0.20	0.19	0.18	0.17	0.21	0.19
3	0.00	0.04	0.05	0.05	0.05	0.05	0.05

b) Calibration QCs--error. Error relative to actual value of each QC

QC		a	b	c	d	e	f
1	error < 5%	1.4%	2.4%	1.0%	6.8%	0.0%	1.2%
2	error < 10%	0.5%	7.4%	11.7%	14.1%	6.7%	3.9%
3	MDL=0.1	<MDL	<MDL	<MDL	<MDL	<MDL	<MDL

c) Laboratory digestion blank

Run ID	Acceptable MDL mg/L	Result mg/L
B4-1	0.01	0.094

d) Duplication. 2nd column is first run, 3rd column is duplicate run, 4th column is error between the two

Sample ID	P mg/L	Dup mg/L	error
Atlas_01_TP	493	498	0.5%

e) Reference Soil: Oldham (from North American Proficiency Testing Program)

	mg/kg	recovery
actual	476	
B4-2	442	92.9%

Run date: 9/2/2020

a) Calibration QCs--results. Second column is certified value, columns a-h are QC results

QC	actual	a	b	c	d	e	f	g	h
	mg/L	mg/L	mg/L	mg/L	mg/L	mg/L	mg/L	mg/L	mg/L
1	5.00	5.00	4.89	4.87	4.87	4.83	4.78	4.74	4.84
2	0.20	0.20	0.20	0.19	0.21	0.21	0.20	0.20	0.18
3	0.00	0.008	-0.004	-0.005	-0.003	-0.008	-0.008	-0.013	-0.007

b) Calibration QCs--error. Error relative to actual value of each QC

QC		a	b	c	d	e	f	g	h
1	error < 5%	0.1%	2.2%	2.7%	2.5%	3.5%	4.4%	5.2%	3.2%
2	error < 10%	0.6%	1.7%	3.8%	4.9%	3.2%	2.4%	2.4%	11.3%
3	MDL=0.1	<MDL	<MDL	<MDL	<MDL	<MDL	<MDL	<MDL	<MDL

c) Laboratory digestion blank

Run ID	Acceptable	Result
	MDL mg/L	mg/L
B5-1	0.01	0.046
B7-1	0.01	0.081

d) Duplication. 2nd column is first run, 3rd column is duplicate run, 4th column is error between the two

Sample ID	P mg/L	Dup mg/L	error
EPSCoR_02_TP	1239	1210	1.2%
Ryder_01_TP	518	522	0.4%
EnosburgFarm02_TP	727	750	1.5%

e) Reference Soil: Oldham (from North American Proficiency Testing Program)

	mg/kg	recovery
actual	476	
B5-2	457	96.0%
B6-2	424	89.1%
B7-2	461	96.9%

Appendix G: Generalized Linear Model Results

Table G1. Model selection results using site-scale data to describe annual phosphorus deposition ($dep_{TP,yr,2ch}$)

Rank	Model for Annual Phosphorus Deposition	df	AIC	delta AIC	AICweight
1	$IR+WS_{IMP}+DA*SSP$	5	226.38	0.00	0.13
2	$WS_{IMP}+DA*SSP$	4	226.65	0.27	0.11
3	$IR+DA*SSP$	4	227.68	1.30	0.07
4	$DA*SSP$	3	227.70	1.32	0.07
5	$WS_{IMP}+W_{FP/CH}+DA*SSP$	5	227.80	1.42	0.06
6	$IR+WS_{IMP}+WS_{GL}+DA*SSP$	6	228.03	1.65	0.06
7	$IR+WS_{IMP}+W_{FP/CH}+DA*SSP$	6	228.32	1.94	0.05
8	$IR+WS_{IMP}+WS_{WET}+DA*SSP$	6	228.33	1.95	0.05
9	$IR+WS_{IMP}+WS_{AG}+DA*SSP$	6	228.38	2.00	0.05
10	$IR+W_{FP}*SSP$	4	228.59	2.21	0.04
11	$W_{FP/CH}+DA*SSP$	4	228.97	2.59	0.04
12	$IR+WS_{GL}+DA*SSP$	5	229.24	2.86	0.03
13	$IR+WS_{AG}+DA*SSP$	5	229.50	3.12	0.03
14	$IR+W_{FP/CH}+DA*SSP$	5	229.64	3.26	0.03
15	$WS_{IMP}+W_{FP/CH}+WS_{GL}+DA*SSP$	6	229.70	3.32	0.02
16	$WS_{IMP}+W_{FP/CH}+WS_{AG}+DA*SSP$	6	229.80	3.42	0.02
17	$IR+WS_{IMP}+WS_{GL}+WS_{WET}+DA*SSP$	7	229.99	3.61	0.02
18	$IR+WS_{IMP}+WS_{GL}+W_{FP/CH}+DA*SSP$	7	230.00	3.62	0.02
19	$W_{FP/CH}*SSP$	3	230.34	3.96	0.02
20	$IR+WS_{GL}+W_{FP}*SSP$	5	230.43	4.05	0.02
21	$IR+WS_{WET}+W_{FP}*SSP$	5	230.44	4.06	0.02
22	$IR+WS_{AG}+W_{FP}*SSP$	5	230.49	4.11	0.02
23	$WS_{GL}+W_{FP/CH}+DA*SSP$	5	230.81	4.43	0.01
24	W_{WET}	2	234.15	7.77	0.00
25	WS_{IMP}	2	234.22	7.84	0.00
26	W_{AG}	2	234.94	8.56	0.00
27	1	1	234.95	8.57	0.00
28	W_{GL}	2	235.53	9.15	0.00
29	IR	2	236.85	10.47	0.00
30	$DA+IR+WS_{IMP}+WS_{AG}$	5	236.89	10.51	0.00
31	$W_{FP/CH}$	2	236.93	10.55	0.00
32	$W_{FP}+IR$	3	237.18	10.80	0.00
33	$W_{FP}+IR+WS_{AG}$	4	237.49	11.11	0.00
34	$DA+IR$	3	237.67	11.29	0.00
35	$DA+IR+WS_{IMP}$	4	237.72	11.34	0.00
36	$W_{FP}+IR+WS_{GL}$	4	237.86	11.48	0.00
37	$DA+IR+WS_{IMP}+WS_{GL}$	5	238.21	11.83	0.00
38	$DA+IR+WS_{GL}$	4	238.45	12.07	0.00

Table G2. Model selection results using site-scale data to describe efficiency.

Rank	Model for Efficiency	df	AIC	delta AIC	AICweight
1	$IR+WS_{IMP}+DA*SSP$	5	11.71	0.00	0.27
2	$IR+WS_{IMP}+WS_{WET}+DA*SSP$	6	13.09	1.37	0.13
3	$IR+WS_{IMP}+WS_{GL}+DA*SSP$	6	13.60	1.89	0.10
4	$IR+WS_{IMP}+W_{FP/CH}+DA*SSP$	6	13.62	1.91	0.10
5	$IR+WS_{IMP}+WS_{AG}+DA*SSP$	6	13.68	1.97	0.10
6	$IR+WS_{IMP}+WS_{GL}+WS_{WET}+DA*SSP$	7	14.93	3.22	0.05
7	$IR+W_{FP}*SSP$	4	15.13	3.41	0.05
8	$IR+WS_{IMP}+WS_{GL}+W_{FP/CH}+DA*SSP$	7	15.53	3.82	0.04
9	$IR+DA*SSP$	4	15.82	4.11	0.03
10	$IR+WS_{WET}+W_{FP}*SSP$	5	16.78	5.07	0.02
11	$IR+WS_{AG}+W_{FP}*SSP$	5	17.04	5.33	0.02
12	$IR+WS_{GL}+W_{FP}*SSP$	5	17.09	5.38	0.02
13	$IR+WS_{GL}+DA*SSP$	5	17.63	5.91	0.01
14	$IR+WS_{AG}+DA*SSP$	5	17.71	6.00	0.01
15	$IR+W_{FP/CH}+DA*SSP$	5	17.76	6.05	0.01
16	$WS_{IMP}+W_{FP/CH}+DA*SSP$	5	19.69	7.98	0.00
17	$WS_{IMP}+DA*SSP$	4	20.48	8.77	0.00
18	$WS_{IMP}+W_{FP/CH}+WS_{AG}+DA*SSP$	5	21.61	9.89	0.00
19	$WS_{IMP}+W_{FP/CH}+WS_{GL}+DA*SSP$	5	21.63	9.92	0.00
20	$W_{FP/CH}+DA*SSP$	4	22.26	10.55	0.00
21	$DA*SSP$	3	22.55	10.83	0.00
22	$DA+IR+WS_{IMP}+WS_{AG}$	5	23.25	11.54	0.00
23	WS_{IMP}	2	23.39	11.67	0.00
24	$W_{FP/CH}*SSP$	3	23.83	12.12	0.00
25	$WS_{GL}+W_{FP/CH}+DA*SSP$	5	24.25	12.54	0.00
26	$DA+IR+WS_{IMP}+WS_{GL}$	5	24.79	13.08	0.00
27	$DA+IR+WS_{IMP}$	4	24.97	13.26	0.00
28	$W_{FP}+IR$	3	25.06	13.35	0.00
29	$W_{FP}+IR+WS_{AG}$	4	25.15	13.44	0.00
30	$W_{FP}+IR+WS_{GL}$	4	25.22	13.51	0.00
31	$DA+IR$	3	26.41	14.70	0.00
32	1	1	26.60	14.89	0.00
33	$DA+IR+WS_{GL}$	4	26.80	15.09	0.00
34	W_{AG}	2	26.94	15.22	0.00
35	$W_{FP/CH}$	2	27.11	15.40	0.00
36	W_{GL}	2	27.19	15.48	0.00
37	IR	2	27.28	15.56	0.00
38	W_{WET}	2	27.78	16.06	0.00

Table G3. Model selection results using plot-scale data to describe phosphorus deposition rates ($dep_{TP,yr}$)

Rank	Model for Annual Phosphorus Deposition Rate	df	AIC	delta AIC	AICweight
1	$\ln(D)+W_{FP/CH}+X_{tree}+Inun+dep_{TP,yr,2ch}+SSP$	7	381.9	0.0	0.45
2	$\ln(D)+W_{FP/CH}+HAND+X_{tree}+Inun+dep_{TP,yr,2ch}+SSP$	8	382.7	0.8	0.31
3	$\ln(D)+X_{tree}+W_{FP/CH}+Inun+dep_{TP,yr,2ch}$	6	386.0	4.1	0.06
4	$\ln(D)+W_{FP/CH}+HAND+Inun+dep_{TP,yr,2ch}$	6	386.4	4.5	0.05
5	$\ln(D)+W_{FP/CH}+HAND+Inun+X_{tree}+dep_{TP,yr,2ch}$	7	386.5	4.6	0.05
6	$\ln(D_{CH})+W_{FP/CH}+HAND+X_{tree}+Inun+dep_{TP,yr,2ch}+SSP$	8	386.9	5.0	0.04
7	$\ln(D)+W_{FP/CH}+Inun+dep_{TP,yr,2ch}$	5	388.4	6.5	0.02
8	$\ln(D)+Inun+HAND+dep_{TP,yr,2ch}$	5	390.1	8.2	0.01
9	$\ln(D_{CH})+W_{FP/CH}+X_{tree}+Inun+dep_{TP,yr,2ch}+SSP$	7	390.4	8.5	0.01
10	$\ln(D)+X_{tree}+Inun+dep_{TP,yr,2ch}$	5	390.6	8.7	0.01
11	$\ln(D)+Inun+dep_{TP,yr,2ch}$	4	391.1	9.2	0.00
12	$\ln(D)+X_{tree}+Inun+HAND+dep_{TP,yr,2ch}$	6	391.2	9.3	0.00
13	$\ln(D)+Inun+HAND+dep_{TP,yr,2ch}+SSP$	6	391.5	9.6	0.00
14	$\ln(D)+X_{tree}+DivAng+Inun+dep_{TP,yr,2ch}$	6	392.1	10.2	0.00
15	$\ln(D)+DivAng+Inun+dep_{TP,yr,2ch}$	5	392.2	10.3	0.00
16	$\ln(D)+Inun+dep_{TP,yr,2ch}+SSP$	5	392.3	10.4	0.00
17	$\ln(D_{CH})+W_{FP/CH}+HAND+X_{tree}+Inun+dep_{TP,yr,2ch}$	7	393.0	11.1	0.00
18	$\ln(D_{CH})+W_{FP/CH}+HAND+Inun+dep_{TP,yr,2ch}$	6	394.1	12.2	0.00
19	$\ln(D_{CH})+X_{tree}+W_{FP/CH}+Inun+dep_{TP,yr,2ch}$	6	396.8	14.9	0.00
20	$\ln(D_{CH})+Inun+HAND+dep_{TP,yr,2ch}$	5	397.4	15.5	0.00
21	$\ln(D_{CH})+X_{tree}+Inun+HAND+dep_{TP,yr,2ch}$	6	397.7	15.8	0.00
22	$\ln(D_{CH})+Inun+HAND+dep_{TP,yr,2ch}+SSP$	6	398.2	16.3	0.00
23	$\ln(D_{CH})+X_{tree}+Inun+dep_{TP,yr,2ch}$	5	401.0	19.1	0.00
24	$\ln(D_{CH})+Inun+dep_{TP,yr,2ch}$	4	405.6	23.7	0.00
25	$\ln(D_{CH})+Inun+dep_{TP,yr,2ch}+SSP$	5	406.0	24.1	0.00
26	$Inun+dep_{TP,yr,2ch}$	3	410.5	28.6	0.00
27	$\ln(D)+HAND+dep_{TP,yr,2ch}+SSP$	5	413.2	31.3	0.00
28	$\ln(D_{CH})+HAND+dep_{TP,yr,2ch}+SSP$	5	418.0	36.1	0.00
29	$\ln(D)+dep_{TP,yr,2ch}$	3	418.7	36.8	0.00
30	$HAND+dep_{TP,yr,2ch}$	3	426.8	44.9	0.00
31	$\ln(D_{CH})+dep_{TP,yr,2ch}$	3	430.0	48.1	0.00
32	$X_{tree}+dep_{TP,yr,2ch}$	3	431.5	49.6	0.00
33	$dep_{TP,yr,2ch}$	2	435.3	53.4	0.00
34	$DivAng+dep_{TP,yr,2ch}$	3	436.2	54.3	0.00
35	Null	1	470.3	88.4	0.00

Appendix H: Floodplain Framework Application Instructions

To adopt the prioritization function:

1) Calculate DA and slope for all reaches within the region of interest and determine if the reach is likely to be depositional (Figure 2).
2) For reaches that are likely to be depositional, calculate or identify *IR*, WS_{IMP}, and *SSP*
3) Apply site-scale $dep_{TP,yr,2ch}$ models to calculate $dep_{TP,yr,2ch}$ for existing conditions
    a. If WS_{IMP} <2.5%, use model#1 (Table 8) to calculate $dep_{TP,yr,2ch}$
    b. Otherwise, use model#3.
4) Lower all IR values to "1" and repeat step (3) to calculate $dep_{TP,yr,2ch}$ for potential conditions
5) Subtract existing from potential to get "potential gain"
6) Identify the 1st, 2nd, 3rd, and 4th quartiles of existing and potential gain and rank reaches.

. The specific steps to apply the intervention function include:

1) Calculate $dep_{TP,yr}$ for existing conditions using GLM models
    a. For site of interest, follow steps 2 through 3 from the prioritization function, described above.
    b. To evaluate changes in floodplain topography or riparian tree planting, use $dep_{TP,yr,2ch}$ from (a), *SSP, and* $W_{FP/CH}$ as input, along with D_{CH}, *Inun HAND,* X_{tree}, values for representative points within the existing floodplain for model #6.
2) Calculate $dep_{TP,yr}$ for proposed conditions using GLM models
    a. If IR changes as a result of intervention, repeat steps 2 through 3 from the prediction function to calculate new $dep_{TP,yr,2ch}$
    b. If evaluating changes in floodplain topography, use the resulting $dep_{TP,yr,2ch}$ from (a) and *SSP and* $W_{FP/CH}$ as input, along with D_{CH} and *HAND* values representative of the proposed floodplain topography, in model #6.
    c. If intervention also includes riparian tree planting, use same in inputs from (b) as well as X_{Tree} representative of targeted canopy cover in model #6.
3) Calculate $dep_{TP,yr}$ for existing conditions using the BRT model.
4) Calculate $dep_{TP,yr}$ for proposed conditions using BRT model.
5) Average results from (1) and (3) to calculate an estimate of and uncertainty associated with phosphorus deposition under existing conditions
6) Average results from (2) and (4) to calculate estimate of and uncertainty associated with phosphorus deposition for proposed conditions